JOINT HUMAN MOTION RECOGNITION AND BREATHING FREQUENCY ESTIMATION FOR INDOOR HEALTHCARE APPLICATIONS

MASTER THESIS REPORT

Irving Maximino Cortés Peralta

JOINT HUMAN MOTION RECOGNITION AND BREATHING FREQUENCY ESTIMATION FOR INDOOR HEALTHCARE APPLICATIONS

Dissertation

To obtain the degree of Master of Science in Electrical Engineering at Delft University of Technology to be defended publicly on 16th of December 2022

by

Irving Maximino Cortés Peralta

Born in Huatusco, Veracruz, Mexico

This thesis has been approved by

Responsible Prof: Dr. F. Fioranelli

Thesis committee:

Dr. F. Fioranelli, EWI-ME-MS3, Technische Universiteit Delft Dr. B. Hunyadi, EWI-ME-CAS, Technische Universiteit Delft PhD Candidate R. Guendel, EWI-ME-MS3, Technische Universiteit Delft



ACKNOWLEDGEMENTS

Growing up happens in a second. We walk in such a hurry through life that we barely realize how important it is to stop for a moment to look and think about who we really are, everything we have achieved, how lucky we are, and everything we are doing to reach the goals we have always dreamed about.

Doubts often paralyze us. We sit around thinking about a problem or a decision that we must take, and it seems that the more we do it, the greater our confusion is. We can only see the beginning of a path, never its route or where it leads ... although I am completely convinced that the path chosen will be neither shorter nor longer than necessary to find our own destiny.

Things never turn out exactly the way we planned. Growing up happens in a heartbeat. One day you are in dippers, next day you are gone. But all the special memories collected through the years will stay with us forever.

It has been an honor for me to be part of TU Delft and particularly of MS3 group. Thank you to all my classmates, PhDs, The Breakdown Club and my dear BME friends for so many laughs, for so many memories, for your songs, for your hugs, for understanding me, for encouraging me, for your trust, and simply, for always being yourselves.

Traveling any new path will always have a meaning behind. Over the years we can decide the distance and direction where to look for new challenges, life gives us opportunities to experiment and enjoy in a very particular way. But the truth is, that independently of the way we decide to follow, we will always find more than one friendly hand that will support us unconditionally to take the next step. Thank you to Francesco, Ronny and Ignacio for being mine.

I find myself very fortunate to have met an amazing group of people like my friends and colleges. I will always admire you and appreciate you with all my heart.

Tough days and bad results will disappoint us many times, but the truth is that history is written with all these experiences and it can be enjoyed even more when the balance, between those things that make us stronger and happier, is completely clear to us.

I will always remember my time at TU Delft, MS3, and The Breakdown Club with a happy smile on my face. :)

Irving Maximino Cortés Peralta

ABSTRACT

The challenge of dealing with patients suffering from chronic diseases and an aging population requires evolving from traditional hospital-based healthcare systems into a person-centered approach, where patients can be monitored remotely via modern technologies by cost-effective and reliable solutions based on emerging technologies in the healthcare domain.

Due to its contactless capabilities, radio-frequency technologies can lead to proactive monitoring of conditions directly related to health statuses. These technologies can include the tracking and monitoring of vital signs or the identification of abnormalities and critical life-threatening events, such as strokes or falls, in order to react before more complex scenarios and non-treatable conditions can appear over time.

This thesis project explores developing, evaluating, and verifying a processing pipeline based on radar sensing technology, jointly exploring human activity recognition and breathing frequency estimation, two of the most immediate capabilities to detect and monitor the general health conditions of a human being.

Through Doppler-Time and Range-Time data domains, the differentiation between translational and in-place activities, namely walking and sitting, is addressed, aiming to successfully identify and locate the segments where the test subject is not moving. This then triggers a proposed pipeline for the continuous estimation of the breathing frequency for the in-place scenario based on a sequential estimator, specifically the extended Kalman filter.

CONTENTS

A	knov	vledgements	V
Al	ostra	t	vi
Li	st of	Figures Control of the Control of th	ix
Li	st of	Tables Cables Ca	хi
Al	brev	iations	xiv
1	Intr	oduction	1
	1.1	Motivation	1
	1.2	Problem Formulation	3
	1.3	Thesis Contribution	4
	1.4	Thesis Structure	5
2	Lite	rature Review	6
	2.1	Radiofrequency sensing technologies for assisted daily living	6
	2.2	Radars in the healthcare domain	8
	2.3	Radar-based human activity recognition	8
		2.3.1 Data domains	9
		2.3.2 Activities	10
	2.4	Radar-based vital signs monitoring	12
		2.4.1 Kalman filter	14
		2.4.2 Particle filter	14
	2.5	Summary	15
3	Pipe	,,,	19
	3.1		19
	3.2		20
			22
			23
	3.3	8 4 5 7	24
		, 1 - 1 - 1 - 1 - 1 - 1 - 1 - 1 - 1 - 1	25
		8 4 3	26
		3 T T T T T T T T T T T T T T T T T T T	27
			28
			31
	3.4	Summary	33

viii Contents

4	Mea	asurement setup and data acquisition	35
	4.1	Radar parameters	35
		4.1.1 Doppler resolution for breathing frequency estimation	36
		4.1.2 Designed waveforms	37
	4.2	Data collection campaign	40
	4.3	Measurement setup	42
	4.4	Summary	44
5	Dat	a analysis and experimental validation	45
	5.1	In-place scenario	45
		5.1.1 Breathing frequency estimation at 1m	46
		5.1.2 Breathing frequency estimation at 2m	50
	5.2	Translational scenario	53
		5.2.1 Activity recognition and segmentation	53
		5.2.2 Breathing frequency estimation	58
	5.3	Summary	59
6	Res	ults and Future Work	62
	6.1	Results	62
	6.2	Recommendations for future research	63
	Refe	erences	65
Aŗ	pen	dix A	73
Aŗ	pen	dix B	76
Aŗ	pen	dix C	84

LIST OF FIGURES

3.1	Overview of the proposed pipeline for joint HAR and vital signs	20
3.2	Geometry of a walking person in line of sight with the radar	21
3.3	Range-Time matrix of the test sequence	22
3.4	Normalized derivative of the Range-Time	23
3.5	Spectrogram of the test sequence	23
3.6	Normalized envelope of the spectrogram for the test sequence with walk-	
	ing back and forth and in-place activities	24
3.7	Identification of data segments to trigger the pipeline for breathing fre-	
	quency estimation	25
3.8	Mechanism of breathing	25
3.9	Inhalation and exhalation motions	26
	Range history derivation based on phase unwrapping approach	28
	Flow diagram of the extended Kalman Filter	32
3.12	Segments for breathing freq. estimation based on the extended Kalman filter	33
4.1	Texas Instruments radar IWR6843 used in this thesis	36
4.2	Single chirp and related parameters from TI IWR6843 radar	37
4.3	Single frame structure from TI IWR6843 radar	38
4.4	Indoor environment for data collection	42
4.5	Respiration belt used for ground-truth	43
4.6	Example of in-place activity, i.e. sitting	43
4.7	Example of translational sequence, i.e. subject walking towards the radar .	44
5.1	Range history with waveform W1: HAR + Vital Signs at 1m	47
5.2	Estimated breathing frequency with waveform W1: HAR + Vital Signs at 1m	48
5.3	Range history with waveform W2: Vital Signs at 1m	48
5.4	Estimated breathing frequency with waveform W2: Vital Signs at 1m	49
5.5	Estimated errors with waveform W2: Vital Signs for the in-place seq. at 1m	49
5.6	Range history with waveform W1: HAR + Vital Signs at 2m	50
5.7	Estimated breathing frequency with waveform W1: HAR + Vital Signs at 2m	51
5.8	Range history with waveform W2: Vital Signs at 2m	51
5.9	Estimated breathing frequency with waveform W2: Vital Signs at 2m	52
5.10	Estimated errors with waveform W2: Vital Signs for the in-place seq. at 2m	52
5.11	Range-Time information with waveform W1: HAR + Vital Signs	54
	Range-Time information with waveform W2: Vital Signs	54
5.13	Threshold found based on Range-Time information and experimental val-	
	idation for activity segmentation	54

X LIST OF FIGURES

5.14	Segmentation between translational and in-place activities based on Range-	
	Time information with the developed waveforms	55
5.15	Segments to apply the extended Kalman filter based on Range-Time infor-	
	mation with the waveform W1: HAR + Vital Signs	56
5.16	Doppler-Time information with waveform W1: HAR + Vital Signs	57
5.17	Threshold found based on Doppler-Time information and experimental	
	validation for activity segmentation	57
5.18	Doppler-Time information with waveform W2: Vital Signs	58
5.19	Estimated errors with waveform W2: Vital Signs for the translational se-	
	quence based on Range-Time segmentation at 1m	59
5.20	Visual capability summary of the obtained results with waveform W1: HAR	
	+ Vital Signs	59
5.21	Visual capability summary of the obtained results with waveform W2: Vital	
	Signs	60

LIST OF TABLES

2.1	Comparison between different technologies for assisted daily living	7
2.2	Examples of data domains used for HAR from the literature	10
2.3	Activities studied in different works in the literature of radar-based HAR .	11
2.4	Summary of some relevant radar-based studies for HAR	16
2.5	Summary of healthcare studies for vital signs estimation	17
3.1	Typical breathing frequencies and amplitudes of a healthy person due to breathing activity	26
4.1	Summary of the key parameters of the two designed waveforms	40
4.2	Sequence of the tests performed for the data collection	40
5.1	Initialization values of the extended Kalman filter	46
6.1	Estimated breathing frequencies and errors with waveform W2: Vital Signs	
	for the in-place sequence at 1m [participants 1-10]	76
6.2	Estimated breathing frequencies and errors with waveform W2: Vital Signs	
	for the in-place sequence at 1m [participants 11-20]	77
6.3	Estimated breathing frequencies and errors with waveform W2: Vital Signs	
	for the in-place sequence at 2m [participants 1-10]	78
6.4	Estimated frequencies and errors with waveform W2: Vital Signs for the	
0.5	in-place sequence at 2m [participants 11-20]	79
6.5	Estimated breathing frequencies and errors based on Range-Time segmen-	00
6.6	tation with waveform W2: Vital Signs at 1m [participants 1-10]	80
0.0	Estimated breathing frequencies and errors based on Range-Time segmentation with waveform W2: Vital Signs at 1m [participants 11-20]	81
6.7	Estimated breathing frequencies and errors based on Range-Time segmen-	01
0.7	tation with waveform W2: Vital Signs at 2m [participants 1-10]	82
6.8	Estimated breathing frequencies and errors based on Range-Time segmen-	02
5.0	tation with waveform W2: Vital Signs at 2m [participants 11-20]	83
6.9	Summary of the test participants' information	84
3.0		- 1

ABBREVIATIONS

```
AKF adaptive Kalman filter. 14, 17
ANN artificial neural networks, 73
AoA angle of arrival. 10
Bi-LSTM bidirectional LSTM. 16, 75
BMI body mass index. 42, 84
CNN convolutional neural networks. 16, 75
CVD cadence velocity diagram. 10, 16, 73
CW Continuous-wave. 8, 12, 16–18
DCNN deep convolutional neural networks. 16, 75
DCT discrete cosine transform, 73
DL deep learning. 74
DoA direction of arrival. 13
ECG electrocardiography. 2
EKF extended Kalman filter. 4, 14, 17, 18, 28, 30, 32, 43, 44, 53
FFT fast Fourier transform. 9, 10, 28, 73
FMCW frequency-modulated continuous-wave. 4, 8, 13, 14, 16–18, 35, 37
GRU gated recurrent unit. 75
HAR human activity recognition. 1–6, 8, 10, 12, 15, 16, 18, 20, 21, 33, 34, 37, 40, 44, 45,
      62, 74, 75
HOG histogram of oriented gradients. 73
ICA independent component analysis. 13
KF Kalman filter. 13, 17
```

Abbreviations xiii

```
KNN K-nearest neighbour. 16, 74
LoS line of sight. 12, 16–18, 20, 40, 44, 46
LPC linear predictive coding. 74
LSTM long-short term memory. 16, 75
MFCC melody-frequency cepstral coefficients. 74
MIMO multiple-input multiple-output. 4, 10, 13, 16
ML machine learning. 74
MLP multilayer perceptron. 73
NCF nearly constant frequency. 14, 28, 30
PCA principle component Analysis. 13, 73
PF particle filter. 13, 17
PRF pulse repetition frequency. 16, 18, 74
PRI pulse repetition interval. 29
RCS radar cross section. 10
RD range-doppler. 9
ResNet residual Networks. 16, 75
RF radiofrequency. 2, 7, 15
RFID radio-frequency identification. 7
RNN recurrent neural networks. 75
RTI range-time information. 9, 22, 53
SCR signal to clutter ratio. 13
SIDS sudden infant death syndrome. 2
SNR signal to noise ratio. 13, 16, 74
STFT short time Fourier transform. 9
SVD singular value decomposition. 73
SVM support vector machine. 16, 74
```

xiv Abbreviations

TIV time-invariant. 15

TVAR time-varying autoregressive. 15

UWB Ultra-wideband. 8, 12, 14, 16, 18

1

INTRODUCTION

This chapter describes the motivation behind the development of a joint approach for radar-based human activity recognition (HAR) and vital signs monitoring in Section 1.1. The problem formulation is defined in Section 1.2 according to the gaps found in existing research, and Section 1.3 summarizes the main contributions of the proposed HAR and breathing frequency approach developed in this thesis. Finally, the structure of this thesis is presented in Section 1.4.

1.1. MOTIVATION

The motivation behind this thesis work is based on the following four questions:

Is it worth exploring emerging technologies for indoor healthcare applications?

Home healthcare devices can significantly improve patients' quality of life suffering from chronic, non-communicable diseases like Parkinson's, dementia, epilepsy, narcolepsy, and multiple sclerosis, by minimizing the disruption to their usual routine and lifestyle [1]. Aging increases the incidence of these diseases, followed by a reduction in mobility due to cardiovascular and musculoskeletal problems. Additionally, the probability of critical life-threatening events, such as strokes or falls, increases as well, together with the incidence of multiple chronic health conditions. In the medical domain, this condition is referred as "multimorbidity", where two or even more chronic diseases can coexist within the same person [2].

The World Health Organization and the United Nations estimate that 30% of the world population will be older than age 65 by 2050 [3]. The challenges to managing the health conditions of an aging population are combined with budget limitations, hence specialized intensive care at hospitals or clinics might result unsustainable for public healthcare systems. In addition, prolonged periods of hospitalization can be unpleasant for patients and their families and can bring risks of exposure to other infections such as antibiotic-resistant bacteria. Therefore, the challenge of dealing with an aging

population is making the case for novel healthcare developments that evolve from the traditional hospital-based system to a person-centric approach where the patients can be observed in their homes remotely via modern technologies. Hence, there is a need to find cost-effective and reliable solutions in the healthcare domain based on emerging technologies [1].

Why explore radiofrequency (RF) approaches? Why focus on HAR and vital signs monitoring?

Various sensors have been used for HAR and assisted living (more details in Chapter 2). Nevertheless, RF has increasing popularity due to its capability of contactless monitoring to identify basic daily life activities, such as walking, kneeling, sitting, or standing up. Therefore, this contactless capability might be advantageous for different groups of people, like those affected by cognitive impairments who might forget to use wearable sensors properly, and even for users' acceptance, for instance in comparison to video-based sensors.

Enabling the recognition of these fundamental activities is important for well-being assessment, as health-related activities, such as exercising, are complex activities composed by fundamental daily activities [4]. Moreover, the way these basic activities are performed has a direct relationship with health statuses, such as arthritis, cardiovascular, or neurodegenerative diseases [5]. RF monitoring systems can also ease the detection of critical events such as falls or other potentially dangerous behavior, and alert family members, caregivers, or first-aid services for immediate support [1]. Furthermore, RF can potentially lead to proactive monitoring of health conditions to identify abnormalities over time and react before more complex and non-treatable conditions can appear.

Regarding vital signs, breathing frequency and heart rate are the two most immediate components while detecting or monitoring the health conditions of human beings, and they can already provide important information on their general health conditions. Traditional methods of vital signs monitoring, such as electrocardiography (ECG) with straps and electrodes, are applicable with intrusive or contact devices, which might have limitations in various scenarios, such as burned skin or sudden infant death syndrome (SIDS) [6–8]. Consequently, contactless vital signs monitoring is an area of interest, and RF implementation is one of the most promising approaches to be further explored.

Why radar sensing?

The fundamentals of radar-based HAR is that each human activity has unique kinematic patterns, which can be represented by intrinsic kinematic features within the radar data. On the other hand, contactless vital signs estimation and monitoring through radar technology is mainly based on capturing the periodic motion of the chest and heart wall due to cardiopulmonary activity. Specifically, the implementation of radar-based approaches provides the following advantages compared to other existing technologies [3, 9]:

 Radar is a non-invasive device, meaning that privacy can be less of a problem than for camera-based sensors.

- It is a non-wearable sensor, so interaction with the radar from the users' side is not required for its functionalities.
- Its functionality is independent of light conditions in the indoor (or outdoor) environment.
- With suitable techniques, the extracted information from the acquired data is still
 accurate and rich in content, even in the presence of noise, clutter, and multipath
 effects.

However, it is important to mention that practical implementation of radars is not wholly feasible yet; further developments in size, costs, and algorithms are still required to bring the current research activities and systems to an actual deployable product. Nevertheless, ongoing research in other fields like autonomous driving is substantially accelerating this process of miniaturization of radar systems and reduction of costs [3].

As a result of the answers obtained from the previous research questions, this thesis project focuses on the *development of a radar-based processing pipeline for joint HAR and vital signs monitoring (i.e., respiration specifically)*, aiming to provide an innovative solution for assisted living technologies in the healthcare domain.

1.2. PROBLEM FORMULATION

By reviewing the literature in Chapter 2, several challenges and limitations of existing solutions for radar-based HAR and vital signs estimation have been found. An overview of these limitations is briefly discussed, together with the open challenges that radar technology is currently facing in the healthcare domain for both fields [1, 3, 9, 10].

- For human activity recognition:
- Identification of the most suitable radar data domains for the specific classification problems to be addressed.
- Dealing with human activities as continuous sequences, where transitions and durations between different movements are not pre-defined.
- It is not yet clear how to train the classification algorithms for unforeseen activities or movements not initially present in the dataset (so-called open set problem).
- Processing of complex scenarios that include, besides noise and clutter, multiple targets and multipath phenomena.
- Implementation of machine learning techniques, which can bring practical challenges like the acquisition and development of labelled datasets to train and test the different classification algorithms, and the interpretability and explainability of the decisions made by these types of classifiers.
- Development of algorithms to combine information from multiple sensors, a process known as data fusion or multimodal fusion, to improve the overall classification performance.
- For vital signs monitoring:
- Validation of breathing frequency and heart rate monitoring on longer distances from the radar and different, unfavourable aspect angles is required.

 More realistic conditions and scenarios need to be tested, in order to extend current capabilities to monitor heartbeat and if possible even blood pressure successfully.

- Evaluating the impact of different radar frequencies with different layers of clothing, such as the ones worn by the subjects (shirts, sweaters, coats) or the ones present in the environment such as blankets or curtains.
- The robustness of the implemented algorithms must be further investigated under different subject orientations in azimuth and elevation, such as lying down or back and side view, rather than frontal and sitting positions typically used in demonstrations in lab-conditions.

Based on these gaps, the problem to be addressed in this thesis work is formulated as follows:

"Development, evaluation, and verification of a proof of concept approach based on radar technology, simultaneously combining HAR and vital signs estimation. Specifically, the proposed approach aims to provide a joint exploration of both aspects, evaluating the feasibility of estimating the breathing frequency of a static and moving target under different test conditions in an indoor environment, while recognizing translational and in-place human motions in a simple sequence."

An important point to stress is that HAR and vital signs estimation are often performed separately, treated as two different problems in the current radar literature. From this comes the wish to implement a unified processing pipeline that can do both tasks given a sequence of radar data. Further details about the proposed pipeline are discussed in Chapter 3.

1.3. THESIS CONTRIBUTION

The main contributions of the proposed joint HAR and breathing frequency estimation system can be summarized as follows:

- 1. A processing pipeline that can segment a sequence of translational activities and in-place activities alternated with static postures is formulated based on range-time and Doppler-time radar data. An extended Kalman filter (EKF) is implemented and used to estimate the breathing frequency when the subject is in a static position (e.g., sitting).
- 2. The pipeline is validated in a proof of concept experiment involving 20 volunteers and simple sequences including walking, sitting, and standing actions. A 60[GHz] frequency-modulated continuous-wave (FMCW) multiple-input multiple-output (MIMO) radar is used for this validation, showing acceptable results in the best-case scenarios (in terms of radar parameters and distance/orientation of the volunteers with respect to the radar).
- 3. This initial study highlighted the importance of choosing suitable parameters for the radar waveform in order to get acceptable performance for both human activity segmentation and estimation of the respiration frequency. A potential trade-off

is found, in a sense that a radar waveform that obtains good performance for both tasks may not be easily implementable with the chosen radar.

1.4. THESIS STRUCTURE

This thesis is structured as follows. Chapter 2 reviews the relevant literature related to radar-based HAR and vital signs monitoring. Chapter 3 introduces the pipeline of the proposed joint classification and respiration estimation approach, presenting the methods and models to be implemented. In Chapter 4, the laboratory measurement setup for data acquisition is fully described. Experimental verification of the joint indoor application is then assessed in Chapter 5. Lastly, the corresponding results together with the outlines for potential future work are summarized in Chapter 6.

LITERATURE REVIEW

In this chapter, the related work regarding HAR and vital signs monitoring through radar implementation is presented. Section 2.1 introduces different radiofrequency techniques currently explored as assisted living technologies. Section 2.2 describes the application of radar systems in the healthcare domain. Recent advances to address HAR and vital signs are studied correspondingly in sections 2.3 and 2.4. As closure, various remarks based on the research done in this chapter are shared with the reader in section 2.5.

2.1. RADIOFREQUENCY SENSING TECHNOLOGIES FOR ASSISTED DAILY LIVING

Recently, as previously mentioned in Chapter 1, there has been significant interest in applying the most advanced technologies to develop integrated health care systems for home environments, commonly referred to as *assisted living technologies*, which have primarily two objectives [3]:

- A proactive approach to provide continuous and reliable monitoring of signs related to worsening health conditions, rather than reacting only when severe symptoms are present.
- Avoid hospitalization and preserve the autonomy and independence of vulnerable people, like older or disabled people.

In the literature, several types of technologies have been investigated regarding assisted living [1]:

- **Vision-based:** Through the implementation of video cameras, a light-dependent approach.
- **Sensor-based:** Based on body-worn sensors, such as magnetic sensors, which the monitored subject must wear.

- **Motion-based:** Employing accelerometers and gyroscopes, usually integrated and carried by the subject in wearable devices.
- Sound-based: Applying ultrasonic acoustic audio, a realization commonly sensitive to noise and interference.

RF offers contactless monitoring capabilities with typically no interaction required from users, and the possibility of leveraging existing communication signals and available infrastructure (like Wi-Fi routers).

The use of RF sensing has also been considered in recent years in the context of assisted living, where the most explored technologies have been [10]:

- Wi-Fi-based: Monitoring a particular area of interest and the subjects there, aiming to detect the temporal amplitude and phase variations from information retrieved from multiple wireless channels.
- radio-frequency identification (RFID)-based: Identifying objects and movements
 utilizing electromagnetic fields to transmit digital encoded data from the RFID
 tags to tags deployed on subjects' bodies or surroundings.
- Radar-based: Emitting different electromagnetic waveforms and analyzing the received echoes to characterize the location and movements of the subjects under the illuminated area.

A more comprehensive comparison between the technologies mentioned above is presented in Table 2.1.

Table 2.1: Comparison between different technologies for assisted daily living [1, 10]

Sensor	Main advantages	Main disadvantages	
	a) Very effective security measure	a) Privacy interference	
Vision-based	b) Storage of records	 b) Dependance of light conditions 	
	b) Storage of records	c) High computational cost	
	a) High detection accuracy	a) Expensive	
Sensor-based	b) Not related with privacy issues	 b) Disturb activities of the users 	
	b) Not related with privacy issues	c) Requires sensors installation and calibration	
	a) High detection accuracy	a) Raise physical discomfort	
Motion-based	b) Not related with privacy issues	b) No direct linear or angular position information	
Wolfoll-Dased	c) Low cost	c) Prone to false detection	
	C) LOW COST	d) Insensitive to very slow motions	
	a) Sensitive to motion	a) Directional functionality (ultrasonic)	
Sound-based	b) It allows to determine precisely objects and distances c) Inexpensive (audio)	b) Sensitive to target temperature and angle (ultrasonic)	
Sound-based		c) It can be influenced by audio signals/noise	
	c) mexpensive (audio)	d) Prone to false detections	
	a) Cost-efficiency: almost everywhere is equipped with Wi-Fi	a) Adjustment is needed in different environments	
Wi-Fi based	b) High detection accuracy	b) Computationally complex	
	c) Acceptable performance in complex environments	c) Sensitive to the noise interference	
	a) High detection accuracy	a) Adjustment is needed in different environments	
RFID-based	b) Respect to privacy	b) Computationally complex	
	b) Respect to privacy	c) Reduced performance in complex environments	
	a) Functionality in darkness	a) Directional functionality	
Radar-based	b) Respect to privacy	b) Sensitivity to temperature and direction of arrival	
	c) Accurate range measurements	c) Required installation and calibration	

Compared to other radiofrequency technologies in the healthcare domain, radars offer privacy in sensitive environments, like bedrooms or bathrooms. At the same time,

users do not need to wear or interact with any external device to modify their daily routine or expected behavior [1]. Further explanation about the use of radars in healthcare applications will be described in the upcoming sections.

2.2. RADARS IN THE HEALTHCARE DOMAIN

Applications of radar in the healthcare domain can be subdivided into three areas [9]:

- Human activity recognition (HAR): To monitor and classify human motions in indoor environments, including but not limited to walking, sitting, standing up, kneeling, carrying objects, crawling, as well as short-term activity pattern monitoring like fall detection for critical events [11–15]. These movements can also be combined to represent daily life activities and more complex scenarios.
- **Gait analysis:** To estimate parameters of gait that can be clinically relevant, such as limping, dragging feet, and frozen gait. Additionally, radar signatures have been implemented to identify irregular gait patterns related to the physical or cognitive worsening of health conditions [16–18].
- **Vitals signs:** To estimate variables related to physiological movements of the body like respiration rate, heart rate, and blood pressure [19–22].

All these applications could potentially be combined to develop an overall health status of the subjects under study and detect anomalies and critical events for indoor scenarios. As this thesis project will focus on addressing HAR and vital signs estimation through the implementation of radar, advances and current tradeoffs from both research fields will be covered in sections 2.3 and 2.4, respectively.

In the literature, the most typical radar architectures used in the domain of health-care have been [9]:

- Continuous-wave (CW) radar, often referred to as Doppler radar.
- Ultra-wideband (UWB) radar, often referred to as pulse-Doppler or pulsed radar.
- FMCW radar, often referred to as range-Doppler radar.

While a detailed discussion about the operating principle behind these types of architectures goes beyond this thesis's scope, it is essential to mention that one of the main differences between FMCW and UWB radars lies in the possibility of measuring Doppler and range to the target, in contrast to a simple CW radar where only Doppler information can be retrieved. Therefore, further discussions will focus only on FMCW and UWB architectures for HAR and monitoring of vital signs.

2.3. RADAR-BASED HUMAN ACTIVITY RECOGNITION

HAR typically relies on different data domains and machine learning algorithms to classify patterns corresponding to different activities, based at the same time on patterns observed in the radar data [23–27]. This section analyzes radar-based HAR's problem from two mutually dependent perspectives: *data domains and analyzed activities*. Further information regarding features extraction and algorithms currently applied for HAR

and classification tasks based on machine learning techniques are shared in Appendix 6.2.

2.3.1. DATA DOMAINS

Activity recognition and vital signs estimation can be related to the detection and characterization of movements from the human body, either by:

- Large movements of the body and limbs while performing daily tasks.
- Small chest movements (for breathing frequency) and internal organs (for heart rate or blood pressure).

Signal processing techniques on radar data aim to characterize these types of movements principally based on three variables [3]:

- *Time*: To evaluate the position of the subject and all the movements involved over the time domain.
- **Range:** To locate the target and its body parts with respect to the radar on a distance base.
- *Velocity:* To estimate the radial velocity at which all these changes occur. This velocity estimation is typically performed based on the Doppler effect.

The combination between these variables leads to represent the radar raw data in different matrix forms, known as data domains [3]:

- a) Range-Time: Also known as range-time information (RTI) matrix, where each radar pulse is digitized, and samples inside the matrix represent the time and distance to the target under study according to the temporal sequence of the pulses. The time or pulse number axis is usually referred to as the slow-time axis, while the range axis is also known as the fast-time axis.
- b) Range-Doppler: Obtained applying a fast Fourier transform (FFT) across the time dimension (across the sequence of radar pulses) of the range-time matrix. This range-doppler (RD) matrix characterizes the overall Doppler pattern of the target in the frequency domain.
- c) **Doppler-Time:** The RD matrix does not include information about how the body and limbs move over time. Therefore, to generate Doppler-time patterns (also known as spectrograms), a short time Fourier transform (STFT) is typically applied. This signal processing technique performs several FFTs on the radar data using shorter and overlapped time windows, producing a column of the spectrogram over time every time an FFT is done. The patterns obtained typically represent the movement of the whole body, torso, and limbs, such as arms and legs. In the literature, signatures related to these micromotions' dynamics are often referred to as the *micro-Doppler effect* due to the induced Doppler modulations in addition to the constant Doppler frequency shift from the bulk motion.

The three data domains described above represent (after clutter filtering, denoising, and interference suppression) the initial input for radar signal processing algorithms aiming to perform HAR and vital signs estimation. Typically, micro-Doppler signatures have been utilized as the primary domain to perform HAR since the past decade [11, 12]. However, research considering other data domains rather than micro-Doppler, and/or the combination between them, is emerging and currently under development, as shown in Table 2.2.

Paper	Data domains		
Jokanović et al. [23] Range information + Micro-Doppler			
Li et al. [24] Range-time + Micro-Doppler + cadence velocity diagram			
Guendel et al. [25]	Phase information from range map + Micro-Doppler		
Aziz et al. [26]	Micro-angular velocity + Micro-Doppler		
Ding et al. [27]	Range + Doppler + radar cross section (RCS) information		

Table 2.2: Examples of data domains used for HAR from the literature

Jokanović et al. [23] studied a combination of range information and micro-Doppler signatures to improve fall detection accuracy through the implementation of deep learning techniques. Li et al. [24] investigated three domains of radar data, namely rangetime, micro-Doppler, and CVD, evaluating which ones were best suited to classify specific daily human movements. CVD is a data domain obtained by taking a further FFT along the Doppler frequency bins spectrograms. This representation normally facilitates highlighting the periodicity of the micro-Doppler modulations over time. Guendel et al. [25] explored the phase information directly extracted from a high-resolution range to classify six different arm gestures and eight gross-motor activities performed bidirectionally. Aziz et al. [26] utilized a MIMO radar for activity recognition, capturing the angle of arrival (AoA) of the scattered waves to characterize the body micro angular displacements, known as micro-angular signatures, based on calculating the rate of change of the AoA with respect to time. Ding et al. [27] incorporated the RCS information from the test subject as a data domain to distinguish falls from other movements like jumping and squatting.

As it can be deduced, different domains can be evaluated and combined to find the ones that best suit the classification of the specific human activities to be addressed. Moreover, different domains have distinctive sensitivity to particular movements, meaning that each domain has its own limitations and advantages. In addition, information fusion between different domains can also be applied to enhance the classification accuracy, compared to the results of using a single data domain.

2.3.2. ACTIVITIES

Postures and activities analyzed for HAR vary from work to work. Table 2.3 presents a brief summary of the different and total number of activities for several works in the literature reviewed in this thesis.

Table 2.3: Activities studied in different works in the literature of radar-based HAR

Paper	No. of activities	Activities			
_		1. Running, 2. Walking			
Vi at al [11]	7	3. Walking without moving arms			
Kim et al. [11]	7	4. Crawling, 5. Boxing			
		6. Boxing while moving forward, 7. Sitting			
		1. Running, 2. Walking			
		3. Walking while holding a stick			
Kim et al. [12]	7	4. Crawling			
		5. Boxing while moving forward			
		6. Boxing while standing in place, 7. Sitting			
		1. Walking, 2. Running			
Çağlıyan et al. [28]	4	3. Crawling directly toward the radar			
,,,,,,,,,,,,,,,,,,,,,,,,,,,,,,,,,,,,,,,		4. Walking at an aspect angle of 75 degrees			
		1. Walking, 2. Sitting			
Jokanović et al. [29]	4	3. Bending and straightening, 4. Falling			
		1. Boxing, 2. Climbing			
		3. Walking, 4. Running, 5. Jumping up			
Du et al. [30]	8	6. Jumping forward, 7. Kicking			
		8. Standing with slight movement			
		1. Jumping, 2. Running			
Yang et al. [31]	6	3. Walking, 4. Crawling			
rang et an [01]		5. Creeping, 6. Boxing			
		1. Walking, 2. Running			
	7	3. Walking while holding a stick, 4. Boxing			
Shao et al. [32]		5. Boxing while moving forward			
		6. Falling, 7. Sitting down			
		1. Walking, 2. Sitting down			
Jia et al. [33]	6	3. Standing up, 4. Picking up an object			
Jia et al. [55]	0	5. Drinking, 6. Falling			
		1. Bending and picking up an object from the floor			
		2. Waving with one hand			
Fioranelli et al. [34]	4	3. Sitting and standing up			
		4. Walking back and forth			
		1. Walking back and forth			
		2. Standing up and sitting			
Yang et al. [35]	6	3. Bending down and standing back up			
langeran [30]	0	4. Moving one arm in a circle while standing			
		5. Pushing, 6. Pulling			
		1. Running forward, 2. Walking forward			
Liotal [36]	6	3. Boxing in place, 4. Running in a circle			
Li et al. [36]	6	5. Jumping forward, 6. Sitting			
		1. Running, 2. Walking			
		3. Walking while holding a stick, 4. Crawling			
Vim et al [27]	7	5. Boxing while moving forward			
Kim et al. [37]	7	6. Boxing while standing in place			
		7. Sitting			

Based on the information from Table 2.3, activities typically studied are:

- Walking
- · Sitting down
- Standing up
- Bending over
- Falling down
- Running
- Crawling

In most studies the average number of classes, defined as the output category of the acquired data, ranges around 6 classes, varying from binary cases for fall detection [29] to cases with even 7 or 8 different classes [30].

It is worth mentioning that walking is an activity always included in any dataset for HAR, with variants like walking without moving the arms [11], walking while holding a stick [32], or walking at an aspect angle of 75 degrees to the line of sight (LoS) of the radar [28]. Additionally, activities such as sitting, bending, standing up, and falling are frequently present [33] [34] [35], since they can show indoor daily life activities that could potentially be applied for human life assistance. Furthermore, most of the related work adopts indoor scenarios with a single radar, and Doppler signatures from activities performed in the LoS, which can be unrealistic constraints for true daily life assistance applications. Exceptions can be found in Çağlıyan et al. [28], where several aspect angles are evaluated for different human activities, and in Guendel et al. [38], where continuous human activity recognition is proposed through the implementation of a network of radars.

As it can be seen, the choice of activities is inherently dependent on the desired application. Therefore, as one of the aims of this thesis project is the development, evaluation, and verification of an indoor healthcare application for daily life assistance, the three common activities of walking, sitting, and standing will be considered in this work for an initial simple proof of concept.

2.4. RADAR-BASED VITAL SIGNS MONITORING

Similar to human activity recognition and classification, radar has also been used to estimate and monitor vital human signs, such as breathing frequency, heart rate, and even blood pressure [21]. Information regarding these biological functions could potentially assess respiratory conditions and the worsening of human health over time.

The analysis of the reflected signals from the human body is generally simplified due to the penetration depth into the skin being 1 mm at most with a 60 GHz radar [39]. In the literature, range displacement of the human body has been measured with UWB radar by Yarovoy et al. [40] and induced Doppler frequency shift with a CW radar by Li et al. [41] to estimate the parameters of chest movement. Moreover, successful monitoring of vital signs has also been demonstrated by Li et al. [41] for different aspect angles and sides from the human body to the radar.

Nevertheless, the application of mm-wave FMCW radars (60 GHz and 77 GHz bands) has recently and widely been investigated as mentioned by Su et al. [22] due to their high Doppler sensitivity. Estimation of respiration movements for contactless monitoring of vital signs utilizing an 80 GHz FMCW radar by Wang et al. [42] showed the possibility to detect respiration rate from the left side of the human body with a relatively low error, and measurements of vital signs with a 96 GHz radar with time and frequency methods were demonstrated by Ayhan et al. [43]. As the estimation of vital signs often has to deal with low signal to noise ratio (SNR) and signal to clutter ratio (SCR) of the received signal, a MIMO system was used by Sakamoto et al. [44] for instantaneous heartrate in a multiple people scenario to estimate their direction of arrival (DoA) while focusing the signals on desired directions to reduce the clutter interference. Range compression and beamforming were applied by Ahmad et al. [45] for vital signs monitoring of multiple people and further extended with a 120 GHz MIMO architecture for 3D localization by Wang et al. [46]. It has been demonstrated that vital signs measurements can be performed with a multiple antenna system and various adaptive signal processing techniques to increase the SNR and enhance the accuracy of the measurements by Aho et al. [47]. Undesired clutter can be suppressed by applying the principle component Analysis (PCA), as shown by Singh et al. [48]. Arctangent demodulation is proposed by Park et al. [49] to solve the problem of DC offset compensation at the in-phase and quadrature channels for Doppler radar systems.

Furthermore, random body movement cancellation is addressed by Li et al. [50] through the implementation of two demodulation techniques: complex signal demodulation and arctangent demodulation, showing that vital signs detection can be feasible with both demodulation techniques if the dc offset of the baseband signal is accurately calibrated; and by taking data simultaneously from both sides, front and back, of the human body to cancel out the random frequency drift derived from the target's random behavior, which can introduce a significant source of noise and affect an accurate detection. Estimation of vital signs has also been explored through empirical mode decomposition and independent component analysis (ICA) by Weishaupt and Mercuri et al. [51, 52], techniques that process the radar data over a long observation time which can oscillate between ten seconds and above one minute. Additionally, Mikhelson et al. [53] used wavelet decomposition to analyze the heartbeat in terms of the phase history. Extraction of vital signs, such as breathing or heartbeat frequencies, is typically based on frequency peak searching in the Doppler power spectrum and/or by unwrapping the phase history of the received signal from which the range history is computed [22]. Therefore, proper signal processing techniques must be implemented to extract this information from the received signals, as addressed by Adib et al. [54], where the Doppler phase history was extracted to estimate breathing and heart rate frequencies.

As continuous information about the targets state is usually required for assisted living technologies, a rapid reaction from the monitoring system is necessary to capture the human body's behavior. However, sequential tracking of vital signs has not been widely investigated yet. Closely related to the fields of tracking human motions and activities, dynamic estimation of vital signs has been addressed by applying estimators, such as the Kalman filter (KF) and the particle filter (PF), to the radar data [55–58].

Further details about these possible estimators for vital signs monitoring are presented in the following sections.

2.4.1. KALMAN FILTER

The key assumptions behind the derivation of the Kalman filter are that the estimation problem to be solved must be linear and Gaussian. Once these conditions are satisfied, the Kalman filter computes the mean and covariance of the true posterior density. However, many practical problems are nonlinear, and several variants of the Kalman filter have been proposed for dealing with these nonlinearities.

In the literature, variants of the Kalman filter have been derived for vital signs monitoring. An adaptive Kalman filter (AKF) technique for heart rate monitoring was implemented by Xu et al. [56], and vital sign integrated tracking through a Kalman filter with UWB radars was performed by Yu et al. [57]. Similarly, heartbeat estimation with an FMCW radar architecture was done via a Kalman filter by Arsalan et al. [58], and dynamical changes in vital signs using a switching Kalman filter were addressed by Almeida et al. [59]. A modified robust Kalman filter for the estimation of heartbeat and respiration rate is discussed by Khan et al. [60], and the estimation of breathing frequency with a modified joint unscented Kalman filter is presented by Uysal et al. [61].

As it can be deduced, the motion of vital signs is an example of a nonlinear problem estimation. An approximate solution has been done by linearizing the state and/or the observation functions of these nonlinear problems. This approximation results in a subsequent application of the Kalman filter for a linear case based on the linearization of a nonlinear model, an implementation referred to as the EKF. Su et al. [22] utilized an EKF for the dynamic estimation of breathing parameters based on the chest movement due to breathing and the unwrapped phase history of the received data, focusing on the sequential estimation of the breathing frequency through the adoption of a nearly constant frequency (NCF) model for the displacement of the chest with an mm-wave FMCW radar, showing that the proposed method can provide accurate information about human breathing after collecting a few seconds of raw data.

In many practical cases, the EKF is a sufficient algorithm for its simplicity and efficient implementation, and for this reason it is used in the proof of concept implemented in this thesis to estimate the respiration frequency. However, its optimality cannot always be guaranteed due to the linearization assumptions [62]; for this reason particle filters are briefly introduced in the next sub-section as a possible hint to future work.

2.4.2. PARTICLE FILTER

Although the Kalman filter and its variants perform as optimal sequential estimators in linear Gaussian cases, the models of vital signs are nonlinear, as mentioned before. Moreover, the linearization extension of the Kalman filter, referred to as the extended Kalman filter, restricts the type of noise to be Gaussian. Generally, the noise is Gaussian in the complex domain, but its magnitude and argument are not if the real and imaginary parts of the noise are mutually independent. Therefore, the noise for the phase typically does not follow a Gaussian distribution.

Sampling-based techniques, often referred to as particle filters, are considered a gen-

15

eralization form of the Kalman filter with the advantage of solving filtering problems for nonlinear and/or non-Gaussian models, which can be more suitable for vital signs estimation and monitoring. Consequently, this estimator has become a popular algorithm with the increase in computational and memory capabilities of modern computers.

A particle filter is then a more advanced and robust solution that starts with a set of samples and recursively computes updates (or even new sets of samples) based on the previously computed set, the system dynamics, and the acquired data. Furthermore, different approaches of the particle filter compute a certain weight for each of the particles, measuring their respective importance and using this information to generate the next set of particles based on the updated weights.

Dynamic respiratory modeling with a particle filter framework was proposed by Yamamoto et al. [63] for non-contact monitoring of chest-wall displacement. Lee et al. [64] combined a particle filtering algorithm with time-invariant (TIV) and time-varying autoregressive (TVAR) models for the extraction of breathing frequencies. Photoplethysmography signals and a particle filter-based algorithm were jointly utilized by Fujita et al. [65] for heart rate estimation. Instead, electrocardiogram signals were used by Nathan et al. [66] to achieve the same goal, and a particle filter's continuous monitoring of heart rate variations was addressed using wearable devices for sensors fusion by Nathan et al. [67] as well. As a result that many unknown parameters are estimated, and a significant number of particles are processed on each iteration; particle filters are still considered as high computational complex algorithms independently of their final application.

Although radar-based estimation of vital signs has been widely explored in recent years, vital signs tracking is challenging even for current radar sensing technologies. Multiple people and multipath environments are complex scenarios where further research needs to be done. Amplitudes of breathing and heartbeat frequencies are very weak and hard to detect since their non-contact nature originates from the minor movement of the chest, which makes the power of the signals lower than the power of clutter. Moreover, perfect models of vital signs do not exist, and uncertainty in monitoring tasks will always be present independently of the estimation technique.

2.5. SUMMARY

In this chapter, the implementation of RF to develop assisted living technologies was first introduced. Specifically, related work was presented to address HAR and vital signs estimation in the healthcare domain through radar sensing technology.

- For *radar-based HAR* tasks, two mutually dependent perspectives were analyzed, namely:
 - **a) Data domains:** Where different representations for the radar data were described, such as *range-time, range-Doppler, and Doppler-time*, introducing the term *micro-Doppler* for the last one.
 - **b) Analyzed activities:** Indicating the type of movements and activities usually studied for HAR.

Table 2.4 summarizes some of the relevant papers reviewed for HAR in this literature

review, with an additional discussion based on the information gathered through this research together with the information from Appendix 6.2.

Paper	No. activities	No. features	Data domain	Classifier	Scenario	Radar type
Kim et al. [12]	7	6	Micro-Doppler	support vector machine (SVM)	Lab 12 subjects	CW 2.4 GHz
Jokanović et al. [23]	4	N/A	Micro-Doppler Range information	Stacked autoenconder Softmax regression	Lab 3 subjects	FMCW 25 GHz
Li et al. [24]	6	21	Micro-Doppler Range-time CVD	SVM K-nearest neighbour (KNN)	Lab 72 subjects	FMCW 5.8 GHz
Aziz et al. [26]	8	N/A	Micro-angular velocity Micro-Doppler	Metric learning	Lab 8 subjects	FMCW MIMO 77 GHz
Çağlıyan et al. [28]	4	10	Micro-Doppler	KNN	Lab 10 subjects	UWB 5.8 GHz
Shao et al. [32]	7	N/A	Range information	deep convolutional neural networks (DCNN)	Lab 6 subjects	UWB 3.2 GHz
Jia et al. [33]	6	36	Range-time Range-Doppler Phase diagrams CVD	SVM Stacked autoencoder convolutional neural networks (CNN)	Lab 83 subjects	FMCW 5.8 GHz
Kim et al. [37]	7	N/A	Micro-Doppler	DCNN	Lab 12 subjects	CW 2.4 GHz
Guendel et al. [38]	9	7	Range-Doppler	Softmax regression	Lab 5 subjects	UWB 4.3 GHz
Zhang et al. [68]	7	N/A	Micro-Doppler	CNN	Lab 1 subject	FMCW 77 GHz
Du et al. [69]	6	N/A	Micro-Doppler	residual Networks (ResNet)	Simulation	CMU Mocap Database
Shrestha et al. [70]	6	N/A	Micro-Doppler Range-time	long-short term memory (LSTM) bidirectional LSTM (Bi-LSTM)	Lab 15 subjects	FMCW 5.8 GHz

Table 2.4: Summary of some relevant radar-based studies for HAR

The main insights derived from this analysis include:

- Different data domains have distinctive sensitivity to certain types of movements, meaning that each domain has its own limitations and advantages. Information fusion between different domains can also be applied to enhance the classification accuracy compared to using a single data domain. However, micro-Doppler is still the domain most explored for HAR.
- Data domains and classifiers are mutually dependent. Therefore, the optimal classifier or data representation does not exist in absolute terms, but a better performance of their combination given a specific task or a set of them, aiming to enhance and ideally optimize the classification performance by exploring different radar data representations and the matching classifier.
- The efficacy of any given feature does not depend only on radar parameters, such as the transmit frequency or the pulse repetition frequency (PRF), but also on external factors, such as the SNR, aspect angle, dwell time, and the classification problem itself.
- Most related work adopts indoor scenarios for a single target with various test subjects, and a single radar for different human activities in the LoS and several aspect angles from the test subject to the radar. Additionally, continuous HAR can potentially be addressed by implementing a network of radars.
- Activities such as sitting, bending, standing up, and falling are frequently included for HAR since they represent indoor daily life activities that can be applied for hu-

17

2

man life assistance. Nevertheless, the choice of activities is inherently dependent on the application to be examined.

- For *radar-based vital signs monitoring*, mainly two types of signal processing techniques were studied:
 - **a) Kalman filter:** Primarily examining derived variants and the linear approximation of this algorithm for non-linear cases referred to as the EKF.
 - **b) Particle filter:** Sampling-based technique to address non-linear problems like the behavior of vital signs.

Similarly, table 2.5 summarizes a few relevant papers for healthcare applications involving the estimation of vital signs, which allowed to reach important remarks listed below.

Paper	Vital sign	Algorithm	Subject orientation	Subject distance	Radar type	
Su et al. [22]	Ducathing funguous	EKF	LoS	2 m	FMCW	
Su et al. [22]	Breathing frequency	EKF	1.05	2 111	77 GHz	
Xu et al. [56]	Heart rate	AKF	N/A	N/A	N/A	
Ancolon et al. [E0]	Heart rate	KF	LoS	0.4 m	FMCW	
Arsalan et al. [58]	неан гате	Nr.	103		60 GHz	
	Breathing frequency	PF		3.25 m	CW	
Yamamoto et al. [63]			30°		24 GHz	
			FF	ГГ	ГГ	гг
					sensor at 0.5 m	
Nathan et al. [66]	Heart rate	PF	N/A	N/A	N/A	

Table 2.5: Summary of healthcare studies for vital signs estimation

- Continuous information about the target state is usually required for assisted living technologies. However, sequential tracking of vital signs through radar sensing has not been widely investigated yet. Nevertheless, dynamic estimation of vital signs has been addressed by applying estimators, such as the Kalman filter and the particle filter, to data acquired from various sources.
- Extraction of vital signs through radar technology, such as breathing or heartbeat
 frequencies, is typically based on frequency peak searching in the Doppler power
 spectrum and/or by unwrapping the phase history of the received signal from
 which the range history is computed.
- Vital signs monitoring is a nonlinear estimation problem. Nevertheless, the EKF
 has proved to be a sufficient algorithm for its simplicity and efficient implementation compared to PF for radar sensing applications, where the PF is still considered
 a high computational complex algorithm due to the many unknown parameters to
 be estimated, and the significant number of particles to be processed on each iteration.
- Validation of breathing frequency and heart rate monitoring on longer distances and different aspect angles is still required.

- As can be deduced, a perfect radar architecture for HAR and vital signs monitoring does not exist, and each radar system has its unique advantages and disadvantages. However, FMCW and UWB radars enable the possibility of measuring Doppler and range to the target, in contrast to simple CW radars where only Doppler information can be acquired. Therefore, FMCW and UWB radars are feasible architectures for HAR and monitoring of vital signs.
- In both architectures, the signals sent are a function of the transmit frequency, bandwidth, pulse duration, and the PRF. Doppler resolution depends upon the PRF, while the transmit frequency affects the Doppler shift induced. Range resolution is limited due to the signal bandwidth.
- Perfect models of vital signs do not exist, and uncertainty in monitoring tasks will
 always be present independently of the estimation technique. Moreover, multiple
 people and multipath environments are complex scenarios where further research
 needs to be done.

As a final conclusion of this literature review, despite the extensive research done in recent years for radar-based healthcare applications, outstanding challenges still remain. Specifically for this thesis, to the best of the author's knowledge HAR and vital signs estimation have not jointly been explored into a single approach. Consequently, a joint exploration of both aspects is proposed as follows:

- Developing and verifying a processing pipeline to recognize and segment a test sequence of in-place and translational activities (e.g., sitting, standing, and walking) based on two data domains with distinctive sensitivity to certain types of movement (e.g., range-time and Doppler-time). For this, an experimental campaign with 20 participants was executed for data collection within an indoor environment.
- Evaluating the feasibility of estimating the breathing frequency when the subject is in a static position (e.g., sitting) at different distances (e.g., 1m and 2m) in LoS with the radar, and implementing an EKF for its simplicity and efficient implementation compared to other estimators such as the particle filter.
- Designing two different waveforms as a function of different FMCW radar parameters, range and Doppler resolutions, and maximum unambiguous range and Doppler to validate their performances for HAR and estimation of breathing frequency according to the proposed processing pipeline.

3

PIPELINE FOR ACTIVITY RECOGNITION AND BREATHING FREQUENCY ESTIMATION

The chapter presents the proposed pipeline for recognizing human activities and estimating the breathing frequency. In Section 3.1, the overview of the proposed pipeline is described, with an explanation of the methods implemented for activity recognition and segmentation, as well as the method for estimating and monitoring the breathing frequency in Sections 3.2 and 3.3, respectively.

3.1. PIPELINE OVERVIEW

The aim of the project is the joint recognition of human activities and the estimation of breathing frequency, with the proposed pipeline presented in Figure 3.1. In this joint pipeline, the differentiation between activities that involve motion and no motion of participants is first addressed by exploring the Range-Time and the Doppler-Time domains. After differentiation between translational and in-place activities, the pipeline for vital signs is triggered for the in-place activities where no motion is present, aiming to estimate the breathing frequency of the target under study in a contactless way through radar sensing.

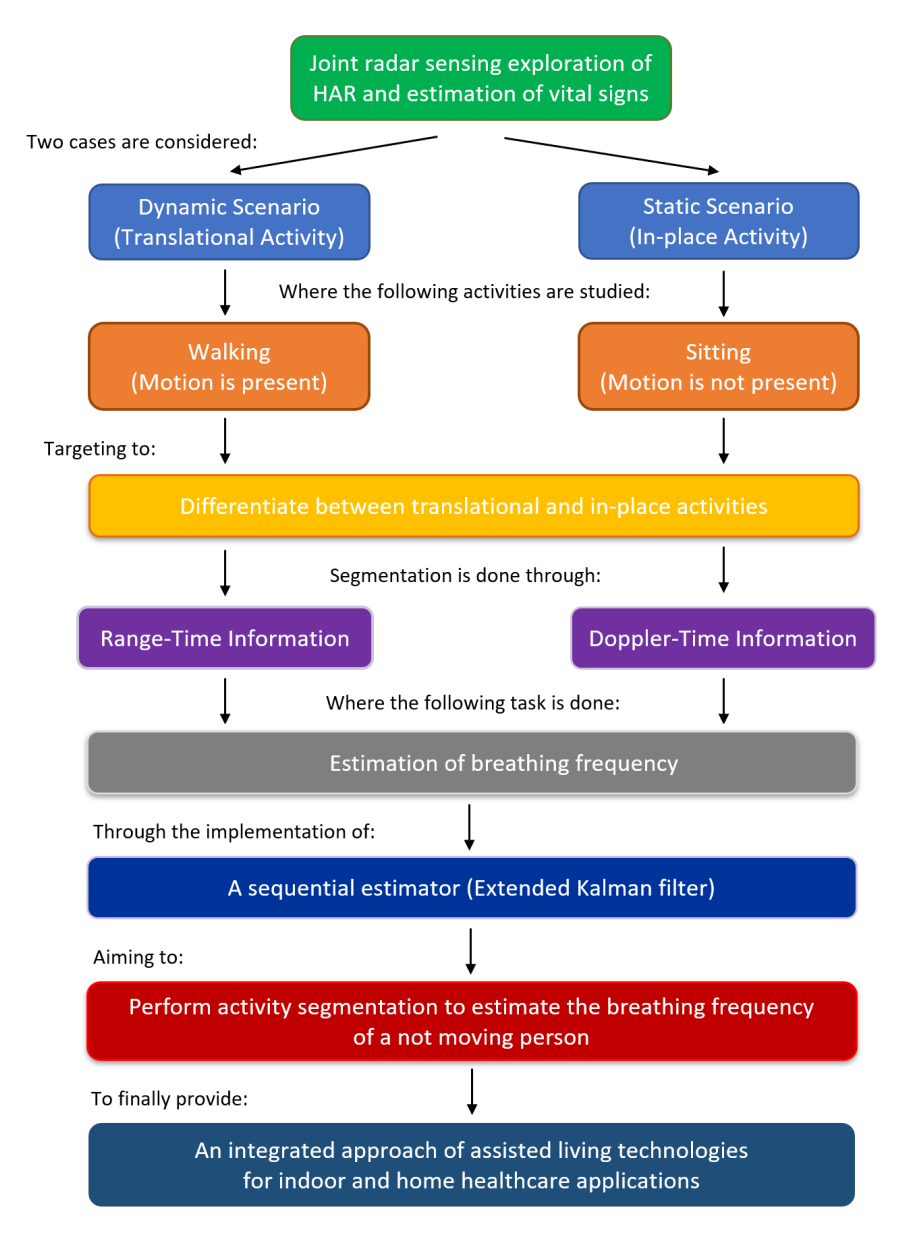


Figure 3.1: Overview of the proposed pipeline for joint HAR and vital signs

3.2. ACTIVITY RECOGNITION AND SEGMENTATION

Assuming an indoor environment where a single person is present and is in LoS with the radar, as shown in Figure 3.2. The reflected signal after impinging the person may potentially contain information related to the vital signs of the target under study, since

the detection of vital signs is based on the fact that the tiny physical movements of the human body can modulate the radar signals scattered after interacting with the body due to breathing and heart beating activities [71].

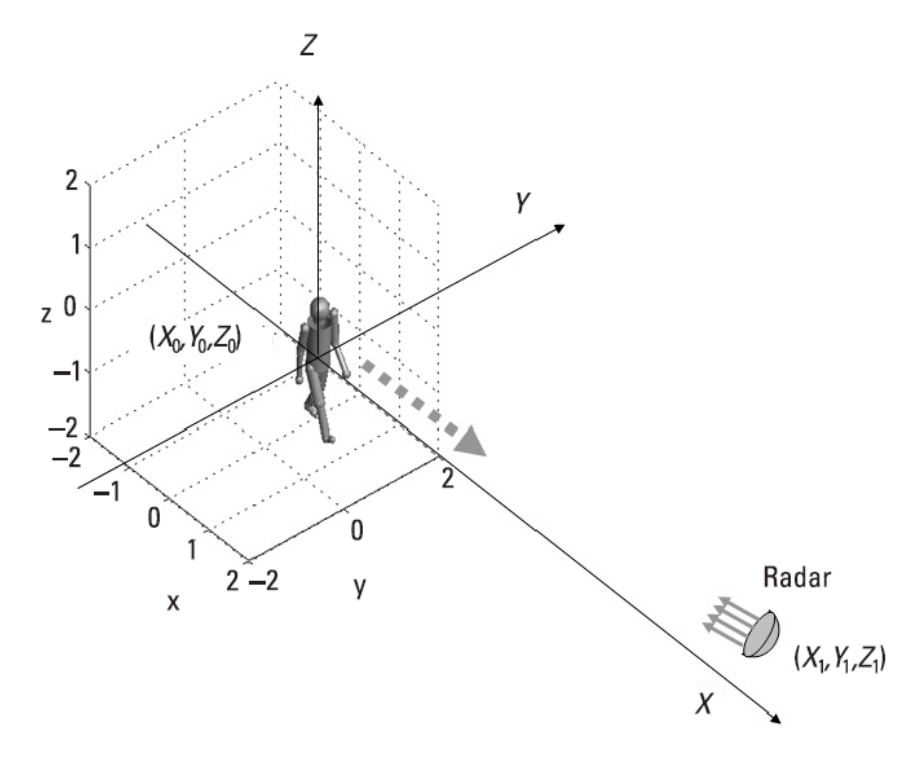


Figure 3.2: Geometry of a walking person in line of sight with the radar [71]

To be able to estimate the breathing frequency of the person within this environment, recognition and segmentation tasks are required to identify the activities where the target is under motion, aiming to isolate the cases where no motion is present to ensure that the signal received has, as a dominant component, the lungs volume change when the person is static and breathing and which encompasses information about vital signs.

For tasks related to HAR and segmentation, two different scenarios are studied, namely:

- *In-place*: Involving a static activity where the person under study has no motion and is static, such as sitting.
- *Translational:* Consisting of dynamic and static activities mixed in a sequence to involve the person's motion and no motion, such as walking and sitting.

More details regarding the test sequence and setup implemented for the experimental validation of the proposed joint pipeline are shared in Chapter 4.

Based on these two scenarios, segmentation between translational and in-place activities is done through two data domains:

- Range-Time: By taking the derivative of the subject position over time.
- *Doppler-Time*: Using the envelope of the spectrogram information.

To trigger the pipeline for breathing frequency estimation once these two activities are distinguished and an in-place activity is identified.

3.2.1. RANGE-TIME INFORMATION

As described in Chapter 2, the RTI matrix is exploited to locate the target' radial range with respect to the radar. Furthermore, a distinction between activities where a motion is present can be made by taking the derivative over the range-time information. An example of the RTI matrix obtained after processing the sequence where in-place and translational activities are jointly combined can be seen in Figure 3.3.

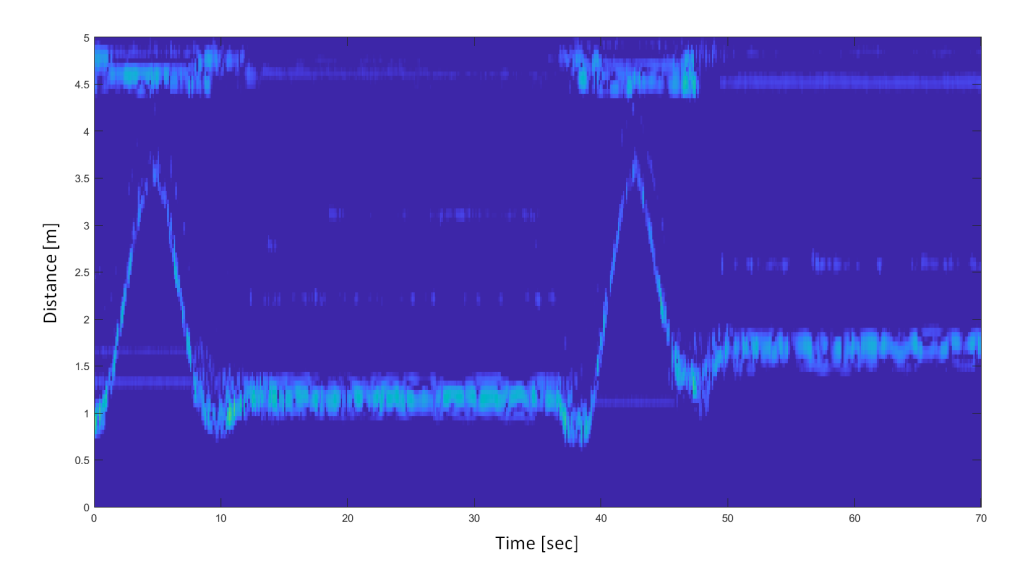


Figure 3.3: Range-Time matrix of the test sequence with walking back and forth and in-place activities

The segmentation procedure to identify translational and in-place activities is discussed in Chapter 5. Nonetheless, it is important to mention that this differentiation is done based on a profile similar to the one shown in Figure 3.4, after taking the derivative of the range history and normalizing the obtained data by dividing over the maximum.

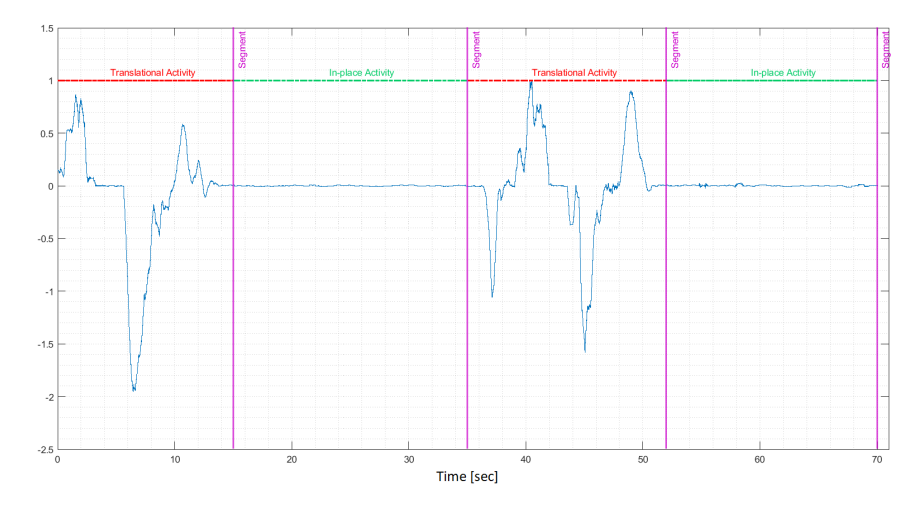


Figure 3.4: Normalized derivative of the Range-Time information of a mixed sequence of walking and in-place activities. This information can be used to segment the data to isolate translational vs in-place activities

3.2.2. DOPPLER-TIME INFORMATION

The individual human body components are tracked by using the mD-spectrogram, also known as micro-Doppler signature, which is a state-of-the-art method used to distinguish between different person's activities. Therefore, to estimate the radial velocity at which the body and limbs of the person move overtime on top of its bulk velocity, micro-Doppler signatures are explored. An example of the mD-spectrogram obtained after processing the test data is shown in Figure 3.5.

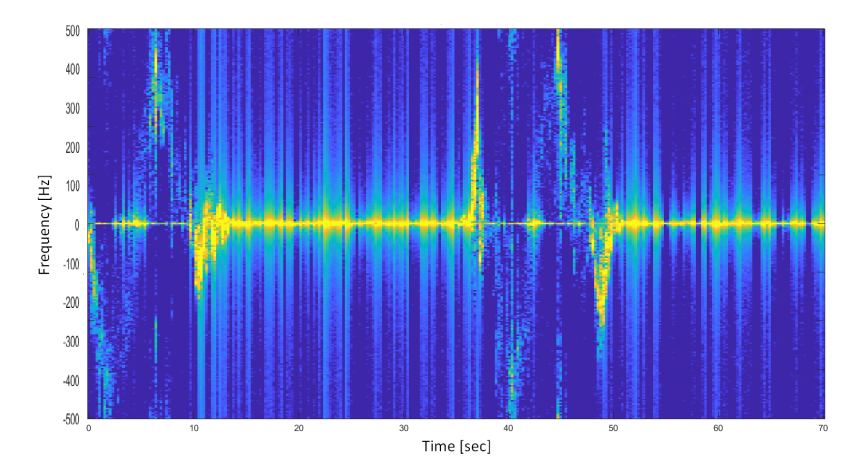


Figure 3.5: Spectrogram of the test sequence with walking back and forth and in-place activities

24

From the spectrogram information, it is proposed to perform segmentation based on the envelope of the obtained signature to differentiate translational and in-place activities through the use of the estimated shape.

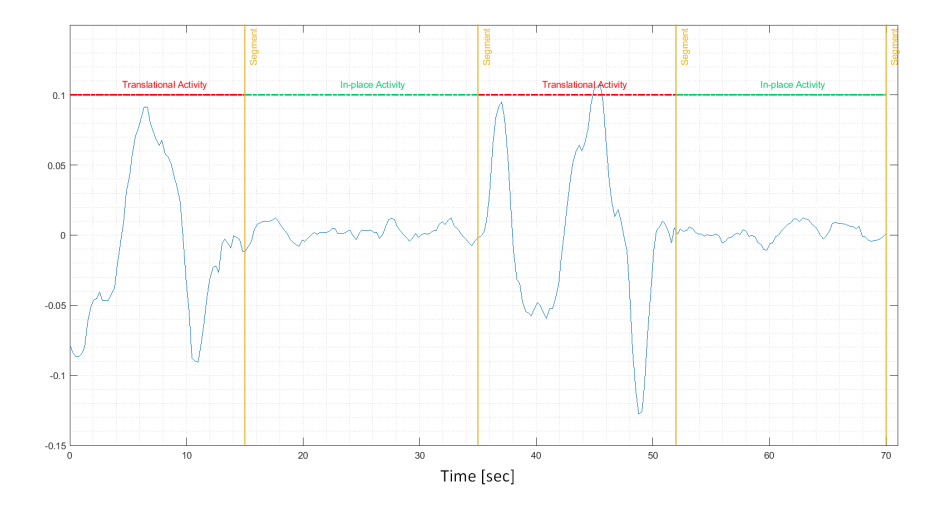


Figure 3.6: Normalized envelope of the spectrogram for the test sequence with walking back and forth and in-place activities

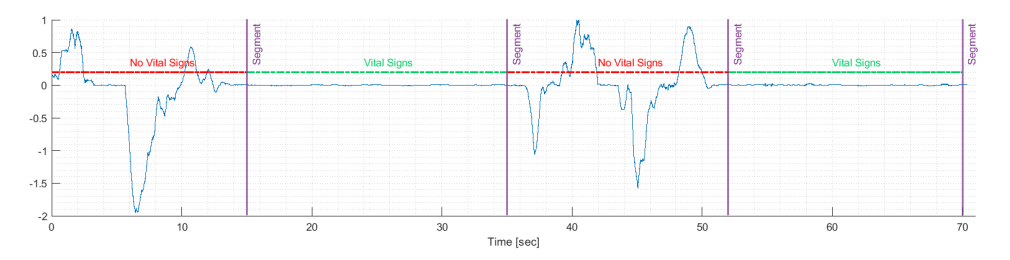
As it can be observed in Figure 3.6, the spectrogram information can exhibit a pattern when activities with motion and no motion are jointly studied. Consequently, the Doppler-Time data domain could be considered as a second data domain that might lead to successful activity differentiation and segmentation.

Further details regarding the segmentation procedure to identify translational and in-place activities based on the spectrogram information are addressed in Chapter 5.

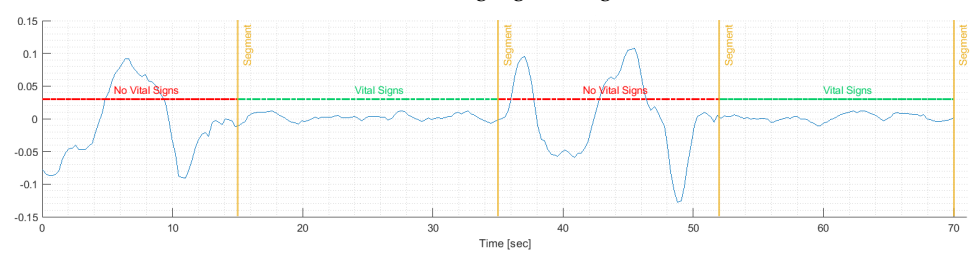
3.3. Breathing frequency

Once translational and in-place activities based on Range-Time and Doppler-Time information are segmented, the pipeline for the continuous estimation of breathing frequency is triggered as shown in Figure 3.7. Typically, the estimation of the breathing frequency has been addressed by frequency peak search in the Doppler power spectrum of the received signal, where a long observation time is usually needed. Therefore, an extended Kalman filter is proposed as studied [22] to continuously estimate the breathing frequency of the subject under study.

Before presenting further details regarding the extended Kalman filter for the estimation of breathing frequency, a brief introduction to the physiology of respiration activity is given in the upcoming subsection.



(a) Segments where the breathing frequency could potentially be estimated based on Range-Time information (highlighted in green)



(b) Segments where the breathing frequency could potentially be estimated based on Doppler-Time information (highlighted in green)

Figure 3.7: Identification of data segments to trigger the pipeline for breathing frequency estimation

3.3.1. PHYSIOLOGY OF RESPIRATION ACTIVITY

The lungs, located in the human thorax, are the main organs responsible for human breathing activity. A complete breathing cycling encompasses two main motions as shown in Figure 3.8:

- Inhalation
- Exhalation

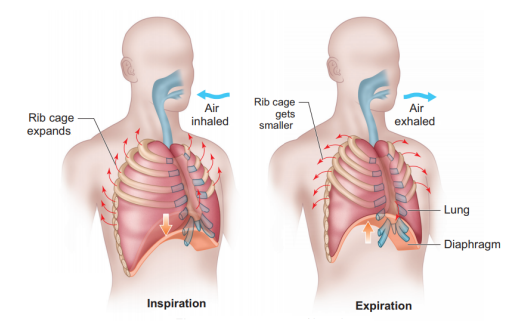


Figure 3.8: Physiological mechanism of breathing [72]

Lungs' expansion leads to inhalation and their volume expansion. On the other hand, lungs' contraction leads to exhalation and their volume contraction. These expansion and contraction motions and the related change in the lungs' volume can be observed in Figure 3.9.



Figure 3.9: Inhalation and exhalation motions [73]

For a healthy adult, the respiratory rate can typically consist of about 6 to 18 breaths per minute, a rate that can be translated into a breathing frequency between 0.1 to 0.3 Hz, while the displacement of prothorax induced by respiration activity ranges from 3 to 11 mm, according to [74]. Table 3.1 summarizes the information previously mentioned.

Table 3.1: Typical breathing frequencies and amplitudes of a healthy person due to breathing activity [74]

Vital Sign	Frequency	Amplitude	
Breathing Activity	0.1 - 0.3 Hz	3 - 11 mm	

Similar to Su et al. [22], the movement of the skin of prothorax due to breathing activity is modeled as a slowly time-varying sinusoidal displacement:

$$R_r(t) \approx \alpha_r \cdot \sin(2\pi f_r \cdot t + \phi_r)$$
 (3.1)

A displacement that leads to a phase shift on the reflected waves due to respiratory activity, and which might potentially be detected by the radar.

Therefore, and since the displacement induced by respiration activity is only several millimeters and no range cell migration is assumed, the phase history of the beat signal plays a key role in the estimation of the breathing frequency.

3.3.2. RADAR RESPONSE OF BREATHING FREQUENCY

Considering the sinusoidal model from Eq. 3.1 and the derivations done by Su et al. [22, 73], the position of the surface skin of prothorax at a distance R_0 can be expressed as:

$$R(n) = R_0 + R_r(n)$$

$$= R_0 + \alpha_r \cdot \sin(2\pi f_r \cdot n + \phi_r)$$
(3.2)

Assuming a constant amplitude for the beat frequency, the phase history $\phi_{ph}(n)$ over slow-time can be written as:

$$\phi_{ph}(n) = \frac{4\pi f_c}{c} \cdot R(n)$$

$$= \frac{4\pi f_c}{c} \cdot (R_0 + \alpha_r \cdot \sin(2\pi f_r \cdot n + \phi_r))$$
(3.3)

An extra phase ϕ_e due to the wrapped phase caused by R_0 is considered, and it can be expressed as:

$$\phi_e = wrap \left[\frac{4\pi f_c}{c} \cdot R_0 \right] \tag{3.4}$$

Therefore, the phase history becomes:

$$\phi_{ph}(n) = \phi_e + \frac{4\pi f_c}{c} (\alpha_r \cdot \sin(2\pi f_r \cdot n + \phi_r))$$
 (3.5)

And the range history over slow-time can be recovered from the phase history of the beat signal as:

$$R(n) = \frac{\phi_{ph}(n)c}{4\pi f_c} \tag{3.6}$$

Finally, considering only respiration activity and its sinusoidal model, the beat signal in the range cell, including R_0 over slow-time can be written as:

$$s(n) = h \exp(j\phi_e) \cdot \exp\left(j\frac{4\pi f_c}{c}(\alpha_r \cdot \sin(2\pi f_r \cdot n + \phi_r))\right) \tag{3.7}$$

Where h is the amplitude of the processed signal.

From this information, it is known that the respiration activity will change the volume of the chest cavity, resulting in the motion of the surface of the skin on the prothorax. Due to the amplitudes related to respiration activity being extremely small, as presented in Table 3.1, radar is considered to detect and monitor the relative motion of the chest rather than its exact position.

3.3.3. Extraction of phase and range history

As previously presented, information regarding respiration activity can be extracted from the motion of the prothorax's surface and the phase information contained in the beat signal.

Assuming that the beat signal is sampled in each chirp and stacked in rows, a raw data matrix D[m, n] can be built, with m being the number of samples per chirp over fast-time and n being the number of chirps over slow-time.

With a preserved coherence of the system, the exact phase history over slow-time can be recovered since the phase information is contained in the exponential term of the received beat signal. Additionally, phase unwrapping can be applied to extracting the phase history, from which the range history can be later computed based on Eq. 3.6.

The calculation of the range history can be divided into the following four steps:

- 1. Perform a FFT over each row of the D[m, n] matrix, resulting in the Range-Time profile matrix RT[r, n], with r being the number of range bins over fast-time.
- 2. Select the desired range bin, denoted as rb, within the target is found based on a peak power search. This signal can be expressed as $s[rb, n] = \operatorname{argmax}(RT[r, n])$.
- 3. Extract the corresponding phase of the signal s[rb, n] and unwrap it, obtaining the phase history $\phi[rb, n]$.
- 4. Estimate the range history based on Eq. 3.6.

The process of range history extraction is summarized below in Figure 3.10.

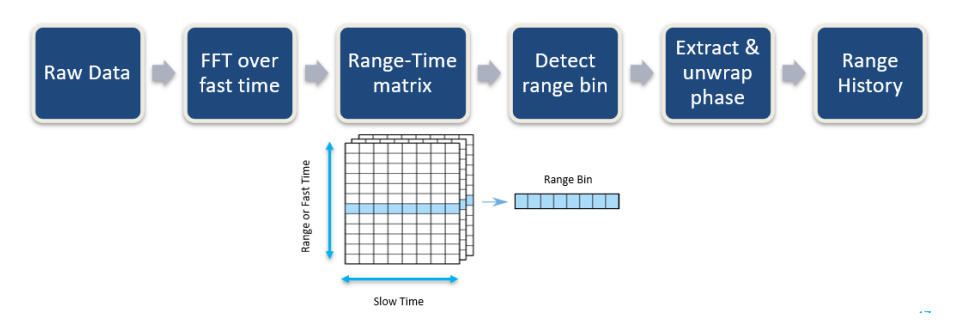


Figure 3.10: Range history derivation based on phase unwrapping approach

3.3.4. STATE AND OBSERVATION MODELS

The state and observation models for estimating the respiration activity parameters are derived in this section because both models are required before introducing the prediction and update steps of the EKF to estimate and monitor the desired parameters from one sweep to another.

A NCF model is adopted for chest movement estimation and tracking due to breathing activity. The choice of the NCF model is determined by its superior performance compared to other models when the frequency varies slowly, the case expected for a healthy person's respiration as proposed by Su et al. [22, 73], presenting the equation derivations from Su's research for the mathematical analysis in this thesis.

By analyzing the structure of the measured data, Eq. 3.8 is derived from Eq. 3.7 with a properly selected range bin, and the breathing model presented in Eq. 3.2:

$$y(n) = h \exp(j\phi_e) \cdot \exp\left(j\frac{4\pi f_c}{c} \cdot (\alpha_r \cdot \sin(2\pi f_r \cdot n + \phi_r))\right) + u \tag{3.8}$$

Where h is the amplitude of the signal, ϕ_e is the extra phase related to both range and scattering properties of the human body, and u is the assumed zero mean, complex white Gaussian noise denoted as:

$$u \sim \mathcal{CN}(0, \sigma_u^2) \tag{3.9}$$

From Eq. 3.8, the unwrapped phase history y_t can be expressed as:

$$y_t = C \cdot \alpha_t \sin(w_t t + \phi_t) + \theta_{av} + u_t \tag{3.10}$$

Where α_t , w_t and ϕ_t are the sinusoidal amplitude, frequency, and phase respectively. u_t is assumed to be additive white Gaussian noise with zero mean, and the constant factor C is given by:

$$C = \frac{4\pi f_c}{c} \tag{3.11}$$

An average phase, θ_{av} , is added to this unwrapped phase history, which is caused by the extra phase ϕ_e , the 2π wrapping effect of the phase history $\phi_{ph}(n)$ at a start point of time, and the reflection coefficient of the target under study.

Eq. 3.10 shows that the unwrapped phase history obtained from the beat signal phase has a sinusoidal shape, which corresponds to the sinusoidal breathing model from Eq. 3.2 with a constant phase scaling factor C.

Furthermore, instead of estimating the frequency w_t and the phase ϕ_t simultaneously, the angle θ_t is estimated:

$$\theta_t = w_t \cdot t + \phi_t \tag{3.12}$$

Applying Taylor series expansion to θ_t and its first derivate:

$$\dot{\theta_t} = \frac{\partial \theta_t}{\partial t} \tag{3.13}$$

The angle θ_t can be written as:

$$\theta_t \approx \theta(t - T_s) + T_s \dot{\theta}(t - T_s) + \frac{T_s^2}{2} \ddot{\theta}(t - T_s)$$

$$\dot{\theta}_t \approx \dot{\theta}(t - T_s) + T_s \ddot{\theta}(t - T_s)$$
(3.14)

Where T_s is the pulse repetition interval (PRI). Additionally, it is assumed that:

$$\begin{aligned} \dot{\theta}_t &= w_t \\ \ddot{\theta}_t &= \dot{w}_t \sim \mathcal{N}(0, \sigma_w^2) \end{aligned} \tag{3.15}$$

Where σ_w^2 is the variance of the frequency w_t . Similarly, the sinusoidal amplitude α_w is approximated as:

$$\alpha_t \approx \alpha(t - T_s) + T_s \, \dot{\alpha}(t - T_s)$$

$$\dot{\alpha}_t \sim \mathcal{N}(0, \sigma_\alpha^2)$$
(3.16)

Based on these assumptions, the four state variables to be estimated in terms of the phase history are: θ_t , w_t , α_t and θ_{av} .

Where a single vector including all these variables, namely the state vector for the NCF model, can be expressed as:

$$x_{t} = \begin{bmatrix} \theta_{t} \\ w_{t} \\ \alpha_{t} \\ \theta_{av,t} \end{bmatrix}$$

$$(3.17)$$

With Eq. 3.14, 3.15, and 3.16, the state dynamic model is:

$$\begin{bmatrix} \theta_t \\ w_t \\ \alpha_t \\ \theta_{av,t} \end{bmatrix} = \begin{bmatrix} 1 & T_s & 0 & 0 \\ 0 & 1 & 0 & 0 \\ 0 & 0 & 1 & 0 \\ 0 & 0 & 0 & 1 \end{bmatrix} \begin{bmatrix} \theta_{t-1} \\ w_{t-1} \\ \alpha_{t-1} \\ \theta_{av,t-1} \end{bmatrix} + \begin{bmatrix} \frac{T_s^2}{2} & 0 & 0 \\ T_s & 0 & 0 \\ 0 & T_s & 0 \\ 0 & 0 & 1 \end{bmatrix} v_t$$
(3.18)

Or written in a simplified form, this state model can be expressed as:

$$x_{t} = f_{m}(x_{t-1}) + B_{m}v_{t}$$

$$= F_{m}(x_{t-1}) + B_{m}v_{t}$$
(3.19)

Where:

- x_t is the state vector containing the current estimates.
- x_{t-1} is the state vector containing the previous estimates.
- f_m is called the evolution/prediction function.
- F_m is called the prediction matrix.
- B_m is called the control matrix.
- v_t is the vector containing the driving noises:

$$v_{t} = \begin{bmatrix} v_{w,t} \\ v_{\alpha,t} \\ v_{\theta_{av},t} \end{bmatrix}$$
(3.20)

With a constant F_m over time, the evolution function f_m of the state vector x_t is linear with the NCF model, an assumption of high importance for the derivation of the EKF.

The covariance matrix of their driving noises can be expressed as:

$$Q = \mathbb{E}[v_t v_t^T] = \begin{bmatrix} \sigma_w^2 & 0 & 0 \\ 0 & \sigma_\alpha^2 & 0 \\ 0 & 0 & \sigma_{\theta_{av}}^2 \end{bmatrix}$$
(3.21)

Due to the amplitude and frequency being assumed as independent variables. Hence, both amplitude and frequency values are uncorrelated.

Finally, the observation model describing the acquired measurements can be expressed in a similar way as:

$$y(t) = g_m(x_t) + u_t = C \cdot x_{3,t} \sin(x_{1,t}) + x_{4,t} + u_t$$
 (3.22)

Where:

- y_t is the measurement vector containing the acquired data.
- x_t is the state vector containing the current estimates.
- g_m is the observation function.
- u_t is the measurement/observation Gaussian noise.

The covariance matrix of the observation noise u_t is:

$$R = \mathbb{E}[u_t u_t^T] = [\sigma_u^2] \tag{3.23}$$

Nevertheless, the observation function g_m is a nonlinear function. The linearization of the observation function can be approximated by taking the first order of its Taylor expansion. Therefore, the corresponding Jacobian matrix is given then by:

$$G_{m,t} = \frac{\partial g_m(x)}{\partial x}|_{x = \hat{x}_{t|t-1}} = \left[C \cdot \hat{x}_{3,t|t-1} cos(\hat{x}_{1,t|t-1}) \ 0 \ C \cdot sin(\hat{x}_{1,t|t-1}) \ \hat{x}_{4,t|t-1} \right]$$
(3.24)

3.3.5. EXTENDED KALMAN FILTER

As mentioned in Chapter 2, the main assumptions behind the derivation of the Kalman filter are that the estimation problem to be solved is linear and Gaussian. Under these conditions, the Kalman filter is an optimal estimator that computes the mean and covariance of the true posterior density.

As the motion of respiration activity is nonlinear, an approximate solution is to linearize the prediction function f_m from the prediction step and/or the observation function g_m from the update step of the Kalman filter.

The linearization of these functions and their corresponding effect on vital signs' estimation parameters was studied by G. Su et al. [22, 73], evaluating the feasibility of

implementing an estimator based on these approximations to monitor and track vital signs' parameters.

The subsequent application of this sequential estimator for a linearized respiration activity case, referred to in the literature as EKF, to estimate the breathing frequency from the state vector from Eq. 3.17, based on the state and observations models derived in the previous subsection is summarized in Figure 3.11.

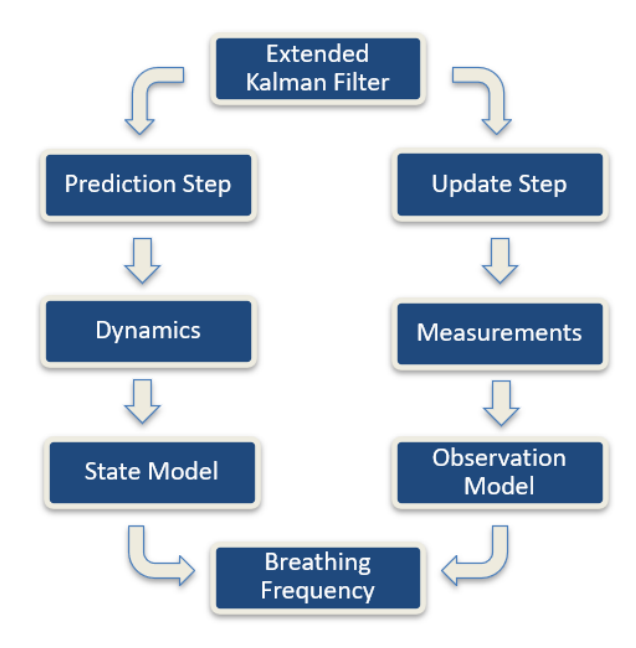


Figure 3.11: Flow diagram of the implemented extended Kalman Filter

And the EKF implemented in the domain of nonlinear functions for the estimation of breathing parameters, based on the state model derived in Eq. 3.19 and the observation model from Eq. 3.22, is given by:

State Prediction: $\hat{x}_{t|t-1} = f_m(\hat{x}_{t-1|t-1})$ Covariance Prediction: $P_{t|t-1} = F_{m,t} P_{t-1|t-1} F_{m,t}^T + B_m Q B_m^T$ Kalman Gain: $K_t = P_{t|t-1} G_{m,t}^T (G_{m,t} P_{t|t-1} G_{m,t}^T + R)^{-1}$

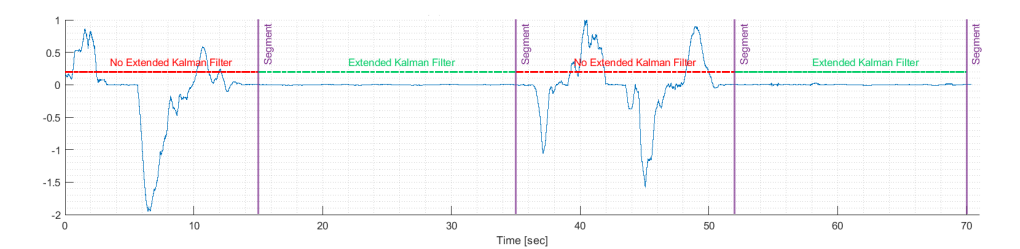
Update Estimation: $\hat{x}_{t|t} = \hat{x}_{t|t-1} + K_t(y_t - g_m(\hat{x}_{t|t-1}))$

Update Covariance: $P_{t|t} = (I - K_t G_{m,t}) P_{t|t-1}$

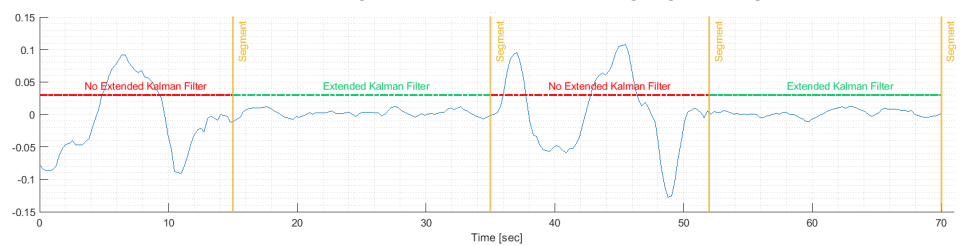
Where the state variables in the state vector from Eq. 3.17 are predicted and updated every time an iteration is performed, having the breathing frequency as the main output estimation.

3.4. Summary 33

Finally, the pipeline for continuous estimation of breathing frequency based on the derived extended Kalman filter is triggered once translational and in-place activities are segmented through the exploration of the information from Range-Time and Doppler-Time data domains, as it can be observed in Figure 3.12.



(a) Segments where the breathing frequency could potentially be estimated based on the derivative of the range information over time highlighted in green)



(b) Segments where the the breathing frequency could potentially be estimated based on the envelope of the spectrogram (highlighted in green)

Figure 3.12: Segments for breathing frequency estimation based on the implemented extended Kalman filter

3.4. SUMMARY

This chapter introduces the pipeline for the joint exploration of HAR and breathing frequency estimation tasks. Moreover, both pipelines are discussed separately after presenting the proposed joint approach, pointing out the following important information:

- For HAR: The two types of activities to be studied are: *translational* (e.g., walking and standing) and *in-place* (e.g., sitting).
- For vitals: The breathing frequency is the estimated variable for vital signs monitoring.

Through Range-Time and Doppler-Time information, the differentiation between translational and in-place activities is addressed, aiming to successfully identify them

and locate the segments where the test subject is stationary. Then, the pipeline is triggered for the estimation of the breathing frequency.

The physiology of human respiration activity was briefly illustrated, describing the radar response in a HAR context. Consequently, for a not moving target a sequential estimator is triggered. Prior is known as the extended Kalman Filter, to estimate and monitor the breathing frequency based on phase unwrapping and range history estimation.

4

MEASUREMENT SETUP AND DATA ACQUISITION

This chapter describes the procedure followed in the experimental campaign performed for the data acquisition, and the information to be used in the next Chapter for the experimental validation of the proposed joint pipeline. In Section 4.1, the radar parameters and the designed waveforms to address activity recognition and segmentation, as well as the estimation of breathing frequency, are introduced. Procedures for data collection and sequences to be studied are mentioned in Section 4.2, while the measurement setup implemented for data acquisition is illustrated in Section 4.3.

4.1. RADAR PARAMETERS

To perform the data collection campaign, the FMCW radar utilized in this project was the Texas Instruments IWR6843, shown in Figure 4.1, operating at a carrier frequency of 60 GHz in the millimeter wave range.

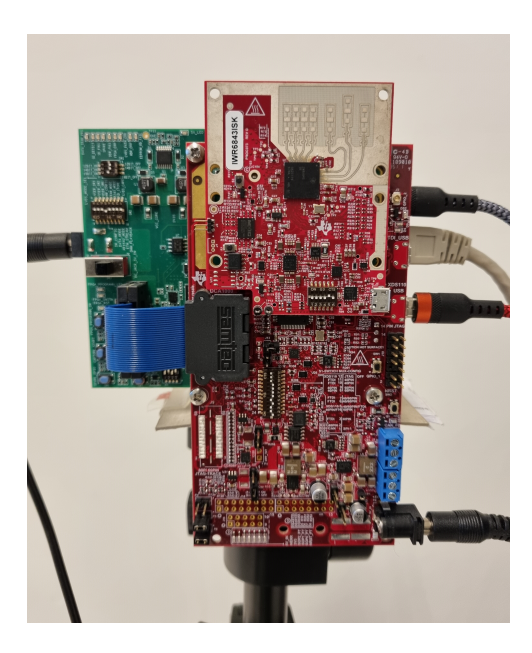


Figure 4.1: Texas Instruments radar IWR6843 used in this thesis

As previously mentioned in Chapter 3 and observed in Table 3.1, the amplitude of the signal related to the respiration activity has a small magnitude. Therefore, the relative motion of the chest is monitored rather than its exact position over time, meaning that a minimum Doppler resolution is required to capture the maximal velocity of the weakest respiration activity. The estimation of this Doppler resolution is described in the following subsection.

4.1.1. Doppler resolution for Breathing Frequency estimation

Recalling Eq. 3.1, the movement of the skin of prothorax due to breathing activity is modeled as a slowly time-varying sinusoidal displacement, given by the expression:

$$R_r(t) \approx \alpha_r \cdot \sin(2\pi f_r \cdot t + \phi_r)$$
 (4.1)

Therefore, the maximal velocity of the weakest respiration activity corresponds to:

$$v_{r,min} = max \left(\frac{dR_r(t)}{dt} \right) \tag{4.2}$$

By taking the derivative over time and applying chain's rule, Eq. 4.2 becomes:

$$v_{r,min} = max \left(\alpha_{r,min} \cdot 2\pi f_{r,min} \cdot cos(2\pi f_{r,min} \cdot t + \phi_r) \right)$$
(4.3)

As the maximum of a cosine function is equal to 1, and $\alpha_{r,min}$ and $f_{r,min}$ are time independent variables, this expression can be simplified to:

$$v_{r,min} = \alpha_{r,min} \cdot 2\pi f_{r,min} \tag{4.4}$$

Substituting $\alpha_{r,min} = 0.003$ m and $f_{r,min} = 0.1$ Hz from Table 3.1 into Eq. 4.4, the maximal velocity calculated for the weakest respiration activity is around 0.0019 m/s. Consequently, in order to measure this maximum velocity, a Doppler resolution $\Delta v_{r,min}$ of at least 0.0019 m/s is required to be able to track the weakest respiration activity of a healthy person. Moreover, the minimum frame duration to ensure a coherent processing interval, T_{CPI} , is given by:

$$T_{CPI} = \frac{\lambda}{2 \cdot \Delta \nu_{r,min}} \tag{4.5}$$

This must be at least 1.31 seconds with an FMCW radar operating at a carrier frequency of 60 GHz. Additionally, as the minimum breathing frequency of a healthy person is around 0.1 Hz, an observation time higher than 10 times the T_{CPI} is proposed to ensure that at least half of the period of the weakest respiration frequency can be captured by the radar.

4.1.2. DESIGNED WAVEFORMS

Based on the requirements for Doppler resolution and the minimum duration of the coherent processing interval, two different waveforms were designed to test their capabilities and overall performance on a test sequence where HAR and estimation of breathing frequency are jointly explored. Figure 4.2 depicts a single chirp and the main associated parameters for the waveforms design employing the TI IWR6843 radar.

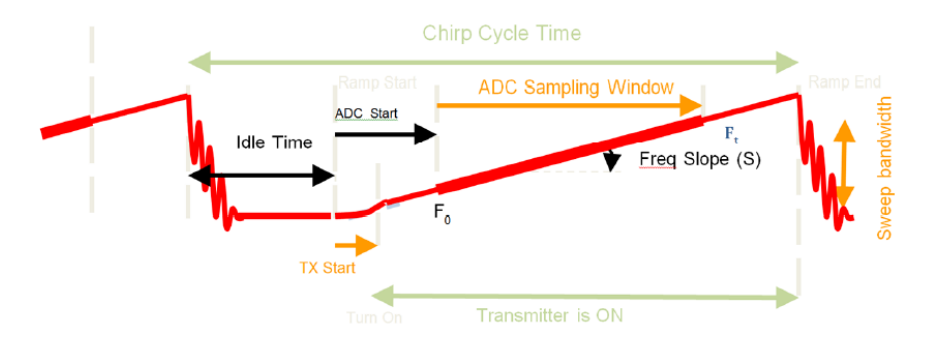


Figure 4.2: Single chirp and related parameters from TI IWR6843 radar [75]

As chirps are usually sent as a set or burst rather than individually, structures similar to the one shown in Figure 4.3 will be considered. These are referred to as 'frames'.

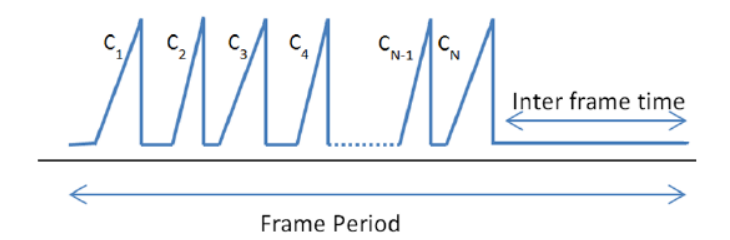


Figure 4.3: Single frame structure from TI IWR6843 radar [75]

The velocity resolution is expressed as:

$$\Delta \nu = \frac{\lambda}{2 \cdot T_{frame}} \tag{4.6}$$

With $\lambda = c/f_c$ and T_{frame} approximated as:

$$T_{frame} = N_{chirp} \cdot T_{chirp} \tag{4.7}$$

Where N_{chirp} is the number of chirps sent in a single frame with a certain T_{chirp} time duration.

The duration of a single chirp is given by:

$$T_{chirp} = T_{idle} + T_{ramp} (4.8)$$

From Figure 4.2, T_{ramp} is the effective time the transmitter is ON while sending a single chirp, and it can be defined as the chirp cycle time minus the idle time. The range resolution and maximum unambiguous range for both designed waveforms are set to be the same, 5cm and 6.4m, respectively, according to Table 4.1, focusing on the velocity resolution to monitor the relative motion of the chest rather than its exact position for the estimation of vital signs, and the maximum unambiguous velocity of the person towards the radar for activity recognition and segmentation.

The range resolution is calculated as:

$$\Delta R = \frac{c}{2 \cdot B} \tag{4.9}$$

With B being the bandwidth, which is given by:

$$B = S \cdot T_{ramp} \tag{4.10}$$

Where *S* refers to the frequency slope from Figure 4.2. As it can deduced from Eq. 4.9 and Eq. 4.10, T_{ramp} plays a key role in the definition of the range resolution ΔR , as these two quantities are inversely proportional, meaning that any increase of T_{ramp} will lead automatically to a finer ΔR .

However, as the maximum unambiguous range is determined by:

$$R_{max} = N_{ADC} \cdot \Delta R \tag{4.11}$$

Where N_{ADC} is the number of ADC range samples per chirp; any increase of T_{ramp} will also lead to a decrease in the R_{max} . Moreover, as the maximum unambiguous velocity can be estimated as:

$$V_{max} = \frac{\lambda}{4 \cdot T_{chirp}} \tag{4.12}$$

 T_{ramp} plays an important role as well in the definition of the V_{max} .

Essentially, the number of chirps N_{chirp} and the idle time T_{idle} could potentially have a major impact based on Eq. 4.6, 4.8 and 4.12 for both the maximum unambiguous velocity V_{max} and the velocity resolution Δv .

Summarizing, as shown in Table 4.1 and as stated at the beginning of this Chapter, two waveforms were designed:

Waveform 1: Developed to have a sufficient maximum unambiguous velocity to
differentiate between translational and in-place activities, sacrificing the velocity
resolution needed for vital signs. This might result in a side effect while capturing
the relative motion of the chest surface for breathing frequency estimation.

This waveform will be referred to as *W1: HAR + Vital Signs* for future reference.

Waveform 2: Built to focus on having a proper velocity resolution to capture the
weakest/smallest respiration activity of the test subject, which might compromise
the satisfactory differentiation between translational and in-place activities due to
resulting potential Doppler ambiguity.

This waveform will be referred to as W2: Vital Signs for future reference.

The overall performance of the two waveforms under the test conditions proposed in the following subsection is fully described in Chapter 5.

Based on Table 4.1, it is important to point out the following:

- Due to the operational conditions of the TI IWR6843 radar, the maximum achievable bandwidth is 4000 MHz, 255 chirps per frame, and a maximum frame duration of 1.342 seconds.
- As the key parameter to monitor the breathing frequency is the velocity resolution, for *W2: Vital Signs* the total chirp duration is designed to make it as long as possible, to achieve the required velocity resolution derived in Subsection 4.1.1.
- However, as the ramp time is directly proportional to the bandwidth, idle time is the key parameter to adapt to accomplish the required resolution.
- Furthermore, as the maximum unambiguous velocity is inversely proportional to the chirp duration, *W1: HAR + Vital Signs* is designed to have at least 1 m/s as maximum unambiguous velocity, an assumption made based on the test conditions developed for this experiment and the average velocity of a person walking.
- As mentioned, it is not necessary to know the chest's exact position to estimate breathing frequency. Therefore, a range resolution of 5 cm with a maximum unambiguous range of 6.4 m is set to both waveforms, sufficient to track the person in the proposed indoor environment to be described in the upcoming subsections.

Parameters	W1: HAR + Vital Signs	W2: Vital Signs
Carrier Frequency [GHz]	60	60
Frequency Slope [MHz/us]	30	30
Number of ADC samples per chip	128	128
Ramp Time [us]	100	100
Idle Time [us]	900	5160
Chip Duration [us]	1000	5260
Number of chirps per frame	255	255
Frame Duration [s]	0.255	1.341
Bandwidth [MHz]	3000	3000
Range Resolution [cm]	5	5
Max. Unamb. Range [m]	6.4	6.4
Velocity Resolution [m/s]	0.0098	0.0019
Max. Unamb. Velocity [m/s]	1.25	0.2376

Table 4.1: Summary of the key parameters of the two designed waveforms

4.2. DATA COLLECTION CAMPAIGN

To test the proposed joint pipeline for HAR and estimation of breathing frequency, two different scenarios are studied with both waveforms derived in the previous subsection. The two proposed scenarios are:

- *In-place scenario:* With the test subject sitting at 1m and 2m in LoS with respect to the radar as an isolate motion, aiming to test the capabilities of both waveforms for the estimation of breathing frequency at different distances.
- Translational scenario: With the test subject walking and sitting in LoS with respect to the radar, performing a sequence where motions are jointly combined, aiming to test the capabilities of both waveforms for the estimation of breathing frequency at different distances and the correct recognition and segmentation of the activities based on Range-Time and Doppler-Time information.

Consequently, 6 different tests were performed, whose description is provided below and its sequence is summarized in Table 4.2.

Waveform	In-place at 1m	In-place at 2m	Translational
W1: HAR + Vital Signs	Test 1	Test 2	Test 5
W2: Vital Signs	Test 3	Test 4	Test 6

• Test 1:

Scenario: In-place

Activity: Sitting

Waveform: W1 - HAR + Vital Signs

- Test duration: 30 sec

- Sequence: Sitting at approx. at 1m

• Test 2:

Scenario: In-placeActivity: Sitting

Waveform: W1 - HAR + Vital Signs

- Test duration: 30 sec

- Sequence: Sitting at approx. at 2m

• Test 3:

Scenario: In-placeActivity: Sitting

- Waveform: W2 - Vital Signs

- Test duration: 30 sec

Sequence: Sitting at approx. at 1m

• Test 4:

Scenario: In-placeActivity: Sitting

- Waveform: W2 - Vital Signs

- Test duration: 30 sec

Sequence: Sitting at approx. at 2m

• Test 5:

- Scenario: Translational

- *Activity:* Walking + Sitting

- Waveform: W1 - HAR + Vital Signs

- Test duration: 70 sec

Sequence: Walking back and forth until 4.5m and sitting at 1m facing the radar in 15 sec + Breathing for 20 sec + Walking back and forth until 4.5m and sitting at 2m facing the radar in 15 sec + Breathing for 20 sec

Test 6:

- Scenario: Translational

Activity: Walking + Sitting

- Waveform: W2 - Vital Signs

- Test duration: 70 sec

 Sequence: Walking back and forth until 5m and sitting at 1m facing the radar in 15 sec + Breathing for 20 sec + Walking back and forth until 5m and sitting at 2m facing the radar in 15 sec + Breathing for 20 sec

Additionally, in the data collection campaign implemented, data from 20 different test subjects were acquired, with 7 females and 13 males between 23 and 37 years old repeating each test 3 times, summing up a total of 18 tests per subject. Appendix 6.2 shows in Table 6.9 the gender, age, height, weight, body mass index (BMI), and clothes worn by each of the volunteers during the data acquisition process.

4.3. MEASUREMENT SETUP

A measurement setup in the indoor environment shown in Figure 4.4 was implemented to execute the data collection campaign. Here, as stated previously, test subjects were requested to perform the tests from Table 4.2.

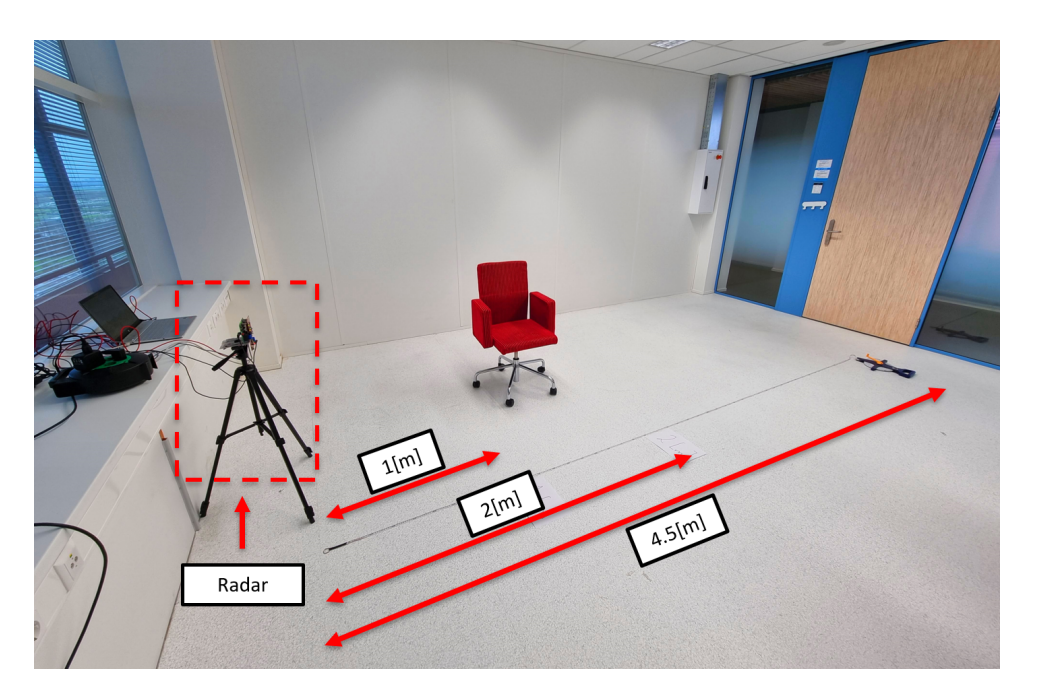


Figure 4.4: Indoor environment for data collection

Furthermore, a respiration belt of the model shown in Figure 4.5 was utilized to measure the true breathing frequency of the person, to be assessed against the estimated values from the EKF.



Figure 4.5: Respiration belt used for ground-truth [76]

Part of the in-place and translational sequences completed by each participant in the described measurement setup can be observed in Figures 4.6 and 4.7, respectively.

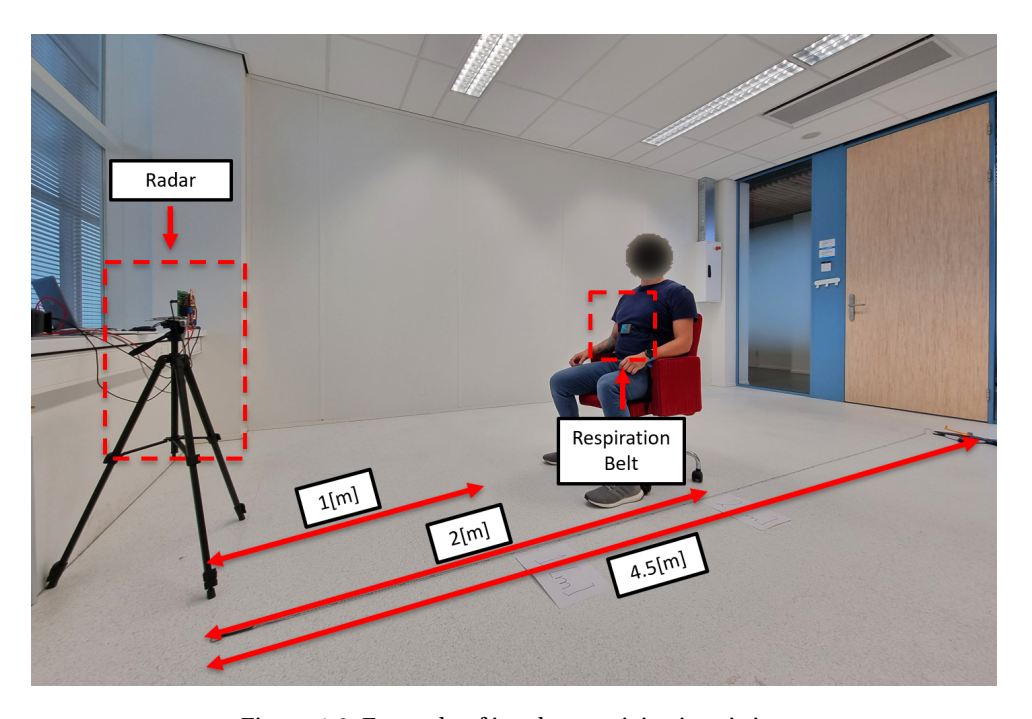


Figure 4.6: Example of in-place activity, i.e. sitting

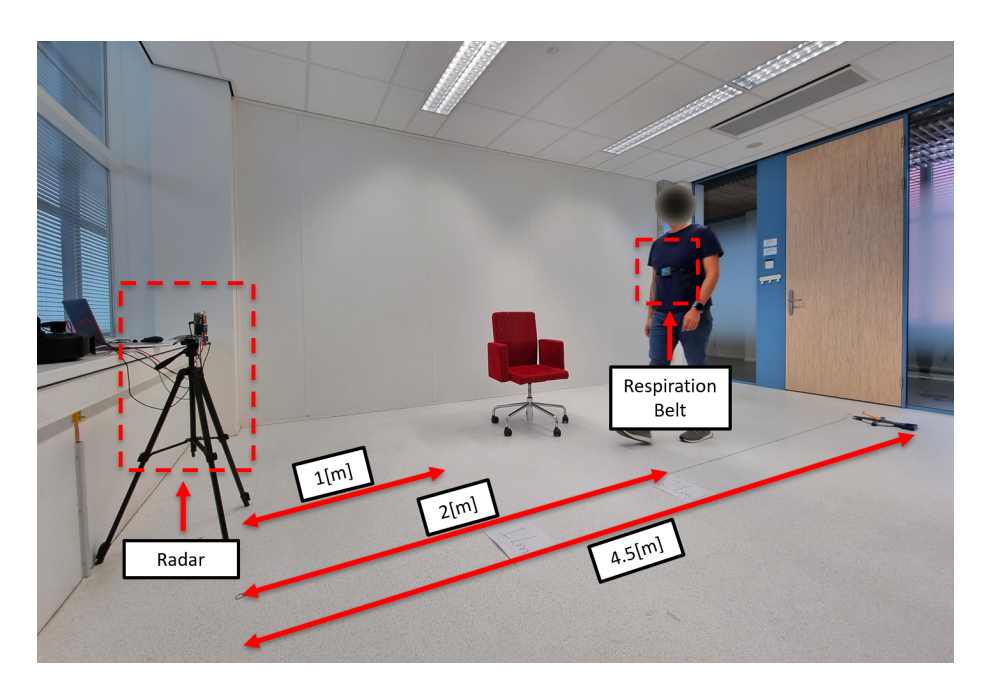


Figure 4.7: Example of translational sequence, i.e. subject walking towards the radar

4.4. SUMMARY

This chapter fully illustrates the setup and measurement campaign developed for the experimental validation of the proposed joint pipeline for HAR and breathing frequency estimation. The importance of different radar parameters, especially the Doppler resolution, for estimating breathing frequency is introduced, deriving two different waveforms to evaluate their performance for activity segmentation and monitoring vital signs. For the data collection campaign, the two sequences of activity performed by each test subject are explained, pointing out the test conditions and the goals behind exploring both scenarios:

- For the in-place scenario: The goal is to test the capabilities of the designed waveforms to estimate the breathing frequency at different distances based on the output from the EKF, requesting the test subjects to sit at 1m and 2m in LoS with respect to the radar to isolate any likely motion or random body movement.
- For the translational scenario: Similar to the previous case, the goal is to test the capabilities of both waveforms for the estimation of breathing frequency at different distances and the correct identification and segmentation of translational and inplace activities based on Range-Time and Doppler-Time information, asking the participants to walk and sit in LoS with respect to the radar executing a sequence where motion and no motion are jointly combined.

For ground truth, a respiration belt is worn and used to estimate the breathing frequency of each participant. Moreover, sequences are timed to know the exact points where each test subject switches between translational and in-place activities.

DATA ANALYSIS AND EXPERIMENTAL VALIDATION

The experimental validation of the proposed joint pipeline for HAR and breathing frequency estimation is described in this Chapter, based on the experimental campaign conducted in Chapter 4. Section 5.1 examines the estimation of breathing frequency for an in-place scenario. In addition, the case with translational and in-place activities jointly combined in a test sequence is presented in Section 5.2, deriving activity segmentation, and the feasibility of estimating breathing frequency through Range-Time and Doppler-Time data domains.

5.1. IN-PLACE SCENARIO

For the in-place scenario, as shown in Figure 3.10, the first step before estimating the breathing frequency of the test target is to obtain the chest surface's range history based on phase unwrapping from the range bin within the target is found after a peak power search.

The estimated range history is utilized during the update step to refine the estimate of the state variables with the available radar measurements. Therefore, as expected, data quality significantly impacts the overall performance of the employed extended Kalman filter and the correct estimation of the target's breathing frequency.

Once the range history is calculated, the extended Kalman filter is initialized to have as its primary output the breathing frequency of the test subject, continuously running the prediction and update steps of this sequential estimator as illustrated in Figure 3.11.

Based on experimental validation and the suggested initialization values from [22], the state vector and the covariance matrix of the extended Kalman filter are initialized

as specified in Table 5.1, with $f_b = 0.3Hz$ and $\alpha = 11mm$ being the upper limits of the breathing frequency and amplitude of a healthy person's respiration activity according to Table 3.1, values utilized in all the tests analyzed in this study.

Table 5.1: Initialization values of the extended Kalman filter

	θ_t	w_t	α_t	$\theta_{av,t}$
State Vector	2π	$2\pi f_b$	α	0
Covariance Matrix	$\pi^2 \cdot 1e4$	$(2\pi f_b)^2 \cdot 1e4$	$0.003^2 \cdot 1e4$	$0.008^2 \cdot 1e4$

Moreover, the error between the true and the estimated breathing frequency to quantify the difference between them is calculated as:

$$Error[\%] = \frac{|a-b|}{a} \cdot 100 \tag{5.1}$$

Where:

- a is the true breathing frequency from the respiration belt in Hz.
- b is the estimated breathing frequency from the extended Kalman filter in Hz.

Defining a successful convergence once the deviation of the estimated breathing frequency is between +/- the current estimation, and the error between the ground truth and output estimation is lower than 10 %.

For this static scenario, the test target remains in sitting position at 1m and 2m in LoS with the radar. The results obtained with both designed waveforms, *W1: HAR + Vital Signs* and *W2: Vital Signs*, at 1m and 2m are discussed in subsections 5.1.1 and 5.1.2, respectively, with respiration rate monitoring considered as vital signs.

5.1.1. Breathing frequency estimation at 1m

As the first experimental validation, the target's breathing frequency estimation is studied for the in-place scenario at a test distance of 1m, where no activity segmentation tasks are required.

Hence, the corresponding range histories is obtained with both waveforms (e.g., *W1: HAR + Vital Signs* and *W2: Vital Signs*) at 1m for the same test subject can be observed in Figures 5.1 and 5.3, with the first figure being the case for the waveform *W1: HAR + Vital Signs*, and the second figure showing the case for the waveform *W2: Vital Signs*.

As waveform *W1: HAR + Vital Signs* is designed to have a sufficient maximum unambiguous velocity to differentiate between translational and in-place activities, it presents the disadvantage of a poor velocity resolution which does not allow capturing the relative motion of the chest surface for breathing frequency estimation independently of the distance, due to the same behavior was observed at the test distance of 2m.

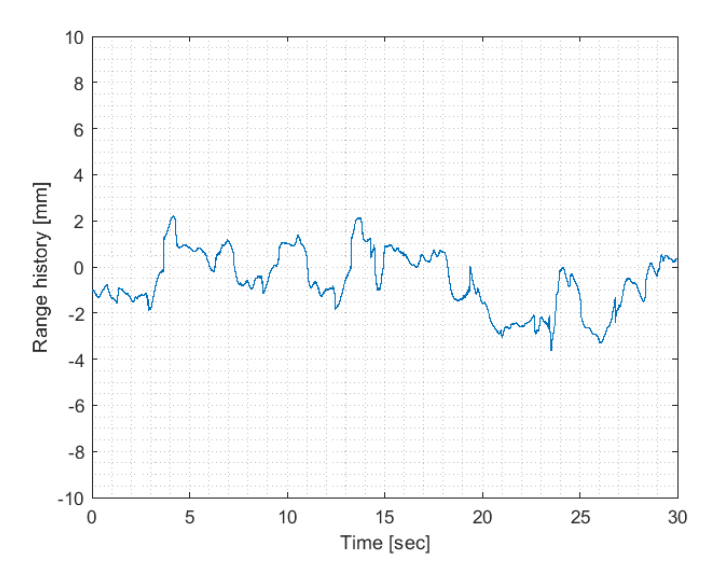


Figure 5.1: Range history with waveform W1: HAR + Vital Signs at 1m shows the target's range displacement

Consequently, the data collected leads the extended Kalman filter to converge to an incorrect breathing frequency, as shown below in Figure 5.2.

This behavior is expected as the measured data does not provide quality information about the target's range history during the update step, where the radar data is used to refine the estimate with the available measurements.

A potential solution, as shared in Chapter 4, is to employ chirps with longer durations to improve the velocity resolution. More specifically, the idle time could be increased to maintain the bandwidth specified in Table 4.1 since an increment in the ramp time would directly impact the bandwidth and decrease the maximum unambiguous range. However, increasing the chirp idle time reduces the maximum unambiguous velocity, one of the main constraints of waveform *W2: Vital Signs*.

Nevertheless, waveform *W2: Vital Signs* is parameterized to have the minimum required velocity resolution to capture the test subject's smallest respiration displacement and shows its capabilities for this first case of study at 1m. The obtained range history for the same test subject using waveform *W2: Vital Signs* can be seen in Figure 5.3, and the output estimation from the extended Kalman filter is displayed in Figure 5.4.

Additionally, Figure 5.5 shows the results obtained for the 20 participants and the 3 tests performed by each subject, with the corresponding data of Tables 6.1 and 6.2 (Appendix 6.2).

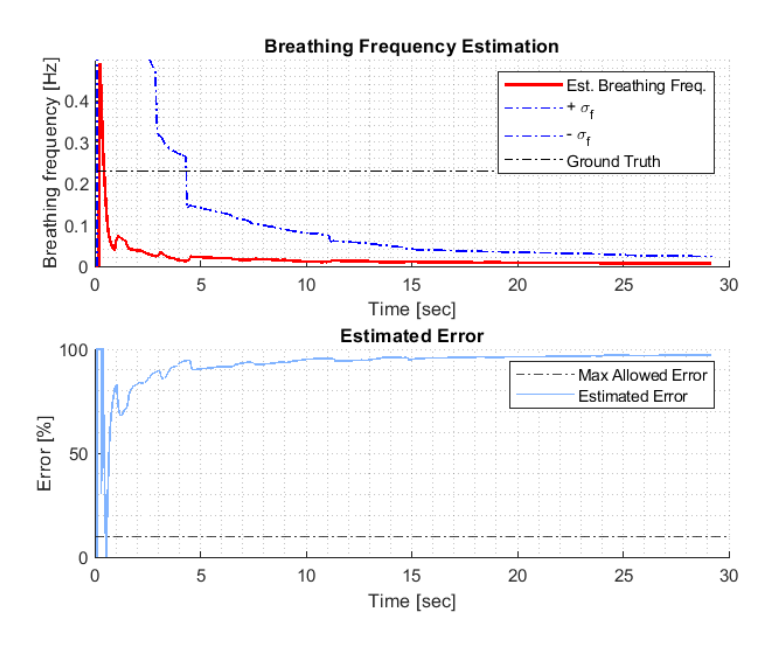


Figure 5.2: Estimated breathing frequency with waveform W1: HAR + Vital Signs for a participant at 1m

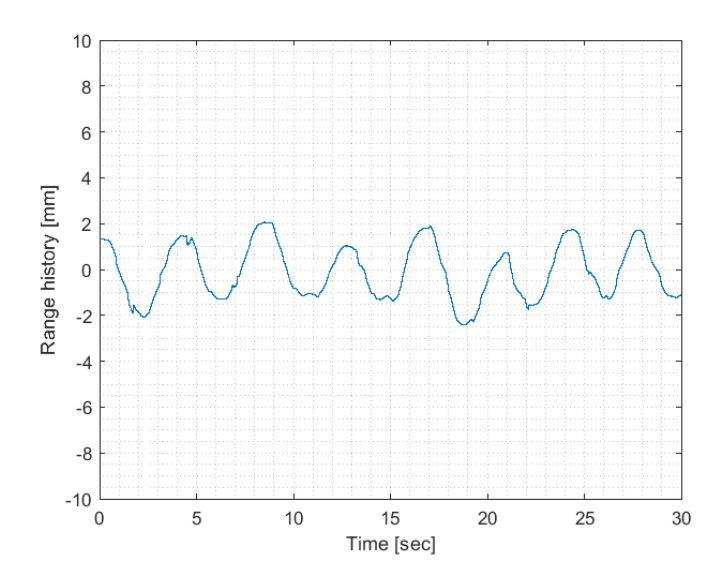


Figure 5.3: Range history with waveform W2: Vital Signs for a participant at 1m, showing the target's range displacement

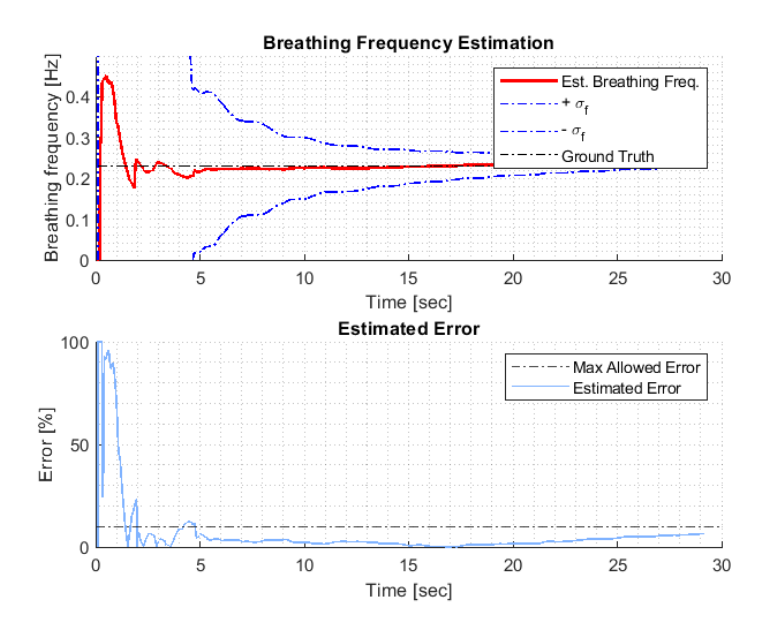


Figure 5.4: Estimated breathing frequency with waveform W2: Vital Signs for a participant at 1m, showing the target's range displacement

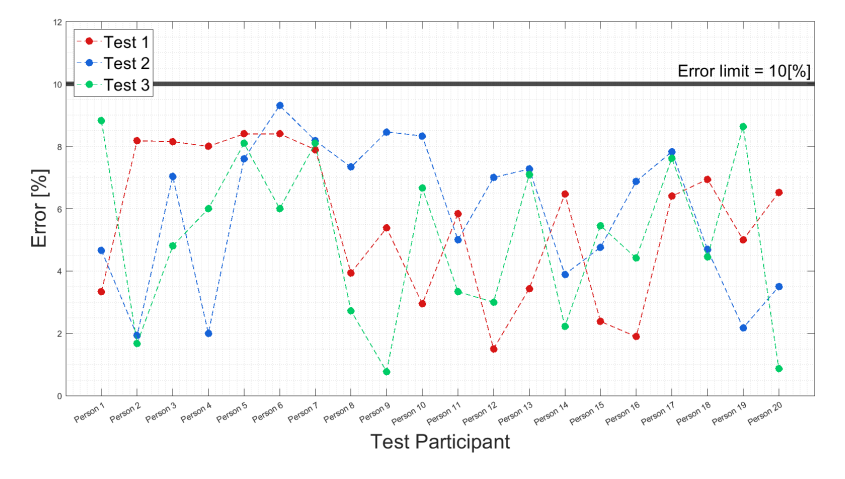


Figure 5.5: Estimated errors for all the participants and tests with waveform W2: Vital Signs for the in-place sequence, i.e. participants sitting at 1m

5.1.2. Breathing frequency estimation at 2m

For the in-place scenario at 2m, the obtained range history from the test subject analyzed in the previous section is presented in Figure 5.6, where a similar low quality data pattern is observed with the waveform W1: HAR + Vital Signs, as in the case at 1m.

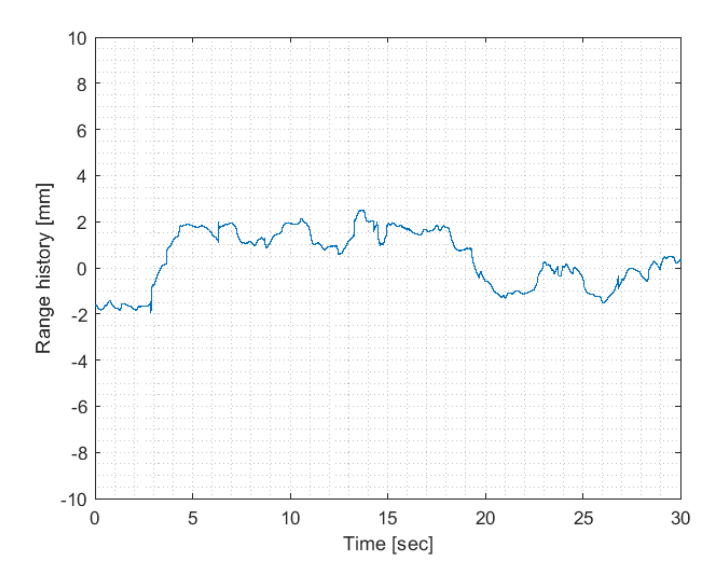


Figure 5.6: Range history with waveform W1: HAR + Vital Signs for a participant at 2m, showing the target's range displacement

Similarly, the poor resolution of the extracted range history leads the extended Kalman to converge to a false breathing frequency, which it is demonstrated in Figure 5.7.

In contrast, waveform *W2: Vital Signs* still presents a sufficient resolution to capture the test subject's respiration activity at the test distance of 2m. Nevertheless, the degradation of the range history quality can evidently be noticed as the distance increases.

The measured range history and the output breathing frequency from the extended Kalman filter with waveform *W2: Vital Signs* are shared in Figures 5.8 and 5.9, respectively.

The estimated breathing frequencies for the 20 participants and the 3 tests performed by each subject are summarized in Tables 6.3 and 6.4 (Appendix 6.2), and the calculated errors between the ground truth and output estimations from the extended Kalman filter can be seen in Figure 5.10.

However, it is relevant to mention that even though for this in-place scenario at 2m the estimated breathing frequencies converged according to the defined criteria, an average of 7/10 tests failed due to the explicit degradation of the reconstructed range history, an important finding to be considered for the following translational sequence.

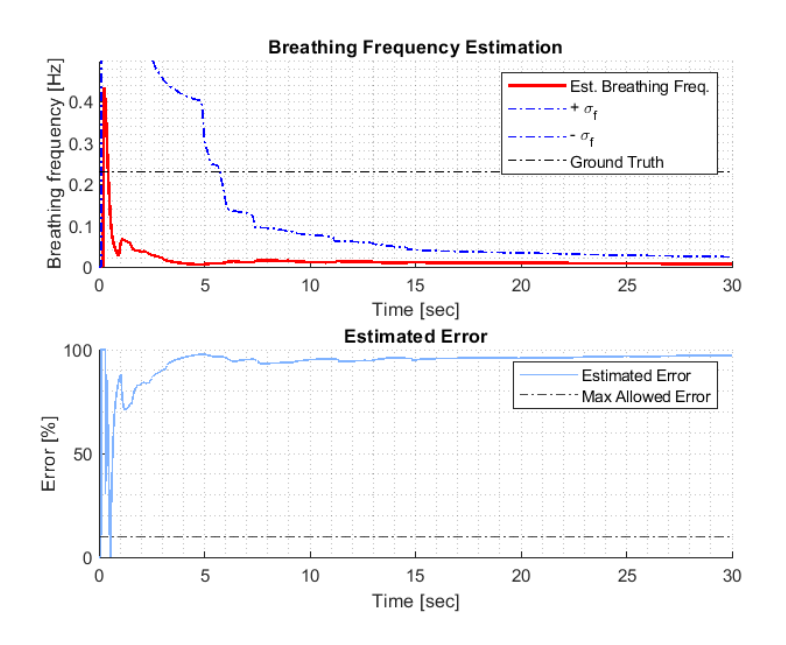


Figure 5.7: Estimated breathing frequency with waveform W1: HAR + Vital Signs for a participant at 2m

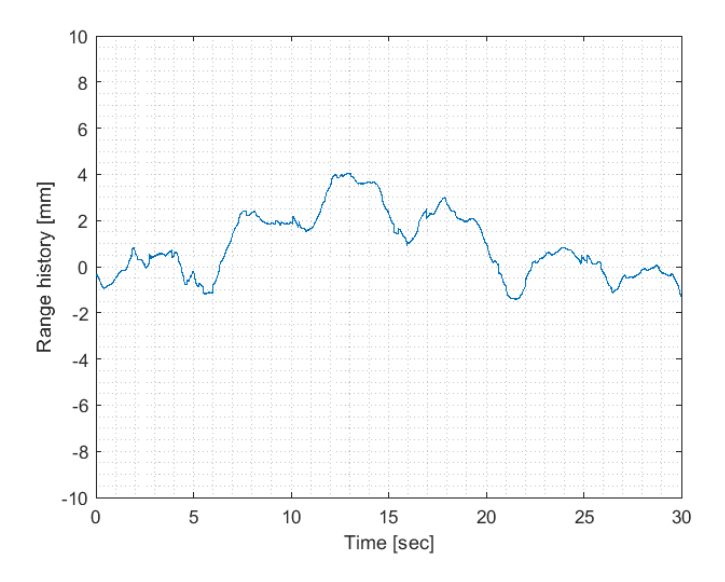


Figure 5.8: Range history with waveform W2: Vital Signs for a participant at 2m, showing the target's range displacement

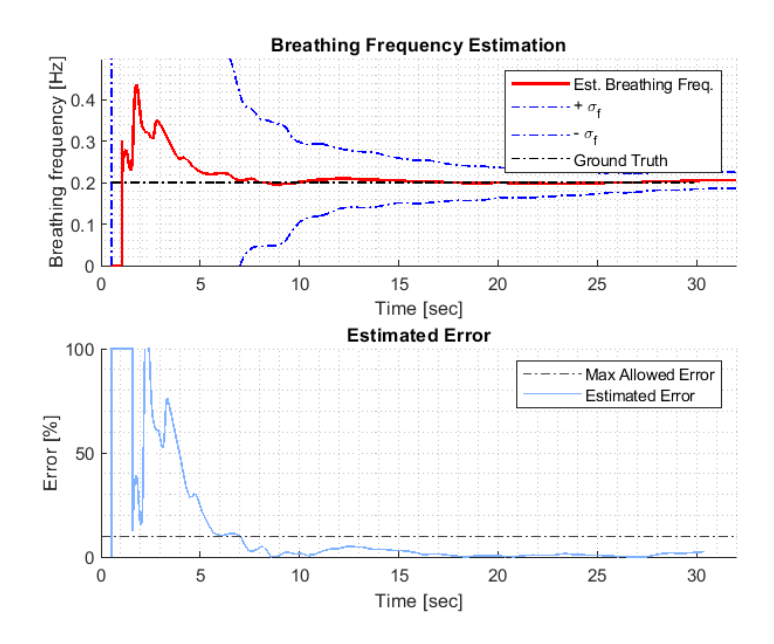


Figure 5.9: Estimated breathing frequency with waveform W2: Vital Signs for a participant at 2m

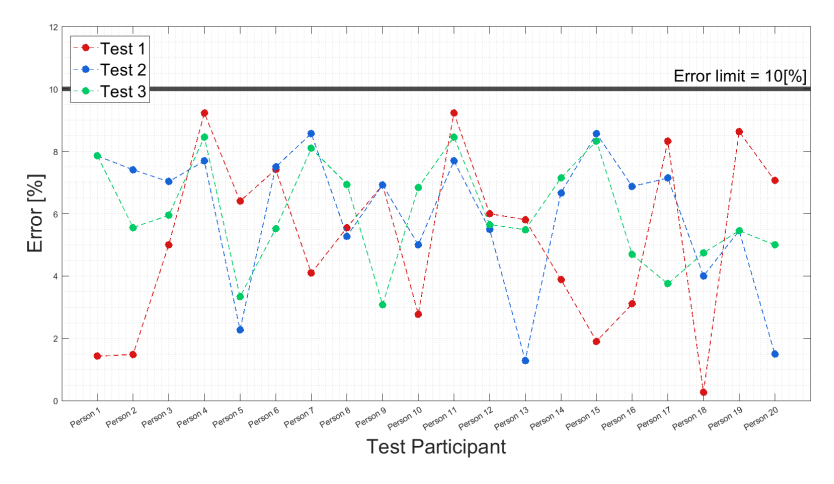


Figure 5.10: Estimated errors for all the participants and tests with waveform W2: Vital Signs for the in-place sequence, i.e. participants sitting at 2m

5.2. Translational scenario

As stated in Chapter 3, to estimate the breathing frequency of a person within an indoor environment, recognition and segmentation between activities where motion is involved are required, to isolate the segments where no motion is present to ensure that the signal reflected back to the radar after interacting with the human body encompasses information about vital signs [71].

Hence, this section introduces the procedure followed for the crucial segmentation between in-place and translational activities, aiming to trigger the EKF for breathing frequency estimation once an in-place activity (e.g., sitting) is distinguished from the translational ones (e.g., walking and standing).

5.2.1. ACTIVITY RECOGNITION AND SEGMENTATION

After reviewing the designed waveforms' performance (e.g., waveform *W1: HAR + Vital Signs* and waveform *W2: Vital Signs*) for breathing frequency estimation in an in-place scenario (e.g., sitting), a test sequence jointly exploring in-place (e.g., sitting) and translational (e.g., walking and standing) activities is proposed to test the waveforms' capabilities for recognition and segmentation tasks based on Range-Time and Doppler-Time information.

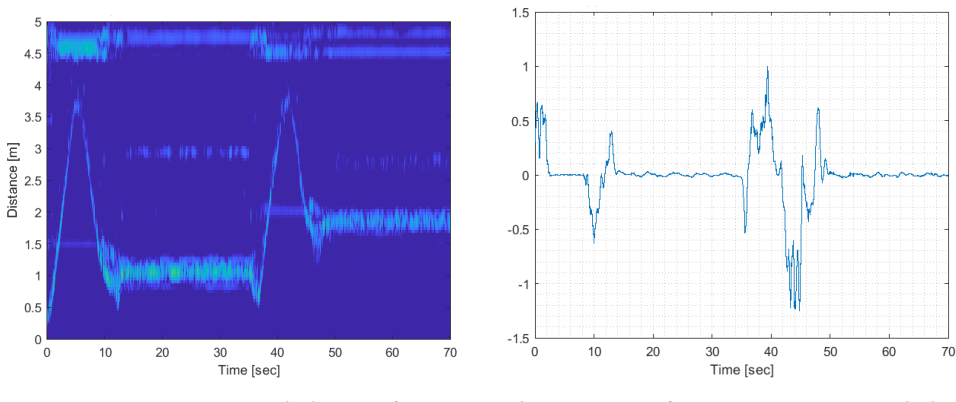
RANGE-TIME INFORMATION

As mentioned above, one of the proposed segmentation methods to distinguish between translational and in-place activities is done by exploring the Range-Time data domain.

By taking the derivative, as proposed by Guendel et al. [77], of the subject position over time and normalizing the obtained profile by its maximum, a shape similar to the one shown in Figure 5.11 is obtained for the waveform *W1: HAR + Vital Signs* based on the RTI matrix from the left side.

Comparably, the profile reproduced with the waveform *W2: Vital Signs* after following the same procedure can be seen in Figure 5.12.

Based on the available data from the executed data campaign, a threshold equal to 0.2, drawn in Figure 5.13 only for the derived profile of the Range-Time information with waveform W1: HAR + Vital Signs, can enable to separate the activities where motion is present, translational or walking activity in this study, from the activities where no motion of the test subject exists, in-place or sitting exercise, in the evaluated test sequence.



- (a) Range-Time matrix with the waveform W1: HAR + Vital Signs
- (b) Derivative of Range-Time matrix with the waveform W1: HAR + Vital Signs

Figure 5.11: Range-Time information with the waveform W1: HAR + Vital Signs

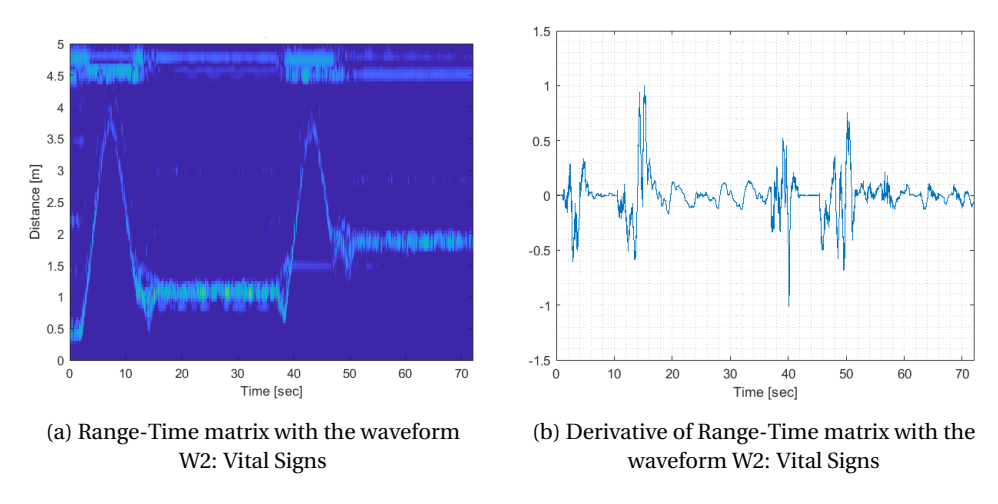


Figure 5.12: Range-Time information with the waveform W2: Vital Signs

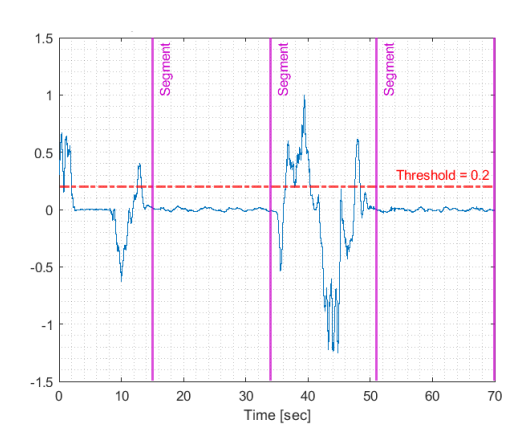
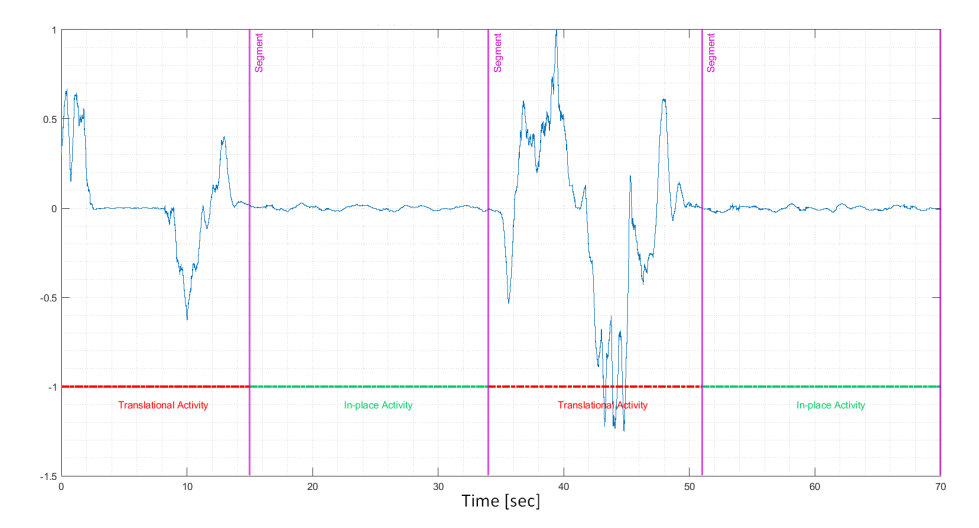
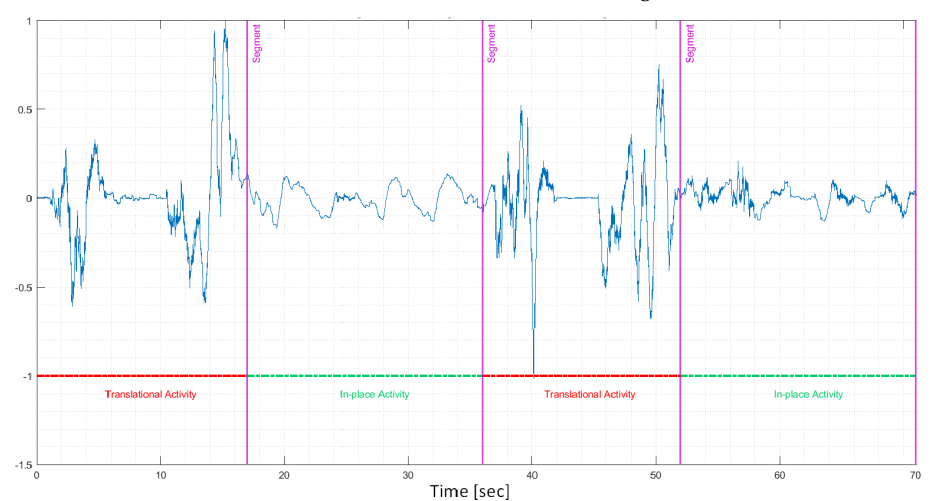


Figure 5.13: Threshold found based on Range-Time information and experimental validation for activity segmentation

Furthermore, it is noticeable that for both cases, the Range-Time information is not influenced by the velocity resolution's constraints from both developed waveforms, and the segmentation to divide the in-place and translational activities can be achieved based on this data domain as shown in Figure 5.14.



(a) Segmentation between translational and in-place activities based on Range-Time information with the waveform W1: HAR + Vital Signs



(b) Segmentation between translational and in-place activities based on Range-Time information with the waveform W2: Vital Signs

Figure 5.14: Segmentation between translational and in-place activities based on Range-Time information with the developed waveforms

Thus, once the segments between the different types of activities are identified, the pipeline for the estimation of breathing frequency based on the derived extended Kalman filter is triggered, restricting the filter to run continuously only in the segments where an in-place activity is detected based on the Range-Time information, as illustrated in Figure 5.15.

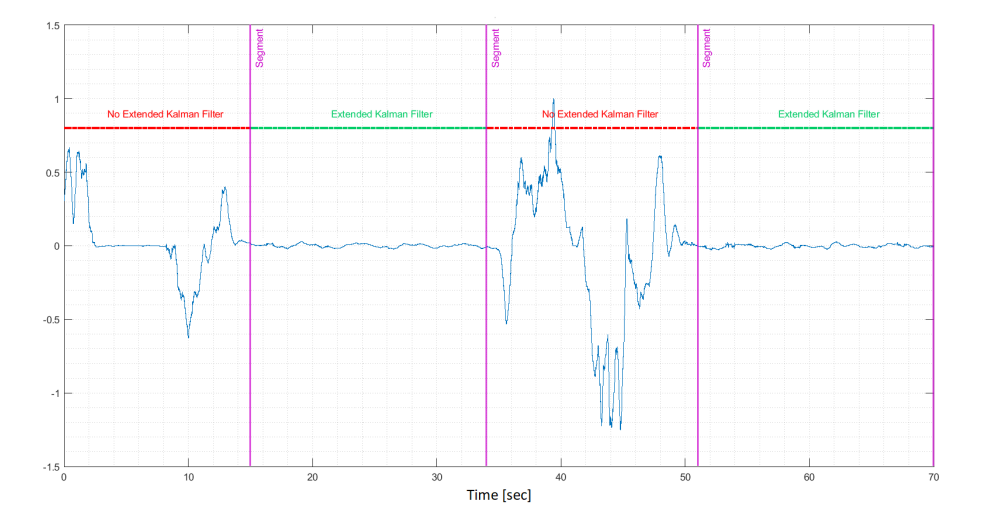


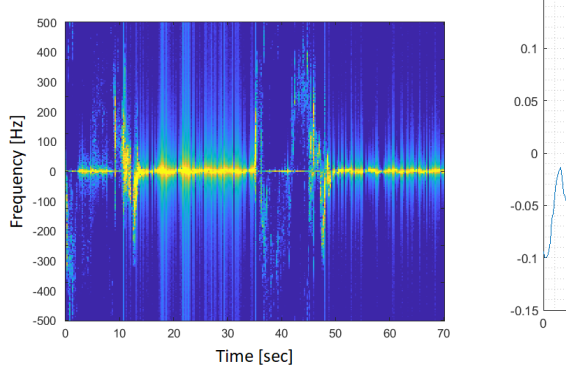
Figure 5.15: Segments to apply the extended Kalman filter based on Range-Time information with the waveform W1: HAR + Vital Signs

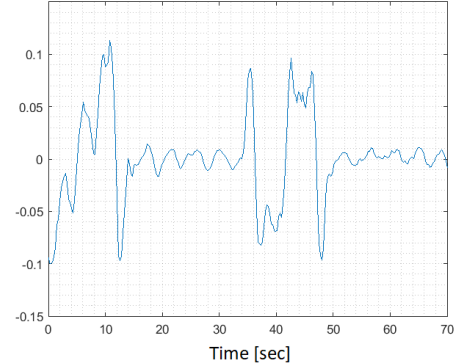
DOPPLER-TIME INFORMATION

The second data domain applied to differentiate between translational and in-place activities is the Doppler-Time information, making use of the envelope of the reconstructed spectrogram after the test subject performs the requested sequence.

In Figure 5.16, the envelope of the micro-Doppler signature from one of the test subjects is displayed, reconstructed with the Doppler-Time information from the left side with waveform W1: HAR + Vital Signs.

The envelope information based on waveform W1: HAR + Vital Signs can be used for activities' differentiation and segmentation. A threshold equal to 0.02 was obtained experimentally using the test data, enabling the separation of the in-place and translational activities, as illustrated in Figure 5.17.





- (a) Spectrogram with the waveform W1: HAR + Vital Signs
- (b) Envelope of the spectrogram with the waveform W1: HAR + Vital Signs

Figure 5.16: Doppler-Time information with the waveform W1: HAR + Vital Signs

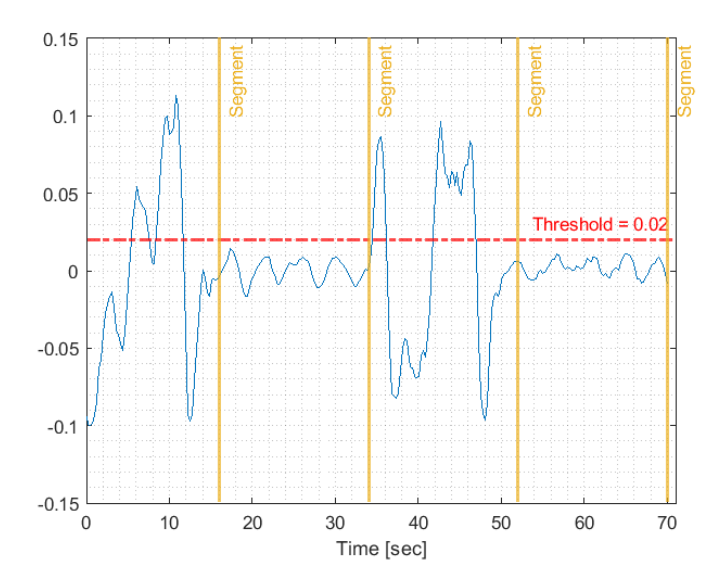


Figure 5.17: Threshold found based on Doppler-Time information and experimental validation for activity segmentation

Nevertheless, this segmentation capability from waveform W1: HAR + Vital Signs is not sufficient for the proper estimation of the breathing frequency, as it was demonstrated in the in-place scenario that this waveform presents the disadvantage of a poor velocity resolution, leading the extended Kalman filter's estimation to converge to a false breathing frequency.

On the other hand, the obtained spectrogram and envelope with the waveform *W2: Vital Signs* are shown in Figure 5.18, where no differentiation is possible between translational and in-place activities through Doppler-Time information due to the maximum ambiguous velocity of this waveform.

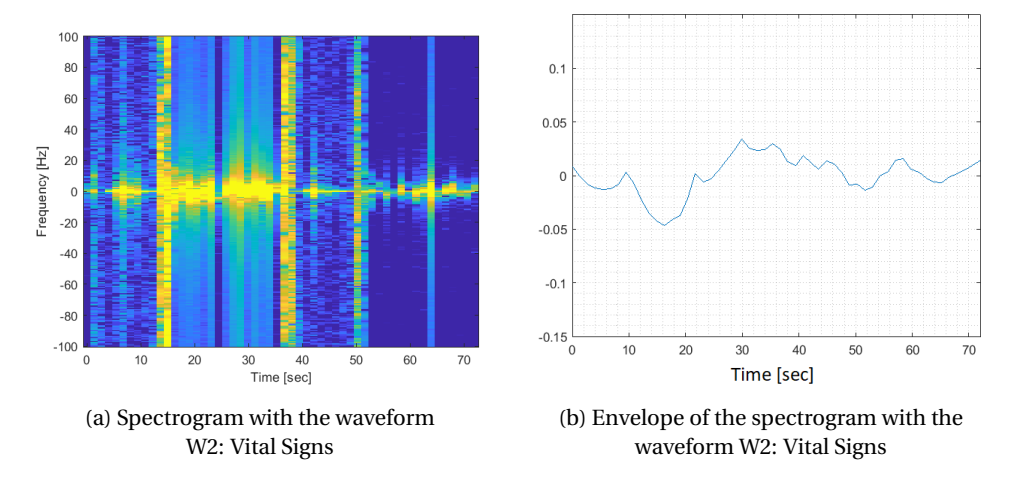


Figure 5.18: Doppler-Time information with the waveform W2: Vital Signs

5.2.2. Breathing frequency estimation

Throughout the work, a fundamental investigation of the vital detection capabilities with respect to the applied radar waveform setting can be concluded. Hence, waveform *W2: Vital Signs* is the only one capable of capturing the chest surface motion due to respiration activity and the Range-Time domain information, compared to the Doppler-Time domain, allows a satisfactory segmentation where classification between translational and in-place activities can be done to trigger the pipeline for the estimation of breathing frequency.

Figure 5.19 shows the calculated errors between the ground truth and the output estimation from the extended Kalman filter for this case at 1m distance, leaving aside the results at 2m due to its low converging rate.

Further comments regarding this choice are shared in the following summary section. Nonetheless, all the numerical results obtained at 1m and 2m are shared in Tables 6.5, 6.6, 6.7, and 6.8, in Appendix 6.2.

5.3. SUMMARY 59

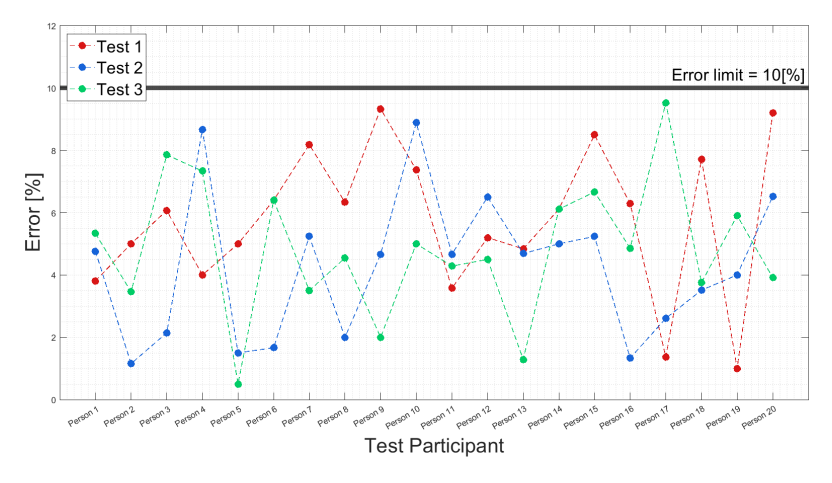


Figure 5.19: Estimated errors for all the participants and tests with waveform W2: Vital Signs for the translational sequence based on Range-Time segmentation with participants sitting at 1m

5.3. SUMMARY

Based on Sections 5.1 and 5.2, Figures 5.20 and 5.21 summarize the results for the cases assessed in this chapter.

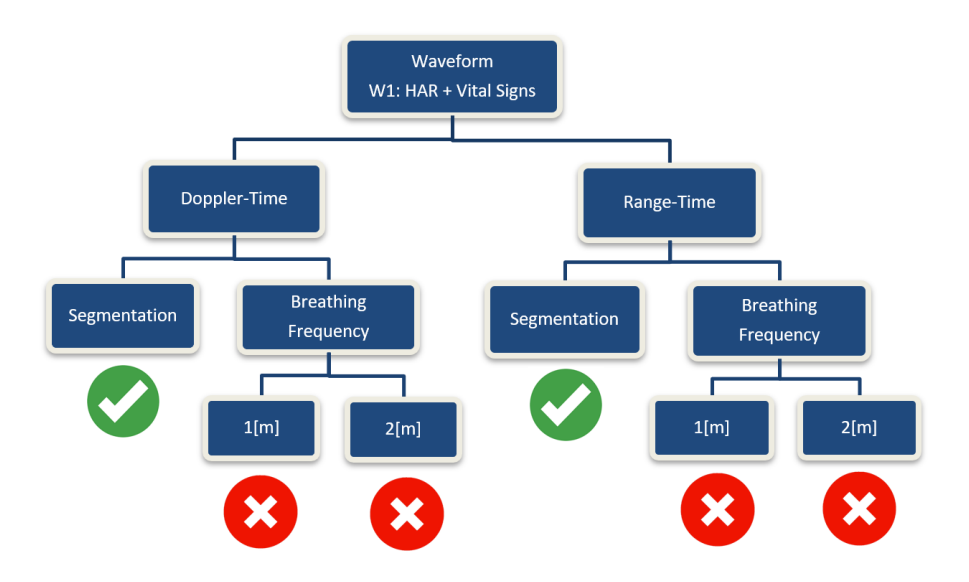


Figure 5.20: Visual capability summary of the obtained results with waveform W1: HAR + Vital Signs

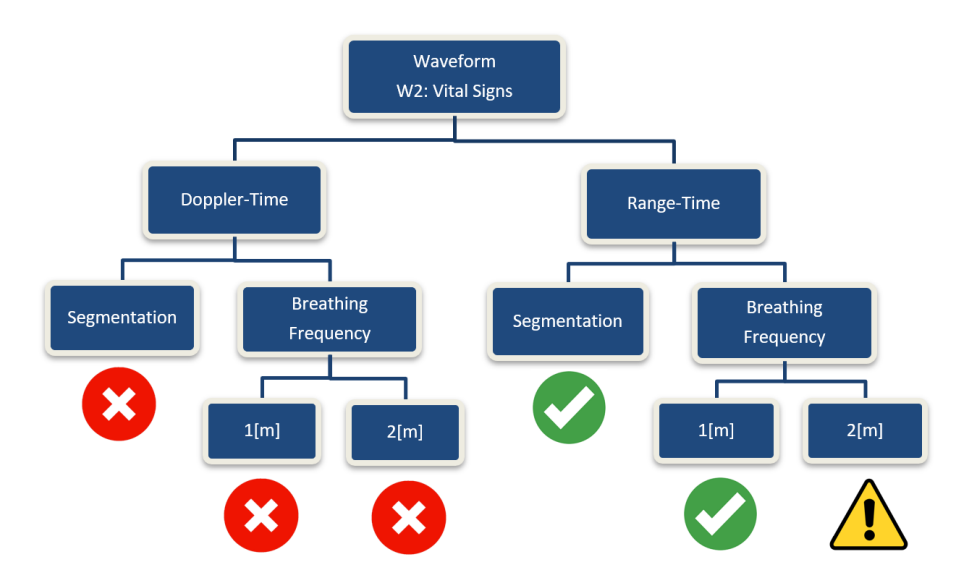


Figure 5.21: Visual capability summary of the obtained results with waveform W2: Vital Signs

From these figures, the main conclusions that can be drawn are:

- In-place scenario:
- Waveform *W1: HAR + Vital Signs*, with a velocity resolution of 0.0098 *m/s* does not have a sufficient velocity resolution to estimate breathing frequency correctly.
- Waveform *W2: Vital Signs* does, with a velocity resolution of 0.0019 *m/s*.
- Translational scenario:
- Waveform W1: HAR + Vital Signs allows activities identification and segmentation through both Range-Time and Doppler-Time domains, with a range resolution of 5cm, a maximum unambiguous range of 6.4m and a maximum unambiguous velocity of $1.25 \ m/s$. Nonetheless, the estimation of breathing frequency is not possible due to its poor velocity resolution as stated before.
- Waveform *W2: Vital Signs* allows activities identification and segmentation only through Range-Time domain, due to this waveform has the same range resolution and maximum unambiguous range as *W1: HAR + Vital Signs*. However, the Doppler-Time information is subject to a poor maximum unambiguous velocity of 0.2376 *m/s*, as a consequence of having a finer velocity resolution.
- Therefore, as segmentation between different activities cannot be done with Doppler-Time information, the pipeline for breathing frequency estimation cannot be trig-

5.3. Summary 61

gered with this data domain and waveform W2: Vital Signs.

• The differentiation between translational and in-place activities based on Range-Time information and the waveform *W2: Vital Signs* allows to trigger the pipeline for breathing frequency estimation, subject to deal with the signal degradation as the distance from the test subject to the radar increases.

• The signal showed a clear degradation pattern at the test distance of 2m, leading to a low convergence rate of the extended Kalman filter for breathing frequency estimation, with 7 out of 10 tests converging to a false breathing frequency value.

5

RESULTS AND FUTURE WORK

As closure for this thesis, Section 6.1 summarizes the key results found during the research. Finally, a few recommendations for future work are shared in Section 6.2, mentioning several directions of work to pursue.

6.1. RESULTS

The main results of the proposed joint HAR and breathing frequency estimation pipeline can be summarized as follows:

- HAR and vital signs estimation have been studied separately, treated as two different research fields according to the current radar literature. This work implements a unified processing pipeline to combine both tasks given a sequence of radar data.
- 2. For classification tasks, Range-Time and Doppler-Time data domains are implemented to distinguish between translational and in-place activities, showing that Range-Time information is sufficient to differentiate activities with a moving subject within an indoor environment, independently of the maximum unambiguous velocity and resolution of the designed waveform.
- 3. As velocity resolution is the crucial parameter to monitor breathing frequency successfully, a trade-off between maximum unambiguous velocity and velocity resolution exists with the used radar due to both being inversely proportional. A finer velocity resolution eases the estimation of breathing frequency, compromising a satisfactory differentiation between translational and in-place activities based on Doppler-Time information.
- 4. Estimation and continuous monitoring of the breathing frequency are possible through a sequential estimator such as the extended Kalman Filter. However, converging to the actual value depends on achieving a proper Doppler resolution and a long enough coherent processing interval to capture the chest surface's smallest

motion due to respiration activity. It is also important to point out that these two requirements might be subject to radar hardware performance limitations.

5. Degradation of the signal (i.e. lower SNR) as the distance increases has an essential impact on the performance of the extended Kalman Filter, where converging to the actual breathing frequency can be challenging. In this case, assuming proper design and choice of a waveform able to measure vital signs and capture the range history of the chest surface, different initialization values for the state vector and covariance matrix might potentially help the filter to converge under this noisy conditions once the segments where the test subject is static and not moving are fully identified.

6.2. RECOMMENDATIONS FOR FUTURE RESEARCH

Based on the results from this thesis project, some recommendations for future research are proposed as follows:

- Human activity recognition
- Exploration of other radar data domains for classification and segmentation tasks, evaluating their capabilities to separate different types of translational and inplace activities, and including critical scenarios that might appear in a real indoor environment, such as falling or falling while sitting down, where immediate action might be needed after their successful identification.
- Dealing with unconstrained continuous sequences, where transitions and durations between each activity are not fixed and pre-defined over time.
- Evaluate more complex scenarios that might include multiple targets and noisy backgrounds, clutter, and even multipath effect.
- Investigation and implementation of machine/deep learning algorithms for classification tasks, where micro-Doppler signatures could also be considered for predicting vital signs based on regression models.
- Modern cognitive radar techniques could be researched to correctly manage and adapt the radar parameters to match them with the desired task: activity identification and triggering of the pipeline for estimating and monitoring the vital signs of the test subject(s).
- Breathing frequency estimation
- Investigate the impact of different initialization values for the mean and variance
 of the state variables and driving noises of the extended Kalman filter, aiming to
 evaluate how this initialization can affect/improve the monitoring of the target's
 breathing frequency.
- Design and implement other sequential estimators, such as the Particle Filter, to evaluate their behavior and robustness within this type of non-linear estimation

problem, their computational complexity, and overall performance compared to the extended Kalman filter employed in this research.

- Validation of breathing frequency on longer distances from the radar and unfavorable aspect angles, extending current capabilities to successfully include and monitor other vital signs such as heartbeat and blood pressure.
- Evaluate the impact of different layers of clothing worn by the test subjects and different orientations of the targets with respect to the radar, such as side, rear, and top view, on the estimation of the breathing frequency and any other integrated vital sign.
- Verify the impact of possible micro motions and the influence of random body
 movement from the test subjects in the final estimation results. These effects may
 be present in any testing environment, and their correct identification could be
 considered in the design of any pipeline aiming to achieve the proper estimation
 and tracking of vital signs.

REFERENCES

[1] S. A. Shah and F. Fioranelli, "Rf sensing technologies for assisted daily living in healthcare: A comprehensive review," *IEEE Aerospace and Electronic Systems Magazine*, vol. 34, no. 11, pp. 26–44, 2019.

- [2] M. E. Salive, "Multimorbidity in older adults," *Epidemiologic reviews*, vol. 35, no. 1, pp. 75–83, 2013.
- [3] F. Fioranelli, J. Le Kernec, and S. A. Shah, "Radar for health care: Recognizing human activities and monitoring vital signs," *IEEE Potentials*, vol. 38, no. 4, pp. 16–23, 2019.
- [4] Z. Hussain, Q. Z. Sheng, and W. E. Zhang, "A review and categorization of techniques on device-free human activity recognition," *Journal of Network and Computer Applications*, vol. 167, p. 102738, 2020.
- [5] B. Najafi, K. Aminian, A. Paraschiv-Ionescu, F. Loew, C. Bula, and P. Robert, "Ambulatory system for human motion analysis using a kinematic sensor: monitoring of daily physical activity in the elderly," *IEEE Transactions on Biomedical Engineering*, vol. 50, no. 6, pp. 711–723, 2003.
- [6] P. K. Capp, P. L. Pearl, and D. Lewin, "Pediatric sleep disorders," *Primary Care: Clinics in Office Practice*, vol. 32, no. 2, pp. 549–562, 2005.
- [7] H. Forster, O. Ipsiroglu, R. Kerbl, and E. Paditz, "Sudden infant death and pediatric sleep disorders," pp. 847–849, 2003.
- [8] N. Hafner, I. Mostafanezhad, V. M. Lubecke, O. Boric-Lubecke, and A. Host-Madsen, "Non-contact cardiopulmonary sensing with a baby monitor," in 2007 29th Annual International Conference of the IEEE Engineering in Medicine and Biology Society, 2007, pp. 2300–2302.
- [9] F. Fioranelli and J. Le Kernec, "Radar sensing for human healthcare: challenges and results," in *2021 IEEE Sensors*, 2021, pp. 1–4.
- [10] H. Raeis, M. Kazemi, and S. Shirmohammadi, "Human activity recognition with device-free sensors for well-being assessment in smart homes," *IEEE Instrumentation Measurement Magazine*, vol. 24, no. 6, pp. 46–57, 2021.
- [11] Y. Kim and H. Ling, "Human activity classification based on micro-doppler signatures using an artificial neural network," in 2008 IEEE Antennas and Propagation Society International Symposium, 2008, pp. 1–4.
- [12] Y. Kim and h. Ling, "Human activity classification based on micro-doppler signatures using a support vector machine," *IEEE Transactions on Geoscience and Remote Sensing*, vol. 47, no. 5, pp. 1328–1337, 2009.
- [13] M. G. Amin, Y. D. Zhang, F. Ahmad, and K. D. Ho, "Radar signal processing for elderly fall detection: The future for in-home monitoring," *IEEE Signal Processing Magazine*, vol. 33, no. 2, pp. 71–80, 2016.

[14] A. Gorji, H.-U.-R. Khalid, A. Bourdoux, and H. Sahli, "On the generalization and reliability of single radar-based human activity recognition," *IEEE Access*, vol. 9, pp. 85 334–85 349, 2021.

- [15] X. Li, Y. He, F. Fioranelli, and X. Jing, "Semisupervised human activity recognition with radar micro-doppler signatures," *IEEE Transactions on Geoscience and Remote Sensing*, vol. 60, pp. 1–12, 2022.
- [16] F. Wang, M. Skubic, M. Rantz, and P. E. Cuddihy, "Quantitative gait measurement with pulse-doppler radar for passive in-home gait assessment," *IEEE Transactions on Biomedical Engineering*, vol. 61, no. 9, pp. 2434–2443, 2014.
- [17] A.-K. Seifert, M. G. Amin, and A. M. Zoubir, "Toward unobtrusive in-home gait analysis based on radar micro-doppler signatures," *IEEE Transactions on Biomedical Engineering*, vol. 66, no. 9, pp. 2629–2640, 2019.
- [18] H. Li, A. Mehul, J. Le Kernec, S. Z. Gurbuz, and F. Fioranelli, "Sequential human gait classification with distributed radar sensor fusion," *IEEE Sensors Journal*, vol. 21, no. 6, pp. 7590–7603, 2021.
- [19] C. Li, P.-I. Mak, R. Gómez-García, and Y. Chen, "Guest editorial wireless sensing circuits and systems for healthcare and biomedical applications," *IEEE Journal on Emerging and Selected Topics in Circuits and Systems*, vol. 8, no. 2, pp. 161–164, 2018.
- [20] Y. Oyamada, T. Koshisaka, and T. Sakamoto, "Experimental demonstration of accurate noncontact measurement of arterial pulse wave displacements using 79-ghz array radar," *IEEE Sensors Journal*, vol. 21, no. 7, pp. 9128–9137, 2021.
- [21] H. Zhao, X. Gu, H. Hong, Y. Li, X. Zhu, and C. Li, "Non-contact beat-to-beat blood pressure measurement using continuous wave doppler radar," in *2018 IEEE/MTT-S International Microwave Symposium IMS*, 2018, pp. 1413–1415.
- [22] G. Su, N. Petrov, and A. Yarovoy, "Dynamic estimation of vital signs with mm-wave fmcw radar," in 2020 17th European Radar Conference (EuRAD), 2021, pp. 206–209.
- [23] B. Jokanović and M. Amin, "Fall detection using deep learning in range-doppler radars," *IEEE Transactions on Aerospace and Electronic Systems*, vol. 54, no. 1, pp. 180–189, 2018.
- [24] Z. Li, F. Fioranelli, S. Yang, L. Zhang, O. Romain, Q. He, G. Cui, and J. Le Kernec, "Multi-domains based human activity classification in radar," in *IET International Radar Conference (IET IRC 2020)*, vol. 2020, 2020, pp. 1744–1749.
- [25] R. G. Guendel, F. Fioranelli, and A. Yarovoy, "Phase-based classification for arm gesture and gross-motor activities using histogram of oriented gradients," *IEEE Sensors Journal*, vol. 21, no. 6, pp. 7918–7927, 2021.
- [26] F. Aziz, O. Metwally, P. Weller, U. Schneider, and M. F. Huber, "A mimo radar-based metric learning approach for activity recognition," *arXiv preprint arXiv:2111.01939*, 2021.

[27] C. Ding, H. Hong, Y. Zou, H. Chu, X. Zhu, F. Fioranelli, J. Le Kernec, and C. Li, "Continuous human motion recognition with a dynamic range-doppler trajectory method based on fmcw radar," *IEEE Transactions on Geoscience and Remote Sensing*, vol. 57, no. 9, pp. 6821–6831, 2019.

- [28] B. Çağlıyan and S. Z. Gürbüz, "Micro-doppler-based human activity classification using the mote-scale bumblebee radar," *IEEE Geoscience and Remote Sensing Letters*, vol. 12, no. 10, pp. 2135–2139, 2015.
- [29] B. Jokanovic, M. G. Amin, and F. Ahmad, "Effect of data representations on deep learning in fall detection," in 2016 IEEE Sensor Array and Multichannel Signal Processing Workshop (SAM), 2016, pp. 1–5.
- [30] H. Du, T. Jin, Y. Song, Y. Dai, and M. Li, "A three-dimensional deep learning framework for human behavior analysis using range-doppler time points," *IEEE Geoscience and Remote Sensing Letters*, vol. 17, no. 4, pp. 611–615, 2020.
- [31] Y. Yang, C. Hou, Y. Lang, T. Sakamoto, Y. He, and W. Xiang, "Omnidirectional motion classification with monostatic radar system using micro-doppler signatures," *IEEE Transactions on Geoscience and Remote Sensing*, vol. 58, no. 5, pp. 3574–3587, 2020.
- [32] Y. Shao, S. Guo, L. Sun, and W. Chen, "Human motion classification based on range information with deep convolutional neural network," in *2017 4th International Conference on Information Science and Control Engineering (ICISCE)*, 2017, pp. 1519–1523.
- [33] M. Jia, S. Li, J. L. Kernec, S. Yang, F. Fioranelli, and O. Romain, "Human activity classification with radar signal processing and machine learning," in *2020 International Conference on UK-China Emerging Technologies (UCET)*, 2020, pp. 1–5.
- [34] F. Fioranelli, M. Ritchie, and H. Griffiths, "Bistatic human micro-doppler signatures for classification of indoor activities," in *2017 IEEE Radar Conference (RadarConf)*, 2017, pp. 0610–0615.
- [35] S. Yang, J. L. Kernec, F. Fioranelli, and O. Romain, "Human activities classification in a complex space using raw radar data," in *2019 International Radar Conference (RADAR)*, 2019, pp. 1–4.
- [36] X. Li, Y. He, F. Fioranelli, X. Jing, A. Yarovoy, and Y. Yang, "Human motion recognition with limited radar micro-doppler signatures," *IEEE Transactions on Geoscience and Remote Sensing*, vol. 59, no. 8, pp. 6586–6599, 2021.
- [37] Y. Kim and T. Moon, "Human detection and activity classification based on microdoppler signatures using deep convolutional neural networks," *IEEE Geoscience and Remote Sensing Letters*, vol. 13, no. 1, pp. 8–12, 2016.
- [38] R. G. Guendel, M. Unterhorst, E. Gambi, F. Fioranelli, and A. Yarovoy, "Continuous human activity recognition for arbitrary directions with distributed radars," in *2021 IEEE Radar Conference (RadarConf21)*, 2021, pp. 1–6.

[39] T. Wu, T. S. Rappaport, and C. M. Collins, "The human body and millimeter-wave wireless communication systems: Interactions and implications," in *2015 IEEE International Conference on Communications (ICC)*, 2015, pp. 2423–2429.

- [40] A. Yarovoy, L. Ligthart, J. Matuzas, and B. Levitas, "Uwb radar for human being detection," *IEEE Aerospace and Electronic Systems Magazine*, vol. 21, no. 3, pp. 10–14, 2006.
- [41] C. Li, J. Lin, and Y. Xiao, "Robust overnight monitoring of human vital signs by a non-contact respiration and heartbeat detector," in *2006 International Conference of the IEEE Engineering in Medicine and Biology Society*, 2006, pp. 2235–2238.
- [42] S. Wang, A. Pohl, T. Jaeschke, M. Czaplik, M. Köny, S. Leonhardt, and N. Pohl, "A novel ultra-wideband 80 ghz fmcw radar system for contactless monitoring of vital signs," in 2015 37th Annual International Conference of the IEEE Engineering in Medicine and Biology Society (EMBC), 2015, pp. 4978–4981.
- [43] S. Ayhan, S. Diebold, S. Scherr, A. Tessmann, O. Ambacher, I. Kallfass, and T. Zwick, "A 96 ghz radar system for respiration and heart rate measurements," in *2012 IEEE/MTT-S International Microwave Symposium Digest*, 2012, pp. 1–3.
- [44] T. Sakamoto, P. J. Aubry, S. Okumura, H. Taki, T. Sato, and A. G. Yarovoy, "Noncontact measurement of the instantaneous heart rate in a multi-person scenario using x-band array radar and adaptive array processing," *IEEE Journal on Emerging and Selected Topics in Circuits and Systems*, vol. 8, no. 2, pp. 280–293, 2018.
- [45] A. Ahmad, J. C. Roh, D. Wang, and A. Dubey, "Vital signs monitoring of multiple people using a fmcw millimeter-wave sensor," in *2018 IEEE Radar Conference (Radar-Conf18)*, 2018, pp. 1450–1455.
- [46] S. Wang, S. Kueppers, H. Cetinkaya, and R. Herschel, "3d localization and vital sign detection of human subjects with a 120 ghz mimo radar," in *2019 20th International Radar Symposium (IRS)*, 2019, pp. 1–6.
- [47] J. Aho, J. Salmi, and V. Koivunen, "Adaptive processing and realistic signal propagation modeling for multiantenna vital sign radar," in *2013 IEEE Radar Conference* (*RadarCon13*), 2013, pp. 1–6.
- [48] V. Singh, S. Bhattacharyya, and P. K. Jain, "Through the wall human signature detection using principle component analysis (pca)," in 2018 IEEE International Symposium on Antennas and Propagation USNC/URSI National Radio Science Meeting, 2018, pp. 1975–1976.
- [49] B.-K. Park, O. Boric-Lubecke, and V. M. Lubecke, "Arctangent demodulation with dc offset compensation in quadrature doppler radar receiver systems," *IEEE Transactions on Microwave Theory and Techniques*, vol. 55, no. 5, pp. 1073–1079, 2007.
- [50] C. Li and J. Lin, "Random body movement cancellation in doppler radar vital sign detection," *IEEE Transactions on Microwave Theory and Techniques*, vol. 56, no. 12, pp. 3143–3152, 2008.

[51] F. Weishaupt, I. Walterscheid, O. Biallawons, and J. Klare, "Vital sign localization and measurement using an lfmcw mimo radar," in *2018 19th International Radar Symposium (IRS)*, 2018, pp. 1–8.

- [52] M. Mercuri, Y.-H. Liu, I. Lorato, T. Torfs, F. Wieringa, A. Bourdoux, and C. Van Hoof, "A direct phase-tracking doppler radar using wavelet independent component analysis for non-contact respiratory and heart rate monitoring," *IEEE Transactions on Biomedical Circuits and Systems*, vol. 12, no. 3, pp. 632–643, 2018.
- [53] I. V. Mikhelson, S. Bakhtiari, T. W. Elmer, and A. V. Sahakian, "Remote sensing of patterns of cardiac activity on an ambulatory subject using millimeter-wave interferometry and statistical methods," *Medical & biological engineering & computing*, vol. 51, no. 1, pp. 135–142, 2013.
- [54] F. Adib, H. Mao, Z. Kabelac, D. Katabi, and R. C. Miller, "Smart homes that monitor breathing and heart rate," in *Proceedings of the 33rd annual ACM conference on human factors in computing systems*, 2015, pp. 837–846.
- [55] S. Groot, R. Harmanny, H. Driessen, and A. Yarovoy, "Human motion classification using a particle filter approach: multiple model particle filtering applied to the micro-doppler spectrum," *International Journal of Microwave and Wireless Technologies*, vol. 5, no. 3, pp. 391–399, 2013.
- [56] M. Xu, A. Goldfain, J. DelloStritto, and S. Iyengar, "An adaptive kalman filter technique for context-aware heart rate monitoring," in 2012 Annual International Conference of the IEEE Engineering in Medicine and Biology Society, 2012, pp. 6522–6525.
- [57] Y. Yu, W. Yin, L. Li, and L. Zhang, "Vital sign integrated tracking by predictive knn and kalman filter with uwb radars," in 2018 10th International Conference on Wireless Communications and Signal Processing (WCSP), 2018, pp. 1–6.
- [58] M. Arsalan, A. Santra, and C. Will, "Improved contactless heartbeat estimation in fmcw radar via kalman filter tracking," *IEEE Sensors Letters*, vol. 4, no. 5, pp. 1–4, 2020.
- [59] V. Almeida and I. T. Nabney, "Detecting dynamical changes in vital signs using switching kalman filter," in 2017 39th Annual International Conference of the IEEE Engineering in Medicine and Biology Society (EMBC), 2017, pp. 2223–2226.
- [60] N. Khan, K. Khan, A. Khan, I. Alam, F. U. Khan, S. U. Khan, and A. Ali, "Accommodate data loss in monitoring vital signs through autoregressive model," *Journal of Medical Imaging and Health Informatics*, vol. 9, no. 6, pp. 1205–1214, 2019.
- [61] C. Uysal, A. Onat, and T. Filik, "Non-contact respiratory rate estimation in real-time with modified joint unscented kalman filter," *IEEE Access*, vol. 8, pp. 99 445–99 457, 2020.
- [62] S. M. Kay, Fundamentals of statistical signal processing: estimation theory. Prentice-Hall, Inc., 1993.

[63] K. Yamamoto, K. Maeno, and T. Kamakura, "Dynamic respiratory modeling for non-contact live monitoring by particle filter approach," in 2013 IEEE 14th International Symposium on Computational Intelligence and Informatics (CINTI), 2013, pp. 25–30.

- [64] J. Lee and K. H. Chon, "Time-varying autoregressive model-based multiple modes particle filtering algorithm for respiratory rate extraction from pulse oximeter," *IEEE Transactions on Biomedical Engineering*, vol. 58, no. 3, pp. 790–794, 2011.
- [65] Y. Fujita, M. Hiromoto, and T. Sato, "Parhelia: Particle filter-based heart rate estimation from photoplethysmographic signals during physical exercise," *IEEE Transactions on Biomedical Engineering*, vol. 65, no. 1, pp. 189–198, 2018.
- [66] V. Nathan, I. Akkaya, and R. Jafari, "A particle filter framework for the estimation of heart rate from ecg signals corrupted by motion artifacts," in 2015 37th Annual International Conference of the IEEE Engineering in Medicine and Biology Society (EMBC), 2015, pp. 6560–6565.
- [67] V. Nathan and R. Jafari, "Particle filtering and sensor fusion for robust heart rate monitoring using wearable sensors," *IEEE Journal of Biomedical and Health Informatics*, vol. 22, no. 6, pp. 1834–1846, 2018.
- [68] R. Zhang and S. Cao, "Real-time human motion behavior detection via cnn using mmwave radar," *IEEE Sensors Letters*, vol. 3, no. 2, pp. 1–4, 2019.
- [69] H. Du, Y. He, and T. Jin, "Transfer learning for human activities classification using micro-doppler spectrograms," in *2018 IEEE International Conference on Computational Electromagnetics (ICCEM)*, 2018, pp. 1–3.
- [70] A. Shrestha, H. Li, J. Le Kernec, and F. Fioranelli, "Continuous human activity classification from fmcw radar with bi-lstm networks," *IEEE Sensors Journal*, vol. 20, no. 22, pp. 13607–13619, 2020.
- [71] V. C. Chen, The micro-Doppler effect in radar. Artech house, 2019.
- [72] "Mechanism of human breathing activity," https://www.brainkart.com/article/Mechanism-of-breathing_33205/, accessed: 2022-12-09.
- [73] G. Su, Sequential Estimator for Breathing and Heart Beat Frequencies Using Radar. Delft University of Technology, 2019.
- [74] K. Konno and J. Mead, "Measurement of the separate volume changes of rib cage and abdomen during breathing," *IEEE Aerospace and Electronic Systems Magazine*, vol. 21, no. 3, pp. 10–14, 2006.
- [75] T. Instruments, *Programming Chirp Parameters in TI Radar Devices*, Texas Instruments, 2017.
- [76] "Go direct respiration belt to measure human respiration rate," https://www.vernier.com/product/go-direct-respiration-belt/, accessed: 2022-12-09.

[77] R. G. Guendel, F. Fioranelli, and A. Yarovoy, "Derivative target line (dtl) for continuous human activity detection and recognition," in *2020 IEEE Radar Conference* (RadarConf20), 2020, pp. 1–6.

- [78] S. Z. Gürbüz, B. Erol, B. Çağlıyan, and B. Tekeli, "Operational assessment and adaptive selection of micro-doppler features," *IET Radar, Sonar & Navigation*, vol. 9, no. 9, pp. 1196–1204, 2015.
- [79] F. Fioranelli, M. Ritchie, and H. Griffiths, "Centroid features for classification of armed/unarmed multiple personnel using multistatic human micro-doppler," *IET Radar, Sonar & Navigation*, vol. 10, no. 9, pp. 1702–1710, 2016.
- [80] C. Clemente, L. Pallotta, A. De Maio, J. J. Soraghan, and A. Farina, "A novel algorithm for radar classification based on doppler characteristics exploiting orthogonal pseudo-zernike polynomials," *IEEE Transactions on Aerospace and Electronic Systems*, vol. 51, no. 1, pp. 417–430, 2015.
- [81] X. Shi, F. Zhou, L. Liu, B. Zhao, and Z. Zhang, "Textural feature extraction based on time–frequency spectrograms of humans and vehicles," *IET Radar, Sonar & Navigation*, vol. 9, no. 9, pp. 1251–1259, 2015.
- [82] P. Molchanov, J. Astola, K. Egiazarian, and A. Totsky, "Ground moving target classification by using dct coefficients extracted from micro-doppler radar signatures and artificial neuron network," in *2011 MICROWAVES, RADAR AND REMOTE SENSING SYMPOSIUM*, 2011, pp. 173–176.
- [83] B. Erol and M. Amin, "Generalized pca fusion for improved radar human motion recognition," in *2019 IEEE Radar Conference (RadarConf)*, 2019, pp. 1–5.
- [84] J. J. M. de Wit, R. I. A. Harmanny, and P. Molchanov, "Radar micro-doppler feature extraction using the singular value decomposition," in *2014 International Radar Conference*, 2014, pp. 1–6.
- [85] B. Erol and S. Z. Gürbüz, "Hyperbolically-warped cepstral coefficients for improved micro-doppler classification," in *2016 IEEE Radar Conference (RadarConf)*, 2016, pp. 1–6.
- [86] H. Li, J. le Kernec, A. Mehul, S. Z. Gurbuz, and F. Fioranelli, "Distributed radar information fusion for gait recognition and fall detection," in *2020 IEEE Radar Conference (RadarConf20)*, 2020, pp. 1–6.
- [87] M. Li, T. Chen, and H. Du, "Human behavior recognition using range-velocity-time points," *IEEE Access*, vol. 8, pp. 37 914–37 925, 2020.
- [88] K. He, X. Zhang, S. Ren, and J. Sun, "Deep residual learning for image recognition," in *Proceedings of the IEEE Conference on Computer Vision and Pattern Recognition (CVPR)*, June 2016.

[89] M. S. Seyfioğlu, A. M. Özbayoğlu, and S. Z. Gürbüz, "Deep convolutional autoencoder for radar-based classification of similar aided and unaided human activities," *IEEE Transactions on Aerospace and Electronic Systems*, vol. 54, no. 4, pp. 1709–1723, 2018.

- [90] X. Li, Y. He, Y. Yang, Y. Hong, and X. Jing, "Lstm based human activity classification on radar range profile," in *2019 IEEE International Conference on Computational Electromagnetics (ICCEM)*, 2019, pp. 1–2.
- [91] G. Klarenbeek, R. I. A. Harmanny, and L. Cifola, "Multi-target human gait classification using lstm recurrent neural networks applied to micro-doppler," in *2017 European Radar Conference (EURAD)*, 2017, pp. 167–170.
- [92] S. Wang, J. Song, J. Lien, I. Poupyrev, and O. Hilliges, "Interacting with soli: Exploring fine-grained dynamic gesture recognition in the radio-frequency spectrum," in *Proceedings of the 29th Annual Symposium on User Interface Software and Technology*, 2016, pp. 851–860.

APPENDIX A

In this appendix, literature regarding feature extraction and selection methods is shared, along with a brief description of different algorithms currently used for human activity recognition and classification based on machine and deep learning techniques. While these techniques were not directly applied in this thesis, they have been reviewed and hence are reported here for future work reference.

FEATURES EXTRACTION AND SELECTION

Features are discriminating properties of the object signatures, expressed in numerical values, that enable its classification. For features extraction, significant research exists on statistical features extracted from spectrograms. As addressed in Chapter 2, micro-Doppler seems to be most commonly used over other data domains [78]. Features proposed in the literature can be divided into several basic types [78]:

- Physical/handcrafted features: These derive quantities based on the physical characteristics of the target and its motion. Physical features, like the ones implemented by Kim and Çağlıyan et al. [12, 28], can include average torso Doppler frequency, total Doppler bandwidth, and torso frequency; while features extracted from the CVD include torso power, harmonic frequencies, and harmonic power. Other features inspired by 2D image representations have been explored by Fioranelli et al. [79] implementing centroid features for classification, and by Clemente et al. [80] using Pseudo-Zernike moments. Textural features extraction was studied by Shi et al. [81] based on targets' spectrograms to calculate the entropy and third-order moment of the statistical histogram to obtain features representing the characteristic of micro-motion targets. The histogram of oriented gradients (HOG) was addressed by Guendel et al. [25] combined with a phase-based classification for arm gestures and gross-motor activities.
- Transform/decomposition-based features: Which use the coefficients of different transforms as features. Commonly used transform-based features include FFT, and discrete cosine transform (DCT) coefficients generally computed from spectrograms. For instance, Molchanov et al. [82] classified ground moving targets using DCT coefficients extracted from micro-Doppler radar signatures with a multilayer perceptron (MLP) classifier based on artificial neural networks (ANN).
- Component analysis features: Where the basis computed from algorithms is utilized as features. Component analysis techniques, such as the PCA by Erol et al. [83], and the singular value decomposition (SVD) by de Wit et al. [84], are part of this category.

• **Speech features:** Designed to process speech signals but implemented for human activity classification as well. Examples of features in this category are melody-frequency cepstral coefficients (MFCC) by Erol et al. [85], and linear predictive coding (LPC) by Gürbüz et al. [78], where the coefficients are directly computed from the raw I/Q data.

Potentially, hundreds of features may be extracted from micro-Doppler signatures and other data domains. However, the combination of all these features does not necessarily lead to optimal classification performance. As a result, and as features work as the input of the classifiers, their optimization is required and done through a technique called "feature selection", which aims to remove redundant or correlated features to improve the accuracy of the classification and reduce the computational load. Feature selection algorithms can be categorized into three main strategies [24, 78]:

- Wrapper methods: These methods consider the different combinations of feature space with a specified classifier. The error rate is used then to find the result with the highest accuracy. Due to the fact that each subset needs to be trained, wrapper methods are normally computationally expensive.
- **Filter methods:** These techniques based their operating principle on evaluating the intrinsic relevance between features based on the metric of class separability, scoring the feature subset, and selecting the features with the highest scores. One of the advantages of filter methods is their independency of the type of classifier.
- **Embedded methods:** Where feature selection is integrated with the classification algorithm.

It is important to mention that the efficacy of any given feature does not depend only on the radar parameters, such as the transmit frequency or the PRF, but also on external factors, such as the SNR, aspect angle, dwell time, and the classification problem itself [78].

ALGORITHMS FOR HUMAN ACTIVITY RECOGNITION

Models for human activity recognition and classification can be categorized into two types of algorithms: machine learning (ML) and deep learning (DL) algorithms, where deep learning techniques are essentially a subset of machine learning. Conventional machine learning algorithms, such as SVM or KNN, are mostly used for classification based on handcrafted features, while deep learning algorithms, such as neural networks, focus on classification through data representation as 2D images or temporal sequences.

Firstly, and as mentioned above, supervised ML algorithms such as KNN [34], SVM [12], Random-Forest [86], Naïve Bayes [87], and may more, are compatible with handcrafted features. In comparison with neural networks, these algorithms are relatively easy to train since DL techniques generally have hundreds of parameters to be trained.

On the other hand, the tendency to use DL techniques to approach radar-based HAR has increased as a result of the fact that supervised ML algorithms work with

high dimensionality, which represents the total number of input variables or features for a given dataset Therefore, handcrafted features may not fully represent all the information required for a satisfactory classification.

- For activity recognition using 2D images as data representation, CNN, including multiple convolution layers, are the primary architectures and have been employed by Zhang et al. [68]. Other popular CNN architectures, such as ResNet, have been adapted by He et al. [88] or directly re-utilized for transfer learning tasks as done by Du et al. [69]. CNN with deeper layers, known as DCNN, have also been used to address human detection and activity classification as done by Kim et al. [37].
 - Combinations of neural network blocks have been explored as well, seeking architectures containing the benefits of different blocks as addressed by Seyfioğlu et al. [89], where the structure of a convolutional layer with an autoencoder was implemented for radar-based classification of aided and unaided human activities.
- Regarding temporal sequences, popular choices for HAR classifiers are recurrent neural networks (RNN) and variants like the LSTM, plus other alternatives like the gated recurrent unit (GRU). For instance, Bi-LSTM by Shrestha et al. [70] and LSTM by Li and Klarenbeek et al. [90] [91] have been studied for human activity and gait classification. Moreover, and as previously described, architectures that handle a unique data representation can potentially benefit from their merge as shown by Wang et al. [92], where a sequence of 2D image data representations was processed by a hybrid CNN-RNN architecture, utilizing the CNN to extract out high dimensional features and exploiting the temporal relations amongst the images with an RNN for human gesture recognition.

As it has been shown, data representations and classifiers are mutually dependent. Therefore, the optimal classifier or data representation does not exist, but a better performance of their combination given a specific task or a set of them, aiming to enhance and ideally optimized the classification performance through the exploration of different radar data representations and the matching classifier.

APPENDIX B

In this appendix, the true breathing frequencies obtained with the respiration belt and the output estimations from the extended Kalman filter are listed in the tables below, together with the calculated errors between them for the in-place and translational sequences studied in this research.

Table 6.1: Estimated breathing frequencies and errors with waveform W2: Vital Signs for the in-place sequence at 1m [participants 1-10]

Test Subject	Test Number	True Value [Hz]	Est. Value [Hz]	Error [%]
	Test 1	0.15	0.155	3.3
1 Male	Test 2	0.15	0.157	4.7
	Test 3	0.17	0.155	8.8
	Test 1	0.22	0.238	8.2
2 Male	Test 2	0.26	0.265	1.9
	Test 3	0.3	0.305	1.7
	Test 1	0.27	0.292	8.1
3 Male	Test 2	0.27	0.289	7
	Test 3	0.25	0.238	4.8
	Test 1	0.15	0.138	8
4 Female	Test 2	0.15	0.147	2
	Test 3	0.15	0.141	6
	Test 1	0.25	0.229	8.4
5 Male	Test 2	0.25	0.269	7.6
	Test 3	0.21	0.157 0.155 0.238 0.265 0.305 0.292 0.289 0.238 0.138 0.147 0.141 0.229	8.1
	Test 1	0.25	0.271	8.4
6 Male	Test 2	0.29	0.263	9.3
	Test 3	0.25	0.265	6
	Test 1	0.19	0.205	7.9
7 Male	Test 2	0.22	0.238	8.2
	Test 3	0.21	0.193	8.1
	Test 1	0.33	0.343	3.9
8 Female	Test 2	0.3	0.322	7.3
	Test 3	0.33	0.339	2.7
	Test 1	0.13	0.137	5.4
9 Male	Test 2	0.13	0.141	8.5
	Test 3	0.13	0.155 0.157 0.155 0.157 0.155 0.238 0.265 0.305 0.292 0.289 0.238 0.138 0.147 0.141 0.229 0.269 0.193 0.271 0.263 0.265 0.205 0.238 0.193 0.343 0.342 0.343 0.322 0.339 0.137 0.141 0.129 0.175 0.165	0.7
	Test 1	0.17	0.238 0.265 0.305 0.292 0.289 0.238 0.138 0.147 0.141 0.229 0.269 0.193 0.271 0.263 0.265 0.205 0.238 0.193 0.343 0.322 0.339 0.137 0.141 0.129 0.175 0.165	2.9
10 Female	Test 2	0.18	0.165	8.3
	Test 3	0.18	0.168	6.7

Table 6.2: Estimated breathing frequencies and errors with waveform W2: Vital Signs for the in-place sequence at 1m [participants 11-20]

Test Subject	Test Number	True Value [Hz]	Est. Value [Hz]	Error [%]
	Test 1	0.12	0.127	5.8
11 Male	Test 2	0.12	0.126	5
	Test 3	0.12	0.127 0.126 0.124 0.203 0.214 0.194 0.331 0.354 0.332 0.181 0.176 0.215 0.2 0.232 0.377 0.298 0.325 0.234 0.248 0.226 0.335 0.335 0.344 0.21 0.235 0.201 0.245 0.193	3.3
	Test 1	0.2	0.203	1.5
12 Male	Test 2	0.2	0.214	7
	Test 3	0.2	0.194	3
	Test 1	0.32	0.331	3.4
13 Male	Test 2	0.33	0.354	7.3
	Test 3	0.31	0.332	7.1
	Test 1	0.17	0.181	6.5
14 Female	Test 2	0.18	0.173	3.8
	Test 3	0.18	0.176	2.2
	Test 1	0.21	0.215	2.4
15 Female	Test 2	0.12 0.127 0.12 0.126 0.12 0.124 0.2 0.203 0.2 0.214 0.2 0.194 0.32 0.331 0.33 0.354 0.31 0.332 0.17 0.181 0.18 0.173 0.18 0.176 0.21 0.215 0.21 0.2 0.22 0.232 0.37 0.377 0.32 0.298 0.34 0.325 0.23 0.248 0.21 0.226 0.36 0.335 0.32 0.335 0.36 0.344 0.2 0.21 0.23 0.235 0.23 0.235 0.22 0.201 0.23 0.245	0.2	4.7
	Test 3	0.22	0.127 0.126 0.127 0.126 0.124 0.203 0.214 0.194 0.331 0.354 0.332 0.181 0.173 0.176 0.215 0.2 0.232 0.377 0.298 0.325 0.325 0.234 0.248 0.226 0.335 0.335 0.335 0.344 0.21 0.235 0.201 0.245 0.193	5.5
	Test 1	0.37	0.377	1.9
16 Male	Test 2	0.32	0.12 0.127 0.12 0.126 0.12 0.124 0.2 0.203 0.2 0.214 0.2 0.194 0.32 0.331 0.33 0.354 0.31 0.332 0.17 0.181 0.18 0.173 0.18 0.176 0.21 0.215 0.21 0.22 0.37 0.377 0.32 0.298 0.34 0.325 0.25 0.234 0.23 0.248 0.21 0.226 0.36 0.335 0.32 0.335 0.33 0.235 0.23 0.235 0.22 0.201 0.23 0.245 0.2 0.193	6.8
	Test 3	0.34		4.4
	Test 1	0.25	0.234	6.4
17 Male	Test 2	0.23	0.248	7.8
	Test 3	0.21	0.226	7.6
	Test 1	0.36	0.335	6.9
18 Female	Test 2	0.32	0.335	4.7
	Test 3	0.36	0.12 0.127 0.12 0.126 0.12 0.124 0.2 0.203 0.2 0.214 0.2 0.194 0.32 0.331 0.33 0.354 0.31 0.332 0.17 0.181 0.18 0.173 0.18 0.176 0.21 0.215 0.21 0.22 0.37 0.377 0.32 0.298 0.34 0.325 0.25 0.234 0.21 0.226 0.36 0.335 0.32 0.335 0.36 0.335 0.36 0.344 0.2 0.21 0.23 0.235 0.23 0.235 0.22 0.201 0.23 0.245 0.2 0.193	4.4
	Test 1	0.2	0.21	5
19 Male	Test 1 0.17 0.181 Test 2 0.18 0.173 Test 3 0.18 0.176 Test 1 0.21 0.215 Test 2 0.21 0.2 Test 3 0.22 0.232 Test 1 0.37 0.377 Test 2 0.32 0.298 Test 3 0.34 0.325 Test 1 0.25 0.234 Test 2 0.23 0.248 Test 3 0.21 0.226 Test 1 0.36 0.335 Test 2 0.32 0.335 Test 3 0.36 0.344 Test 1 0.2 0.21 Test 2 0.23 0.235	2.2		
	Test 3	0.22	0.127 0.126 0.124 0.203 0.214 0.194 0.331 0.354 0.332 0.181 0.173 0.176 0.215 0.2 0.232 0.377 0.298 0.325 0.325 0.234 0.248 0.226 0.335 0.335 0.335 0.344 0.21 0.235 0.201 0.245 0.193	8.6
	Test 1	0.23	0.245	6.5
20 Female	Test 2	0.2	0.193	3.5
	Test 3	0.23	0.232	0.9

Table 6.3: Estimated breathing frequencies and errors with waveform W2: Vital Signs for the in-place sequence at 2m [participants 1-10]

Test Subject	Test Number	True Value [Hz]	Est. Value [Hz]	Error [%]
	Test 1	0.14	0.138	1.4
1 Male	Test 2	0.14	0.129	7.8
	Test 3	0.14	0.138 0.129 0.151 0.266 0.25 0.285 0.396 0.392 0.118 0.12 0.141 0.266 0.225 0.203 0.333 0.296 0.306 0.229 0.228 0.227 0.34 0.341 0.335 0.121 0.139 0.134 0.175 0.171	7.8
	Test 1	0.27	0.266	1.4
2 Male	Test 2	0.27	0.25	7.4
	Test 3	0.27	0.138 0.129 0.151 0.266 0.25 0.285 0.396 0.392 0.118 0.12 0.141 0.266 0.225 0.203 0.333 0.296 0.306 0.229 0.228 0.227 0.34 0.341 0.335 0.121 0.139 0.134 0.175 0.171	5.6
	Test 1	0.3	0.285	5
3 Male	Test 2	0.37	0.396	7
	Test 3	0.37	0.138 0.129 0.151 0.266 0.25 0.285 0.285 0.396 0.392 0.118 0.12 0.141 0.266 0.225 0.203 0.333 0.296 0.306 0.229 0.228 0.227 0.34 0.341 0.335 0.121 0.139 0.134 0.175	5.9
	Test 1	0.13	0.118	9.2
4 Female	Test 2	0.13	0.12	7.7
	Test 3	0.13	0.138 0.129 0.151 0.266 0.25 0.285 0.285 0.396 0.392 0.118 0.12 0.141 0.266 0.225 0.203 0.333 0.296 0.306 0.229 0.228 0.227 0.34 0.341 0.335 0.121 0.139 0.134 0.175 0.171	8.5
	Test 1	0.25	0.266	6.4
5 Male	Test 2	0.22	0.225	2.3
	Test 3	0.21	0.138 0.129 0.151 0.266 0.25 0.285 0.396 0.392 0.118 0.12 0.141 0.266 0.225 0.203 0.333 0.296 0.306 0.229 0.228 0.227 0.34 0.341 0.335 0.121 0.139 0.134 0.175 0.171	3.3
	Test 1	0.31	0.333	7.4
6 Male	Test 2	0.32	0.296	7.5
	Test 3	0.29	0.138 0.129 0.151 0.266 0.25 0.285 0.396 0.392 0.118 0.12 0.141 0.266 0.225 0.203 0.333 0.296 0.306 0.229 0.228 0.227 0.34 0.341 0.335 0.121 0.139 0.134 0.175 0.171	5.5
	Test 1	0.22	0.229	4.1
7 Male	Test 2	0.21	0.228	8.6
	Test 3	0.21	0.227	8.1
	Test 1	0.36	0.34	5.5
8 Female	Test 2	0.36	0.341	5.2
	Test 3	0.36	0.138 0.129 0.151 0.266 0.25 0.285 0.396 0.392 0.118 0.12 0.141 0.266 0.225 0.203 0.333 0.296 0.306 0.229 0.228 0.227 0.34 0.341 0.335 0.121 0.139 0.134 0.175 0.171	6.9
	Test 1	0.13	0.138 0.129 0.151 0.266 0.25 0.285 0.285 0.396 0.392 0.118 0.12 0.141 0.266 0.225 0.203 0.333 0.296 0.306 0.229 0.228 0.227 0.34 0.341 0.335 0.121 0.139 0.134 0.175 0.171	6.9
9 Male	Test 2	0.13		6.9
	Test 3	0.13		3.1
	Test 1	0.18	0.175	2.7
10 Female	Test 2	0.18	0.12 0.141 0.266 0.225 0.203 0.333 0.296 0.306 0.229 0.228 0.227 0.34 0.341 0.335 0.121 0.139 0.134 0.175 0.171	5
	Test 3	0.19	0.177	6.8

Table 6.4: Estimated frequencies and errors with waveform W2: Vital Signs for the inplace sequence at 2m [participants 11-20]

Test Subject	Test Number	True Value [Hz]	Est. Value [Hz]	Error [%]
	Test 1	0.13	0.118	9.2
11 Male	Test 2	0.13	0.12	7.7
	Test 3	0.13	0.141	8.5
	Test 1	0.2	0.212	6
12 Male	Test 2	0.2	0.211	5.5
	Test 3	0.23	0.217	5.6
	Test 1	0.31	0.292	5.8
13 Male	Test 2	0.31	0.314	1.3
	Test 3	0.31	0.327	5.5
	Test 1	0.18	0.187	3.9
14 Female	Test 2	0.18	0.168	6.7
	Test 3	0.14	0.15	7.1
	Test 1	0.21	0.206	1.9
15 Female	Test 2	0.21	0.228	8.6
	Test 3	0.18	0.118 0.12 0.141 0.212 0.211 0.217 0.292 0.314 0.327 0.187 0.168 0.15 0.206	8.3
	Test 1	0.29	0.281	3.1
16 Male	Test 2	0.32	0.298	6.8
	Test 3	0.32	0.118 0.12 0.141 0.212 0.211 0.217 0.292 0.314 0.327 0.187 0.168 0.15 0.206 0.228 0.195 0.281 0.298 0.305 0.26 0.225 0.249 0.379 0.336 0.362 0.201 0.208 0.232 0.182 0.203	4.7
	Test 1	0.24	0.26	8.3
17 Male	Test 2	0.21	0.225	7.1
	Test 3	0.24	0.249	3.8
	Test 1	0.38	0.379	0.2
18 Female	Test 2	0.35	0.336	4
	Test 3	0.38	0.362	4.7
	Test 1	0.22	0.217 0.292 0.314 0.327 0.187 0.168 0.15 0.206 0.228 0.195 0.281 0.298 0.305 0.26 0.225 0.249 0.379 0.336 0.362 0.201 0.208 0.232	8.6
19 Male	Test 2	0.22	0.208	5.5
	Test 3	0.22	0.12 0.141 0.212 0.211 0.217 0.292 0.314 0.327 0.187 0.168 0.15 0.206 0.228 0.195 0.281 0.298 0.305 0.26 0.225 0.249 0.379 0.336 0.362 0.201 0.208 0.232 0.182 0.203	5.5
	Test 1	0.17	0.327 0.187 0.168 0.15 0.206 0.228 0.195 0.281 0.298 0.305 0.26 0.225 0.249 0.379 0.336 0.362 0.201 0.208 0.232 0.182 0.203	7.1
20 Female	Test 2	0.2	0.203	1.5
	Test 3	0.2	0.21	5

Table 6.5: Estimated breathing frequencies and errors based on Range-Time segmentation with waveform W2: Vital Signs at 1m [participants 1-10]

Test Subject	Test Number	True Value [Hz]	Est. Value [Hz]	Error [%]
	Test 1	0.21	Est. Value [Hz]	3.8
1 Male	Test 2	0.21		4.7
	Test 3	0.15		5.3
	Test 1	0.26	0.247	5
2 Male	Test 2	0.26	0.257	1.1
	Test 3	0.26	0.202 0.22 0.142 0.247 0.257 0.251 0.297 0.274 0.258 0.144 0.163 0.139 0.21 0.203 0.201 0.234 0.295 0.266 0.202 0.199 0.207 0.319 0.306 0.315 0.164 0.143 0.153 0.204 0.196	3.4
	Test 1	0.28	0.297	6.1
3 Male	Test 2	0.28	0.274	2.1
	Test 3	0.28	0.258	7.8
	Test 1	0.15	0.144	4
4 Female	Test 2	0.15	0.163	8.6
	Test 3	0.15	0.202 0.22 0.142 0.247 0.257 0.251 0.297 0.274 0.258 0.144 0.163 0.139 0.21 0.203 0.201 0.234 0.295 0.266 0.202 0.199 0.207 0.319 0.306 0.315 0.164 0.143 0.153 0.204 0.196	7.3
	Test 1	0.2	0.21	5
5 Male	Test 2	0.2	0.202 0.22 0.142 0.247 0.257 0.251 0.297 0.274 0.258 0.144 0.163 0.139 0.21 0.203 0.201 0.234 0.295 0.266 0.202 0.199 0.207 0.319 0.306 0.315 0.164 0.143 0.153 0.204 0.196	1.5
	Test 3	0.2		0.5
	Test 1	0.25	0.234	6.4
6 Male	Test 2	0.3	0.295	1.6
	Test 3	0.25	0.202 0.22 0.142 0.247 0.257 0.251 0.297 0.274 0.258 0.144 0.163 0.139 0.21 0.203 0.201 0.234 0.295 0.266 0.202 0.199 0.207 0.319 0.306 0.315 0.164 0.143 0.153 0.204 0.196	6.4
	Test 1	0.22	0.202	8.1
7 Male	Test 2	0.21	0.199	5.2
	Test 3	0.2	0.207	3.5
	Test 1	0.3	0.319	6.3
8 Female	Test 2	0.3	0.306	2
	Test 3	0.33	0.202 0.247 0.247 0.257 0.251 0.297 0.274 0.258 0.144 0.163 0.139 0.21 0.203 0.201 0.234 0.295 0.266 0.202 0.199 0.207 0.319 0.306 0.315 0.164 0.143 0.153 0.204 0.196	4.5
	Test 1	0.15	0.202 0.22 0.142 0.247 0.257 0.251 0.297 0.274 0.258 0.144 0.163 0.139 0.21 0.203 0.201 0.234 0.295 0.266 0.202 0.199 0.207 0.319 0.306 0.315 0.164 0.143 0.153 0.204 0.196	9.3
9 Male	Test 2	0.15		4.6
	Test 3	0.15		2
	Test 1	0.19	0.204	7.3
10 Female	Test 2	0.18	0.196	8.8
	Test 3	0.18	0.189	5

Table 6.6: Estimated breathing frequencies and errors based on Range-Time segmentation with waveform W2: Vital Signs at 1m [participants 11-20]

Test Subject	Test Number	True Value [Hz]	Est. Value [Hz]	Error [%]
	Test 1	0.14	0.135 0.157 0.146 0.237 0.187 0.191 0.295 0.335 0.306 0.169 0.171 0.191 0.183 0.221 0.224 0.328 0.296 0.367 0.223 0.224 0.23 0.224 0.23 0.323 0.323 0.357 0.332 0.202 0.192 0.207	3.5
11 Male	Test 2	0.15	0.157	4.6
	Test 3	0.14	0.146	4.2
	Test 1	0.25	0.237	5.2
12 Male	Test 2	0.2	0.187	6.5
	Test 3	0.2	4 0.135 .5 0.157 .4 0.146 .5 0.237 2 0.187 2 0.191 .6 0.295 .8 0.169 .8 0.171 .8 0.191 .2 0.183 .21 0.224 .5 0.328 .3 0.296 .8 0.367 .2 0.23 .3 0.224 .21 0.23 .3 0.323 .3 0.357 .3 0.357 .3 0.332 .2 0.202 .2 0.273 .3 0.245	4.5
	Test 1	0.31	0.295	4.8
13 Male	Test 2	0.32	0.335	4.6
	Test 3	0.31	0.306	1.3
	Test 1	0.18	0.169	6.1
14 Female	Test 2	0.18	0.171	5
	Test 3	0.18	0.14 0.135 0.15 0.157 0.14 0.146 0.25 0.237 0.2 0.187 0.2 0.191 0.31 0.295 0.32 0.335 0.31 0.306 0.18 0.169 0.18 0.171 0.18 0.191 0.2 0.183 0.21 0.221 0.21 0.224 0.35 0.328 0.3 0.296 0.35 0.367 0.22 0.223 0.23 0.224 0.21 0.23 0.23 0.323 0.37 0.357 0.32 0.332 0.2 0.202 0.2 0.192 0.2 0.202 0.2 0.207 0.25 0.273	6.1
	Test 1	0.2	0.183	8.5
15 Female	Test 2	0.21	0.221	5.2
	Test 3	0.21	0.135 0.157 0.146 0.237 0.187 0.191 0.295 0.335 0.306 0.169 0.171 0.191 0.183 0.221 0.224 0.328 0.296 0.367 0.223 0.224 0.23 0.323 0.323 0.357 0.332 0.302 0.192 0.207 0.273 0.245	6.6
	Test 1	0.35	0.328	6.2
16 Male	Test 2	0.3	0.296	1.3
	Test 3	0.35	0.135 0.157 0.146 0.237 0.187 0.191 0.295 0.335 0.306 0.169 0.171 0.191 0.183 0.221 0.224 0.328 0.296 0.367 0.223 0.224 0.323 0.323 0.357 0.332 0.3032 0.202 0.192 0.207 0.273 0.245	4.8
	Test 1	0.22	0.223	1.3
17 Male	Test 2	0.23	0.224	2.6
	Test 3	0.21	0.23	9.5
	Test 1	0.35	0.323	7.7
18 Female	Test 2	0.37	0.357	3.5
	Test 3	0.32	14 0.135 15 0.157 14 0.146 25 0.237 .2 0.187 .2 0.191 31 0.295 32 0.335 31 0.306 18 0.169 18 0.171 18 0.191 .2 0.183 21 0.224 35 0.328 .3 0.296 35 0.367 22 0.223 23 0.224 21 0.23 35 0.323 37 0.357 32 0.332 .2 0.202 .2 0.192 22 0.207 25 0.273 23 0.245	3.7
	Test 1	0.2	0.202	1
19 Male	Test 2	0.2	0.192	4
	Test 3	0.22	0.135 0.157 0.146 0.237 0.187 0.191 0.295 0.335 0.306 0.169 0.171 0.191 0.183 0.221 0.224 0.328 0.296 0.367 0.223 0.224 0.323 0.323 0.323 0.323 0.357 0.332 0.202 0.192 0.207 0.273 0.245	5.9
	Test 1	0.25	0.273	9.2
20 Female	Test 2	0.23	0.224 0.328 0.296 0.367 0.223 0.224 0.23 0.323 0.357 0.332 0.202 0.192 0.207 0.273 0.245	6.5
	Test 3	0.23	0.221	3.9

Table 6.7: Estimated breathing frequencies and errors based on Range-Time segmentation with waveform W2: Vital Signs at 2m [participants 1-10]

Test Subject	Test Number	True Value [Hz]	Est. Value [Hz]	Error [%]
	Test 1	0.2	0.192	4
1 Male	Test 2	0.15	0.163	8.6
	Test 3	0.15	N/A	N/A
	Test 1	0.25	N/A	N/A
2 Male	Test 2	0.2	N/A	N/A
	Test 3	0.26	0.192 0.163 N/A N/A	N/A
	Test 1	0.25	0.246	1.6
3 Male	Test 2	0.3	N/A	N/A
	Test 3	0.25	N/A	N/A
	Test 1	0.15	N/A	N/A
4 Female	Test 2	0.15	N/A	N/A
	Test 3	0.15	0.192 0.163 N/A N/A N/A N/A N/A N/A N/A 0.246 N/A	N/A
	Test 1	0.2	N/A	N/A
5 Male	Test 2	0.2	N/A	N/A
	Test 3	0.18	0.167	7.2
	Test 1	0.3	N/A	N/A
6 Male	Test 2	0.3	0.287	4.3
	Test 3	0.3	0.192 0.163 N/A N/A N/A N/A N/A N/A 0.246 N/A N/A N/A N/A N/A N/A N/A N/A N/A 0.167 N/A 0.287 0.319 N/A	6.3
	Test 1	0.19	N/A	N/A
7 Male	Test 2	0.22	N/A	N/A
	Test 3	0.2	0.192 0.163 N/A N/A N/A N/A N/A N/A 0.246 N/A	N/A
	Test 1	0.3	N/A	N/A
8 Female	Test 2	0.35	0.333	4.8
	Test 3	0.3	2 0.192 15 0.163 15 N/A 25 N/A 2 N/A 26 N/A 26 N/A 27 N/A 28 N/A 29 N/A 20 N/A 20 N/A 20 N/A 21 N/A 21 N/A 22 N/A 23 N/A 24 N/A 25 N/A 26 N/A 27 N/A 28 N/A 29 N/A 20 N/A 20 N/A 21 N/A 21 N/A 22 N/A 22 N/A 23 N/A 24 N/A 25 N/A 26 N/A 27 N/A 28 N/A 29 N/A 20 N/A 20 N/A 21 N/A 22 N/A 22 N/A 23 N/A 24 N/A 25 N/A 26 N/A 27 N/A 28 N/A 29 N/A 20 N/A 20 N/A 21 N/A 22 N/A 23 N/A 24 N/A 25 N/A 26 N/A 27 N/A 28 N/A 29 N/A 20 N/A 20 N/A	N/A
	Test 1	0.2	0.163 N/A N/A N/A N/A N/A N/A 0.246 N/A N/A N/A N/A N/A N/A N/A N/A N/A 0.167 N/A 0.287 0.319 N/A	4.5
9 Male	Test 2	0.15	0.141	6
	Test 3	0.2	N/A	N/A
	Test 1	0.2	N/A	N/A
10 Female	Test 2	0.19	N/A	N/A
	Test 3	0.19	N/A	N/A

6

Table 6.8: Estimated breathing frequencies and errors based on Range-Time segmentation with waveform W2: Vital Signs at 2m [participants 11-20]

Test Subject	Test Number	True Value [Hz]	Est. Value [Hz]	Error [%]
	Test 1	0.15	N/A	N/A
11 Male	Test 2	0.14	0.128	8.5
	Test 3	0.14	N/A	N/A
	Test 1	0.2	0.194	3
12 Male	Test 2	0.2	N/A	N/A
	Test 3	0.2	N/A	N/A
	Test 1	0.31	N/A	N/A
13 Male	Test 2	0.33	N/A	N/A
	Test 3	0.32	N/A N/A N/A N/A N/A N/A N/A N/A	N/A
	Test 1	0.18	0.165	8.3
14 Female	Test 2	0.2	N/A	N/A
	Test 3	0.18	N/A	N/A
	Test 1	0.21	N/A	N/A
15 Female	Test 2	0.21	.15 N/A .14 0.128 .14 N/A .12 0.194 .12 N/A .13 N/A .13 N/A .31 N/A .32 N/A .32 N/A .18 0.165 .19 N/A .19 N/A .19 N/A .10 N/A .10 N/A .10 N/A .10 N/A .11 N/A .12 N/A .13 N/A .21 N/A .33 N/A .34 0.356 .2 N/A .35 N/A .36 N/A .37 N/A .38 N/A .39 N/A .39 N/A .30 N/A .31 N/A .32 N/A .33 N/A .34 0.356 .2 N/A .22 N/A .23 N/A .34 0.356 .2 N/A .35 N/A .36 N/A .37 N/A .38 N/A .39 N/A .39 N/A .39 N/A .30 N/A .31 N/A .32 N/A .33 N/A .34 N/A .35 N/A .35 N/A .36 N/A .37 N/A .38 N/A .39 N/A .39 N/A .39 N/A .39 N/A .30 N/A .30 N/A .31 N/A .32 N/A .33 N/A .34 N/A .35 N/A .35 N/A .36 N/A .37 N/A .38 N/A .39 N/A	N/A
	Test 3	0.21		N/A
	Test 1	0.3	N/A	N/A
16 Male	Test 2	0.35	N/A	N/A
	Test 3	0.34	N/A 0.128 N/A 0.128 N/A 0.194 N/A N/A N/A N/A N/A N/A N/A N/	4.7
	Test 1	0.2	N/A	N/A
17 Male	Test 2	0.2	N/A	N/A
	Test 3	0.21	N/A	N/A
	Test 1	0.35	N/A	N/A
18 Female	Test 2	0.36	N/A	N/A
	Test 3	0.36	N/A	N/A
	Test 1	0.25	N/A	N/A
19 Male	Test 2	0.22	0.15 N/A 0.14 0.128 0.14 N/A 0.2 0.194 0.2 N/A 0.2 N/A 0.31 N/A 0.32 N/A 0.18 0.165 0.2 N/A 0.18 N/A 0.21 N/A 0.21 N/A 0.21 N/A 0.33 N/A 0.34 0.356 0.2 N/A 0.21 N/A 0.22 N/A 0.21 N/A 0.22 N/A 0.23 N/A 0.24 N/A 0.25 N/A 0.25 N/A 0.25 0.263 0.2 N/A	5
	Test 3	0.22		N/A
	Test 1	0.25	0.263	5.2
20 Female	Test 2	0.2	N/A	N/A
	Test 3	0.22	N/A	N/A

APPENDIX C

This appendix presents a summary of the test participants' information during the data collection campaign executed in this thesis project, including the gender, age, height, weight, BMI, and clothes worn by each of the volunteers.

Table 6.9: Summary of the test participants' information

Gender	Age	Height [cm]	Weight [kg]	BMI	Clothes
1 Male	23	180	90	27.8	Sweatshirt
2 Male	25	179	74	23.1	T-shirt
3 Male	30	176	70	22.6	T-shirt
4 Female	26	168	52	18.4	Tank top
5 Male	23	165	67	24.6	T-shirt
6 Male	37	170	73	25.3	Cotton jumper
7 Male	26	191	80	21.9	T-shirt
8 Female	24	166	52	18.9	Knit cardigan
9 Male	32	180	70	21.6	T-shirt
10 Female	25	165	55	20.2	Long sleeve top
11 Male	24	175	70	22.9	T-shirt
12 Male	24	175	48	15.7	T-shirt
13 Male	29	167	77	27.6	T-shirt
14 Female	24	161	60	23.1	T-shirt
15 Female	25	166	56	20.3	T-shirt
16 Male	36	182	82	24.8	T-shirt
17 Male	23	175	74	24.2	T-shirt
18 Female	24	162	58	22.1	Тор
19 Male	25	185	90	26.3	T-shirt
20 Female	26	170	48	16.6	Sweater